Sub-wavelength platinum wires as bolometers: Fabrication and Optimization

Pauline Renoux

Faculty of Physical Sciences
University of Iceland
2014

SUB-WAVELENGTH PLATINUM WIRES AS BOLOMETERS: FABRICATION AND OPTIMIZATION

Pauline Renoux

Thesis submitted in partial fulfillment of a
Philosophiae Doctor degree in Physics

Advisor
Prof. Snorri Þ. Ingvarsson

Ph.D. committee
Prof. Snorri Þ. Ingvarsson
Dr. Kristján Leósson
Prof. Einar Sveinbjörnsson

Opponents
Prof. Joseph J. Talghader
Department of Electrical and Computer Engineering, University of Minnesota, Minneapolis, USA
Prof. Frank Niklaus
School of Electrical Engineering, KTH Royal Institute of Technology, Stockholm, Sweden

Faculty of Physical Sciences
School of Engineering and Natural Sciences
University of Iceland
Reykjavik, March 2014

Sub-wavelength platinum wires as bolometers: Fabrication and Optimization

Faculty of Physical Sciences
School of Engineering and Natural Sciences
University of Iceland
VRII, Hjardarhagi 2-6
107, Reykjavik
Iceland

Telephone: 525 4000

Bibliographic information:
Pauline Renoux, 2014, Sub-wavelength platinum wires as bolometers: Fabrication and Optimization, Ph.D. thesis, Faculty of Physical Sciences, University of Iceland.

ISBN 978-9935-9140-4-0

Printing: Háskólaprent, Fálkagata 2, 107 Reykjavík
Reykjavik, Iceland, March 2014

Abstract

This thesis presents results on nano- to microscopic bolometers. They are made of polycrystalline metallic thin-films shaped into narrow wires that sense infrared radiation in the near- to mid-infrared (IR) range. Using state-of-the-art e-beam lithography and metal deposition, the wires were fabricated on Si/ SiO_2 wafers. The central part has lateral dimensions ranging from hundreds of nanometers to several micrometers, while the metallic thin-film has a thickness between 2 and 80 nm. By illuminating the bolometers with light from a ceramic blackbody infrared source (1060 K, peak wavelength at 2.74 μm), we monitor the change in resistance ΔR in the structures. The resistance change is a direct result of infrared heating and the corresponding temperature change ΔT can be characterized thanks to the approximately linear relationship between resistance and temperature characterized by α, the temperature coefficient of resistance (TCR) of platinum wire. Based on the extracted temperature change of the bolometers, we calculate two figures of merit to characterize the sensitivity of our devices: the responsivity ($\Re$) and the specific detectivity (D^*).

The performance of our bolometers has been optimized through multiple experiments carried out for several years. We studied the influence on performance of physical and operating parameters such as oxide thickness, bolometer dimensions, platinum thickness or drive current. Depending on sample dimension and surroundings, a responsivity of 10^4 to 10^5 V/W was achieved, as well as a detectivity of 10^7 to 10^8 cmHz$^{1/2}$/W, which is comparable to the latest literature results in the field of thermal detectors.

At the size range of our bolometers, changes in absorption properties due to sample dimensions were observed. Antenna-like resonances in IR absorption and enhanced responsivity for narrow wires have been revealed and discussed. It is also suggested that as the width is reduced, the wires become selective to the polarization of light they absorb. Bolometers thinner than 40 nm present altered electronic properties, such as a lower TCR value and a higher resistivity. Detectivity is maximized for thicknesses equal or larger than 40 nm. A silicon dioxide thickness of 350 nm or 1 μm leads to an improved infrared sensitivity. For the latter thickness value, interference effects of infrared light reflected at the interface between silicon dioxide and silicon contribute to the sensitivity.

Finally, the time response of our thin-film bolometers has been calculated to be less than 4 ns, which is a great improvement compared to the general time response of thermal detectors. This value can be further reduced by reducing the metallic film thickness. Similarly, the sensitivity can be improved by reducing the 1/f noise component.

Útdráttur

Í þessari ritgerð eru settar fram niðurstöður mælinga á smásæjum varmageislunarmælum. Mælarnir eru búnir til úr fjölkristalla platínuþynnum sem eru mynstraðar í granna víra, sem nema innrauða geislun á nær- til miðinnrauða bylgjulengdasviðinu. Vírarnir hvíla á Si/SiO_2 undirlagi og eru mynstraðir með rafeindaprentun. Miðhluti vírsins er allt frá hundruðum nanómetra upp í nokkra míkrómetra að breidd, en þykktin er á bilinu 2 til 80 nm. Lýst er á varmageislamælana með svarthlutsljósgjafa (1060 K, hámarksljósafl við bylgjulengd 2.74 μm) og fylgst með viðnámsbreytingum vírsins. Breyting í viðnámi svarar til hitabreytingar í vírnum, en þar á milli er í mjög góðri nálgun línulegt samband sem lýst er með hitaviðnámsstuðli platínuvírsins, α. Frá niðurstöðunum má reikna út næmni varmageislamælisins, sem er gefin til kynna með tveimur kennistærðum, næmi ($\Re$) og sértæku viðtaki (D^*).

Áhrif ýmissa breyta á frammistöðu varmageislunarmælanna hafa verið rannsökuð, svo sem oxíðþykktar, stærðar mælis í plani, platínuþykktar og straumálags. Bestu mælarnir hafa sýnt næmi upp á 10^4 til 10^5 V/W, og sértækt viðtak 10^7 til 10^8 $cmHz^{1/2}/W$, sem er sambærilegt við nýlegar niðurstöður fyrir aðrar gerðir skyldra varmageislunarmæla.

Áhrif stærðarskala varmageislunarmælanna koma fram í ísogseiginleikum þeirra. Einnig sjást merki um loftnets-líkar hermur í innrauðu ísogi og aukningu í næmi grannra víra. Að auki eru leiddar að því líkur að þegar vírarnir verða nógu grannir þá víxlverki þeir eingöngu við ákveðna skautun ljóss sem á þeim lendir. Varmageislunarmælar þynnri en 40 nm eru með lægri hitaviðnámsstuðul og hærra eðlisviðnám. Sértækt viðtak er hámarkað í vírum sem eru þykkari en 40 nm. Kísildíoxíðlög upp á 350 nm annars vegar og 1 μm hins vegar gáfu aukna næmni fyrir innrauðri geislun. Við síðarnefndu oxíðþykktina leggja víxlhrif vegna speglunar innrauðrar geislunar frá mörkum kísildíoxíðs og kísilundirlags sitt af mörkum til aukinnar næmni.

Að lokum er sýnt fram á með útreikningum að varmageislunarmælarnir ættu að hafa viðbragðstíma undir 4 ns, sem er mörgum stærðargráðum hraðari svörun en aðrir skyldir, en stærri, nemar. Svöruninni má enn flýta með því að þynna filmurnar. Eins má auka næmnina með því að minnka framlag 1/f suðs.

Acknowledgments

First and foremost, I would like to thank Snorri Þorgeir Ingvarsson for his supervision on this doctoral project. I feel lucky to have had the opportunity to work with him. Always available for any discussion or problem, he showed boundless patience and dedication. I have seldom met a person this kind, yet fair. Thank you for guiding me through the (sometimes tough) path of research, and for offering me so many opportunities to go abroad and broaden my horizons.

I am also very grateful to my group co-workers I met during these past years, specially to Gabriel Vasile whose help was deeply appreciated. Thanks also to Mustafa Arikan for showing me around the different cleanroom processes and such. It was also super nice to go on trips in the wilderness all together.

I am also very grateful towards all the professors and researchers at Háskóli Íslands: Kristján Leósson, Einar Sveinbjörnsson, Ivan Shelykh, Svein Ólafsson, Ari Ólafsson, Hafliði Pétur Gíslason. They are always smiling and ready to discuss new ideas or to lend a hand with projects. I was also very happy to spend two weeks among the MST group in KTH, Sweden. Thanks to Kristinn B. Gylfason and Floria Ottonello Briano for their warm welcome. Thanks also to Prof. Talghader and Prof. Niklaus, flying over to Iceland to be part of the jury.

The VR-III North open space team also deserves a big thanks, for all the cakes, waffles and burgers celebrating summer, birthdays, or just another good day at the office. Past and present members include: Torben, Anna, Virginia, Sasha, Kristinn, Einar, Frímann, Lukas, Hörður, Balthasar, Árni, Fridrik, Anna Karin, Bassi, Kristján, Bing, Cosmin, Jen, Tibi, and I could keep going! Thanks for the good times.

Also I'd like to thank the French interns who came regularly in Iceland, for the work well done together and the bribery with French goods. All my gratitude goes to Alice, Magali, Dorine, Patrice and Sylvain.

I've been told that I don't look so stressed for a Ph.D. student. The thing is, of course stress kicked in sometimes (and Snorri is ready to confirm this), but how can you stay worried when you're surrounded by so many great friends? They make it all worthwhile. Malcolm for being so Malcolm-ey, Elisa, Fabio and Anna for your superb Italian touch and deep kindness (and your illustrations!), Dr. Morgan who is always ready for a new adventure, Pauline for your understanding and unconditional support

– Is it because we share the same name? Julien the hermit of Skaftafell, Peter for movies and whisky, David, Henrike, Milosz, Gro, Ana, Ute and all the fellow scientists for their all-time enthusiasm, Björn, Kasia, Ana, Karol and Anya, and all the French expats met here: Sigurlína, Fabien, Mickaël, Xavier, Julia and Sébastien, Charlotte, Léa and Nicolas, Féline... Also the French embassy should be thanked, for providing us regularly with free wine and food so we don't get too homesick. I am also very glad that my long-time friends from school and university are still present in my life: Agathe, Céline, Julien, Déborah, Rémi, Caroline, les Gredins Denis, Rémi, Maheata and Guilhem, Delphine and all the others.

I also want to thank my housemates, past and present, the list is too long but my gratitude goes especially to Hannes, Nicola, Behnood, Gabriele, Lara and Philip, Gustav and Marcel for feeling at home at Njarðargata 37.

Finally, my family. There are not enough words to tell them how much I have missed them and how much I love them. My mother Françoise is somebody I look up to, and she is always here when I need her. My sister Louise, who is probably the most awesome person on Earth and beyond. My grand-mother Paulette, my late grand-parents Martine and Pierre, my uncles and aunts, my cousins, with a particular thought for Yannick and Fabien who are like big brothers to me. Thank you all for the support and thoughtfulness. I have a special thought for my late dad Olivier.

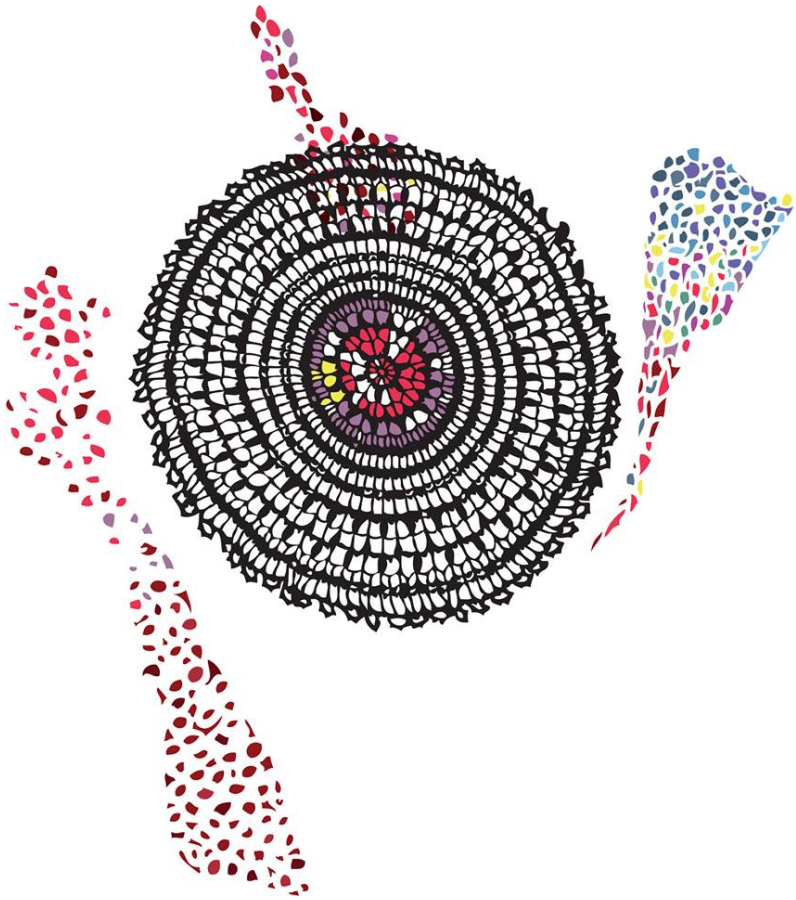

Nobody's easier to fool,
than the person who is
convinced that he's right.
- HARUKI MURAKAMI (1949 -)

Contents

List of Figures

List of Tables

1. Introduction

Infrared radiation is everywhere. It provides us warmth, coming from artificial heating systems or simply from the sun. Our body absorbs and emits it. The first temperature sensor is the human eye, with which we can determine the temperature of an object by assessing the wavelength of its emitted radiation. Calibration of the human eye is based on experience, and one quickly learns that a glowing red metal shall not be touched (hence the term "red-hot"). From antiquity to the present time, craftsmen have employed their vision to discern when heated materials are ready to be cut or shaped. Nowadays, glass makers still visually assess the temperature of melted glass to know if it is ready to be molded.

And yet, it was not until the 19^{th} century that the infrared spectrum was discovered. In 1800, Sir William Herschel was studying the temperature of the visible spectrum, by moving a thermometer along the prism-decomposed light on a table (see fig. 1.1). Much to his surprise, as he moved the thermometer towards the red-end of the spectra, not only was the temperature increasing, but furthermore no maximum was obtained until the thermometer was moved beyond the limit of the visible spectrum (Herschel 1800).

During the next thirty years little progress was made in characterizing the infrared radiation, mostly because no detector other than the thermometer was available. In 1830, Nobili invented the thermocouple, a much more precise device that enabled Herschel and other scientists to make further progress in characterizing the infrared radiation. Finally Langley invented in 1880 a bolometer simply designed as a Wheatstone bridge with two arms made of platinum wires (Langley 1880). A change in temperature of the Pt wires caused by incoming infrared radiation would change the resistance of the bridge. Since this advance in detection, infrared sensors have been exhaustively researched and improved.

It was only after the Second World War that the first modern radiation thermometers became available. Military institutions were investing in infrared sensing technology, specifically in the range of the infrared spectra emitted by humans (around 10 μm). A great emphasis was made on cooled photon detectors until the 1990's. Due to their higher performance and fast response compared to thermal detectors, they seemed very promising. Between 1980 and 1990, major companies in the USA developed successful sensors based on thermal detection (Wood et al. 1992). This prompted DARPA, the national agency for defense-oriented research, to change its funding policy and

invest more towards uncooled technology. Nowadays, there is still a strong demand for infrared detectors for military and space applications, but also for astronomy and telecommunications. There are also an increasing number of commercial applications that require infrared detectors. These include medical instruments, industry processes (e.g. nuclear power plants), earth resources and energy monitoring, etc. The demand from the civilian field is quickly growing, and brings new challenges for researchers.

Since their invention by Langley in 1880, bolometers have been extensively studied and developed. Several categories can be defined, as very different types of materials can be used as bolometric material. The core principle stays the same: upon encountering infrared radiation, the temperature of the material rises, leading to a measureable change in electrical resistance in the device. Metallic bolometers are common, made of bismuth, platinum, titanium or nickel (Block & Gaddy 1973, Kuzmichev et al. 2004, Liddiard 1984, Mei et al. 2002, Saxena, Bhan, Jalwania & Khurana 2008, Shie et al. 1996, Yoneoka et al. 2011, Zhang et al. 2005). Also, metallic antennas can be coupled to the infrared-sensitive element to enhance radiation collection (Bean et al. 2011, Grossman et al. 1998, Krenz et al. 2012). There has been recent improvement in semiconductor-based bolometers, specifically made of vanadium oxide (Aliev & Bortnikov 2011, Chen et al. 2007, Chi-Anh et al. 2005, Han et al. 2005, Ozcelik et al. 2013). Silicon slabs can also be used as bolometers (Boragno et al. 1987), but more recently poly Si-Ge structures (Sedky et al. 1999, 1998) or amorphous alloys (Kosarev et al. 2008, Torres et al. 2003) have also appeared. Finally, with the emergence of graphene technology and optical metamaterials, a wide range of novel bolometers have been proposed, made of diamond (Galkina et al. 2007, Klokov et al. 2010), carbon nanotubes (Aliev 2008, Lu et al. 2009, Mahjouri-Samani et al. 2013, Xiao et al. 2011), graphene (Xia et al. 2009) or metamaterial (Niesler et al. 2012). Also, some bolometric devices are based on the hot-electron effect (Dobrovolsky & Sizov 2007) or quantum wells (Forsberg et al. 2013). However, even if these new devices present some peculiar advantages, their sensitivity usually needs improvement.

The present thesis summarizes the work that has been done on fabricating and optimizing metallic bolometers made of platinum. The idea behind this Ph.D. project comes from a previous characterization of thermal emitters carried out in our lab. Such samples were made of a thin-film of platinum, usually thinner than 100 nm, that emits infrared radiation when biased by a DC current. They are designed as a rectangular or square central part attached to four leads connecting to contact pads. Through several studies, it has been shown that such samples exhibit peculiar infrared emission properties, especially as the dimensions of the central constriction are varied (Au et al. 2008, Ingvarsson et al. 2007). The coherence of the emitted infrared spectra is also affected by the dimensions of the central part (Klein et al. 2008) as well as its polarization (Klein et al. 2009). With Kirchhoff's principle in mind, we became interested in testing such devices not as infrared emitters but as infrared sensors. By biasing them with DC current and measuring the change in electrical resistance of the central part as the sample is under infrared illumination, their performance as bolometers was characterized. A ceramic heater at a temperature of 1060 K was used

as a blackbody source, with a peak wavelength of 2.74 μm. Several peer-reviewed papers were published during this Ph.D. project, describing the influence of different parameters on the bolometers' responsivity and detectivity. Renoux et al. (2011) concerns the evolution of the bolometer performance with its central part's length and is included at the end of this thesis as **Paper 1**. Later, the influence of the insulating layer of the device (SiO_2) and of the bias current on responsivity and detectivity were investigated (Renoux et al. 2012). This article is referred as **Paper 2**. Renoux et al. (2013) shows how the metallic film thickness affects several electronic characteristics of the device as well as its sensitivity (**Paper 4** at the end of the thesis). Recently published, Renoux & Ingvarsson (2013) focuses on the effect of the samples' lateral dimensions on the responsivity and detectivity. It is included as **Paper 3** in this work. Also, the noise sources in the samples as well as their self-heating mechanisms were constantly monitored, and conclusions were drawn about their impact and effects. The time response of bolometers was modeled and studied as a function of the film thickness.

This project has unveiled specific absorption properties due to the reduced size of the bolometers studied. Depending on their lateral dimensions, some of them are smaller than the wavelength that they sense. In this size range, surface effects can become dominant compared to volume ones. This significantly affects their absorption mechanisms, for example via boundary scattering or antenna resonance. This thesis work shows that the performance of such bolometers can be tailored according to specific needs (fast response time, absorption at a specific wavelength, etc.) by tweaking fabrication processes and bias. The sensitivity achieved by our devices is comparable to current state-of-the-art, and we give suggestions about how to improve it. We believe that these bolometers are very promising, as they are simple to fabricate and use. They do not need any encapsulation nor cryogenics, and no side circuits such as Wheatstone bridges. Moreover, a key advantage is their micro- to nanoscopic size, which enables their embedding on MEMS structures like waveguides. With their high sensitivity and expected fast response, they offer a promising solution to the requirements of both defense and civilian infrared sensing market.

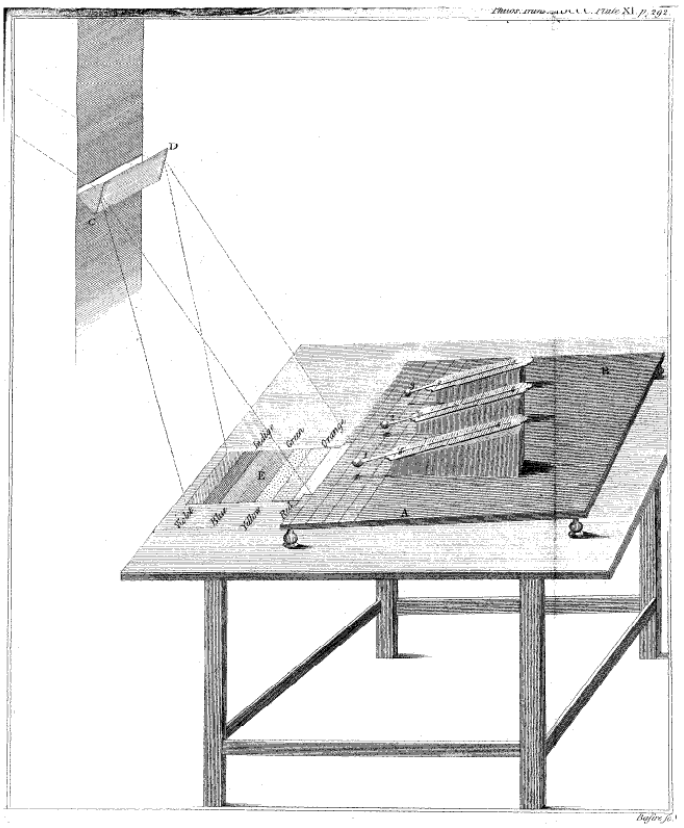

Figure 1.1: Herschel's experiment from 1800 that led to the discovery of the infrared radiation. The incoming solar radiation is decomposed by the prism into the visible spectrum. The violet end of the spectrum is located at the edge of the table, and the red end closer to the thermometers. Thermometers are located on a moving platform, to measure the temperature of each part of the spectrum. Illustration from Herschel (1800).

2. Fundamentals of infrared engineering

This chapter will introduce the reader to the fundamentals of the physics related to infrared detection. The general classification of infrared detectors is also presented, as well as the figures of merit used to evaluate their performance. We will then focus on the type of detector studied in this thesis, namely the bolometer. Its characteristics are described, thereby setting out the key requirements for a sensitive detector.

2.1. Fundamentals of radiometry

2.1.1. Radiance and irradiance of a light source

There are two ways of describing and measuring the propagation of electromagnetic waves radiated by light sources. Radiometry is based on the entire radiant power produced by the source, whereas photometry refers only to the light perceived by the human eye. These two systems carry their own sets of units that are analogous, but which should not be mixed up. The relationship between photometric and radiometric units is linked by the established value of spectral luminous efficacy for human vision: 683 lumens/watt. Radiometry uses units like radiant flux, irradiance or radiance. A brief description is given here.

Every light source is characterized by its radiant flux, also known as radiant power. It is expressed as the energy Q in Joules radiated by a source per unit of time:

$$\Phi = \frac{dQ}{dt} \tag{2.1}$$

The unit of the radiant flux is Watt. Radiant intensity is the radiant flux emitted

from a point source per unit solid angle in a given direction, expressed as:

$$I = \frac{d\Phi}{d\Omega} \tag{2.2}$$

where $d\Phi$ is the radiant flux leaving from the source, propagating in the element of solid angle $d\Omega$. The unit is Watt, but is often expressed in W/sr. The solid angle is itself expressed as:

$$d\Omega = \frac{dA}{r^2} \tag{2.3}$$

Finally, the irradiance is expressed in $\mathrm{W.m^{-2}}$ and indicates the density of incident flux received by the surface A of an object at a certain distance r from the radiant source, as illustrated by fig. 2.1. It is expressed as:

$$Irr = \frac{\partial\Phi}{\partial A} = \frac{\partial^2 Q}{\partial t \partial A} \tag{2.4}$$

with $\partial\Phi$ is the radiant flux incident on ∂A, an element of the object's surface. Combining eq. (2.2), eq. (2.3) and eq. (2.4) one can find the irradiance falling off by $1/r^2$:

$$Irr = \frac{\Phi}{A} = \frac{I}{r^2} \tag{2.5}$$

Figure 2.1 below illustrates the irradiance fall-off with the distance r from the source. Irradiance is a value used in infrared sensing to characterize IR sources. Combined with the area of the detector, it will give the power received by the sensor (see eq. (2.17)).

2.1.2. Blackbody radiation and spectra

All objects are composed of atoms that continually absorb radiation and vibrate. The more energy these atoms have, the more they vibrate; the vibration of all charged particles generates electromagnetic waves. The higher the temperature of the object is, the more its atoms vibrate, thus the higher radiant energy they generate. This means that every object continuously emits radiation at a rate with a wavelength distribution that depends on its temperature and spectral emissivity, $\epsilon(\lambda)$.

The concept of blackbody is very important in radiometry. A blackbody is defined as an ideal object that absorbs all incident radiation, and, according to Kirchhoff's law,

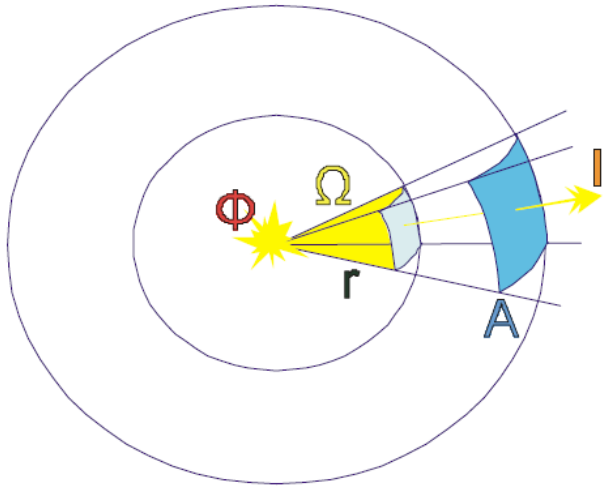

Figure 2.1: Irradiance from a point-like source, falling off as $1/r^2$.

is also a perfect radiator. Thus, the energy emitted by a blackbody is the maximum theoretically possible at a given temperature. Blackbody radiation is considered as incoherent and unpolarized, and its spectrum is described by Planck's law. The following equations describe the spectral radiant exitance of a blackbody as a function of its temperature and frequency or wavelength:

$$M_\lambda(T) = \frac{2\pi hc^2}{\lambda^5}\left[\exp\left(\frac{hc}{\lambda k_B T}\right) - 1\right]^{-1} \tag{2.6}$$

$$M_\nu(T) = \frac{2\pi h\nu^3}{c^2}\left[\exp\left(\frac{h\nu}{k_B T}\right) - 1\right]^{-1} \tag{2.7}$$

where λ is the wavelength, ν the frequency, T the temperature, h is Planck's constant, c is the velocity of light and k_B is the Boltzmann's constant.

Figure 2.2 depicts several emission spectra of blackbodies at different temperatures. As the temperature increases, the amount of energy emitted at each wavelength increases too. Also, the wavelength of the peak emission decreases. The peak emission wavelength corresponds to the solution of the derivative of the spectral radiant exitance function set to zero:

$$\frac{dM(\lambda, T)}{d\lambda} = 0 \tag{2.8}$$

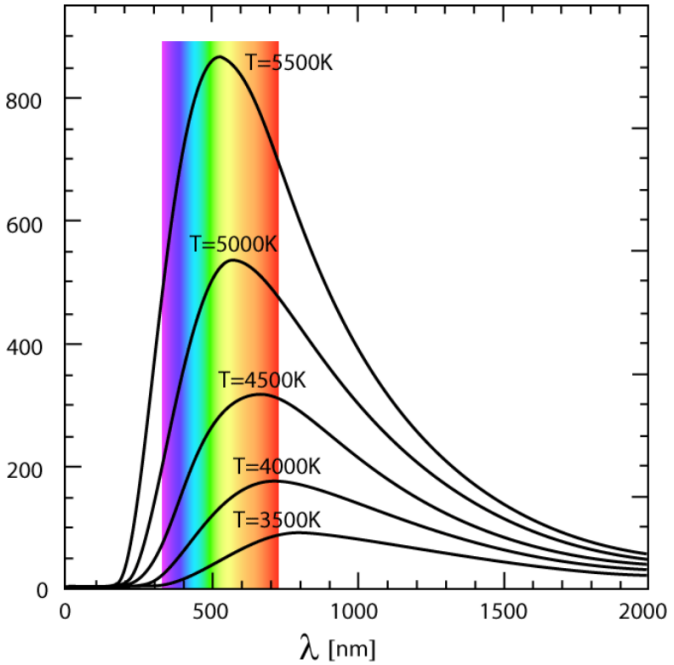

Figure 2.2: Spectral radiance (arbitrary units) of blackbodies at different temperatures, calculated from Planck's law (license GFDL).

The solution provides the relationship between the peak emission of a blackbody and its temperature, called Wien's displacement law.

$$\lambda_{max} T = 2898 \ \mu m K \tag{2.9}$$

Integrating the spectral exitance of a blackbody at temperature T over all wavelengths gives the total radiance exitance. It is called the Stefan-Boltzmann law and is expressed as below, per unit time:

$$M_\lambda(T) = \int_0^\infty M_\lambda(\lambda, T) d\lambda = \int_0^\infty \frac{2\pi h c^2}{\lambda^5 \left[\exp(\frac{hc}{\lambda k T} - 1)\right]} d\lambda = \sigma T^4 \tag{2.10}$$

where $\sigma = 2\pi^5 k^4 / 15 c^2 h^3$ is the Stefan-Boltzmann constant with an approximate value of $\sigma = 5.67 \times 10^{-12}$ W/cm^{2}K^4. Basically this equation can be viewed as the area under the spectral exitance curve as seen in fig. 2.2, for a given temperature. In radiometry, radiant emissions are often treated in terms of the idea of a blackbody. Most sources of

radiation emit energy in a way that can be described as a blackbody emitting through a filter. Thus this concept is of crucial use in radiometry.

2.1.3. Emissivity

The blackbody represents a perfect emitter and absorber, but most real sources are not perfect. Some of them are called graybodies, i.e. they emit radiation with the same spectral distribution as a blackbody, but the intensity of the radiation is reduced. In this sense, the blackbody radiation can be seen as a reference, and the emissivity of an object can be defined as:

$$\epsilon = \frac{M(\lambda, T)_{source}}{M(\lambda, T)_{blackbody}} \tag{2.11}$$

where ϵ is dimensionless and less than or equal to 1. Of course the emissivity of a perfect blackbody is $\epsilon = 1$. The emissivity of a graybody is independent of the wavelength, but dependant on temperature, and the emissivity of a selective source depends on both. Figure 2.3 below illustrates the three concepts of radiators.

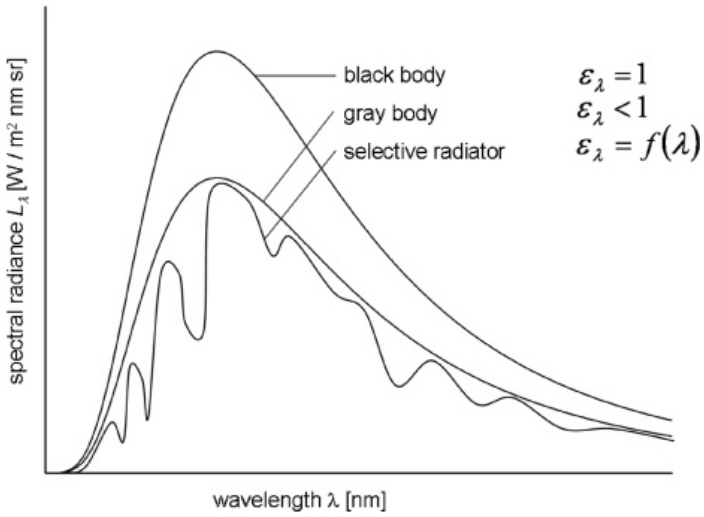

Figure 2.3: Spectral radiance L of blackbodies of three different types of emittors (from Schöpp et al. (2012)).

For a greybody, the Stefan-Boltzmann equation can be modified with eq. (2.11) and

thus be expressed as:

$$M^{gb}(T) = \epsilon\sigma T^4 \tag{2.12}$$

It is of common knowledge that when radiant energy is incident on a surface, a part of it α is absorbed, another part r is reflected, and the rest t is transmitted. This leads to the following energy conservation relationship:

$$\alpha + r + t = 1 \tag{2.13}$$

Kirchhoff observed that the ratio of the radiant exitance of a source to its absorption coefficient is equal to the radiant exitance of a blackbody, i.e.:

$$\frac{M(\lambda, T)_{source}}{\alpha} = M(\lambda, T)_{blackbody} \tag{2.14}$$

Thus it follows from eq. (2.11) that $\epsilon = \alpha$. This means that the emissivity of any materials at a given temperature is equal to its absorptance at this temperature. In the case of an opaque material that does not transmit any energy ($t = 0$), we have $\alpha + r = 1$ and:

$$\epsilon = 1 - r \tag{2.15}$$

In the literature it is possible to find tabulated emissivity values for different temperatures. Many materials have different emissivity depending on the wavelength of radiation. At certain wavelengths some have a low absorption hence a low emissivity, whereas they can be totally absorbent at others. For many substances, the emissivity decreases as wavelength increases. Generally, for metallic substances, emissivity is low at room temperature and increases linearly with temperature. As for non-metallic substances, they often have $\epsilon > 0.8$ at room temperature, and it decreases as wavelength increases (see table 2.1).

Table 2.1: Examples of emissivity values for metals and non-metals, from Omega Engineering (2002).

Metal	Temperature	Emissivity
Platinum (Pt)	260°C	0.05
	540°C	0.1
Chromium (Cr)	38°C	0.08
	540°C	0.26
Non-metal	Temperature	Emissivity
Paper	38-371°C	0.93
Glass, opaque	299°C	0.92
	838°C	0.68

2.2. Classification of infrared detectors

The infrared wavelength region spans from 0.78 μm to 1000 μm, and is divided into three ranges: near-infrared ([0.78 - 3] μm), mid-infrared ([3 - 50] μm) and far-infrared ([50 - 1000] μm). However in infrared detection, the area of interest is commonly between 1 μm and 40 μm. This leads to another classification of infrared regions, as there are two spectral windows of great importance in infrared detection. One is from 3 μm to 5 μm, called MWIR (middle wavelength IR) while the other spans from 8 μm to 14 μm, called LWIR (long-wavelength infrared). The MWIR range encompasses the thermal signature of jet-engines, but also the absorption peaks of some gases (e.g. CO_2 or CO, see Siebert & Müller (2005)). From eq. (2.9) one can see that this range of peak wavelengths is associated to the temperature span [500 - 1000] K. The LWIR range however includes lower-temperature emitting bodies such as humans, animals, but also some celestial objects; as its associated temperature range is [200 - 350] K. Recently, interest towards longer wavelength in detection has increased, motivated by potential space applications. Infrared detectors are usually divided in two categories, photon detectors and thermal detectors. The underlying principle of operation, as well as their advantages and drawbacks as detectors, are utterly different. Historically, the first detector was made by Langley in 1880 (Langley 1881), a platinum thin wire in which electrical resistance would change when being heated by incident radiation. In 1930, photon detectors were brought forward, and the infrared detection in general has been an active research area since the Second World War.

In photon detectors, the incoming radiation is absorbed by the material through the interaction with electrons bound either to lattice atoms or impurity atoms, or free electrons. This induces a change in the electronic distribution, which leads to a modified electrical output signal of the detector. They are mostly semiconductors, and the diverse optical excitation processes in such photon detectors is illustrated in fig. 2.4.

This involves a strong dependency of the sensitivity to the wavelength of the detected

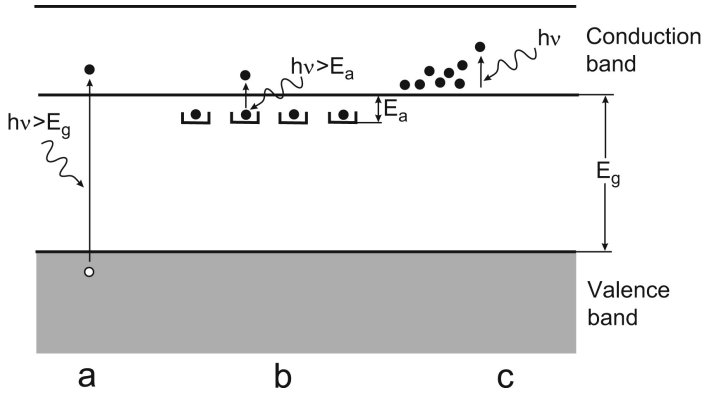

Figure 2.4: Fundamental electronic transitions in semiconductors : (a) intrinsic absorption (b) absorption by impurities or dopants (c) free carrier absorption (from Rogalski (2003)).

signal. However, photon detectors exhibit a good signal-to-noise ratio, leading to overall good sensitivity. They also have a very fast response (below milliseconds). Photon detectors for infrared radiation often require cryogenic cooling to prevent thermal generation of charge carriers. This class of detectors is further divided according to the nature of the interaction with the incoming light. Table 2.2 gives all the classification details, examples of detectors and a summary of the advantages and drawbacks of each type.

In thermal detectors, the incoming radiation is absorbed by the material, changing its temperature. This leads to a modification of its electronic properties that affects the output voltage of the device. Thermal detectors are subdivided according to which electronic property is modified by the temperature change, see table 2.3.

Because the principle of operation of thermal detectors lies in the change in temperature caused by the incoming radiation, they are generally wavelength independent in the infrared range. Thus the output signal depends on the radiant power rather than on its spectral content. Thermal detectors have then a broad spectral response; however they usually exhibit a lower sensitivity and a slower response than photon detectors. They do not need cryogenic cooling and are generally operated at room temperature, making them cheap and easy-to-use devices. Rogalski (2012) gives a detailed overview on the state-of-the-art of infrared sensors. Dillner et al. (2013) describes the figures of merit used for bolometers and thermopiles (see table 2.3), while Bhan et al. (2009) focuses on the state-of-the-art of bolometers with a special emphasis on Ti microbolometers arrays. Finally, Boreman (2012), Talghader et al. (2012) reviews the latest progress made on spectral detectivity in IR thermal detectors.

Table 2.2: Comparison of infrared detectors with their advantages and drawbacks, adapted from Rogalski (2011).

Detector type	Subtype	Advantages	Drawbacks
Thermal	*Bolometers, Thermopile, Pyroelectric*	Light, reliable, low cost, room temperature operation	Low detectivity at high frequency, slow response (ms)
Photon	*Intrinsic: IV-VI (e.g. PbS)*	Easy to prepare, stable materials	Large permittivity and high thermal expansion coefficient
	Intrinsic: II-VI (e.g. HgCdTe), III-V (e.g. InSb)	Easy bandgap tailoring and possible monolithic integration	High cost of processing, risk of large lattice mismatch
	Extrinsic: e.g. Si:Ga, Ge:Cu	Long wavelength operation, relatively simple technology	High thermal generation, extremely low temperature operation
	Free carriers: e.g. PtSi, IrSi	Low cost, high yields	Low temperature operation
	Quantum wells and quantum dots	Good uniformity over large area, easy wavelength control	Complicated design and growth

Table 2.3: Sub-division of thermal infrared detectors, adapted from Rogalski (2011).

Detector	Method of Operation
Bolometer	Change in electrical conductivity
Metal	
Semiconductor	
Superconductor	
Ferroelectric	
Hot electron	
Thermocouple / thermopile	Voltage generation caused by change in temperature of the junction of two dissimilar materials
Pyroelectric	Changes in spontaneous electrical characterization
Golay cell / gas microphone	Thermal expansion of gas
Absorption edge	Optical transmission of a semiconductor
Pyromagnetic	Changes in magnetic properties
Liquid crystal	Changes of optical properties

2.3. Figures of merit for infrared sensors

The essential way to characterize a sensor is to evaluate its sensitivity, i.e. the ratio between the output signal and the measured property. Ideally the output signal has an amplitude as large as possible, and the sensor stays insensitive to any other stimulation. In practice a sensor always presents a drift in the signal. This and several noise sources affect the quality of its performance. In infrared detection there are two main figures of merit that evaluate the performance of a sensor.

2.3.1. Responsivity

Responsivity, usually denoted $\Re$, relates to the amplitude of the output signal generated compared to the incoming detected radiation. This evaluates the sensitivity of the sensor. The output signal can be current or voltage, in which case responsivity is expressed respectively in A/W or V/W. In our case, where we detect an output voltage, it can be written as:

$$\Re = \frac{V_s}{P_{inc}} \tag{2.16}$$

with V_s the signal voltage due to P_{inc}, the incoming power received by the detector sensing area. The output signal voltage will be expressed differently depending on the class and type of the detector, as it relies on its physical mechanism. In the

case of thermal detectors, V_s is caused by the change in temperature ΔT caused by the incoming radiation. In photon detectors, it is the photon absorption in the semiconductor that will generate the output signal V_s.

In this work we studied bolometers, where the infrared radiation causes a change in temperature, leading to a measureable rise in electrical resistance. Thus we can express $V_s = \Delta R \times I_{bias}$ and the responsivity can be expressed as:

$$\Re = \frac{\Delta R \times I_{bias}}{\mathcal{A} \times \mathrm{Irr}} \tag{2.17}$$

with I_{bias} the current biasing the sensor, $\mathcal{A}$ the area of its sensing core, and Irr the irradiance of the infrared source (see section 2.1.1). It is clear that the responsivity is directly proportional to the bias current. The area of the sensing core will also play a role, influencing both ΔR and $\mathcal{A}$.

2.3.2. Detectivity

Specific detectivity D^* links the sensitivity, expressed by $\Re$, to the noise sources. It is expressed in $\mathrm{cmHz}^{1/2}/\mathrm{W}$, this unit also being recently called "Jones". It is expressed as (Chen et al. 2001):

$$D^* = \frac{\Re \times \sqrt{\mathcal{A}}}{V_n} \tag{2.18}$$

with V_n the root mean square (RMS) voltage fluctuation caused by noise sources. For a thermal detector operated at room temperature, its theoretical maximal specific detectivity has been calculated as $D^*_{max} = 1.98 \times 10^9$ $\mathrm{cmHz}^{1/2}/\mathrm{W}$ (Rogalski 2011). This fundamental limit is obtained when the sensitivity of the sensor is limited by temperature fluctuation noise (TCN).

2.3.3. Noise mechanisms

To be able to determine the detectivity D^*, it is necessary to evaluate the noise in the device. For any detector there are a number of noise sources that will impose limits on the detection sensitivity. One noise source for thermal detectors is the Johnson-

Nyquist noise, expressed as:

$$V_{JN}^2 = 4k_B RT\Delta f \tag{2.19}$$

where k_B is the Boltzmann constant and Δf is the frequency band. This noise has a white character (i.e. spectrally flat) and is due to thermal equilibrium resistance fluctuations. Johnson-Nyquist noise can be strong in metallic thin-film conductors where their electrical resistance is high compared to the bulk. Another source of noise is the thermal conductance noise. It arises from the statistical nature of thermal equilibrium. The temperature of a body is determined by a statistical exchange of energy between the body and its surroundings. This causes temperature variations in the detector around a mean value T. This noise depends strongly on the thermal conductance between the sensor and its surroundings, and is written as:

$$V_{TCN}^2 = \frac{4k_B T^2 \Delta V}{G_{th}\Delta T}\Delta f \tag{2.20}$$

with ΔV the output voltage caused by a change in temperature of ΔT, and G_{th} is the thermal conductance from the conductor to its surroundings, measured in W/K. To a good approximation, the electrical resistance in a bolometer changes proportionally with its temperature. This holds in our temperature range. According to (Smith et al. 1957), one can express it as:

$$R = R_0(1 + \alpha\Delta T) \tag{2.21}$$

with α known as the temperature coefficient of resistance (TCR), expressed in K^{-1} (see section 2.4.2), and R_0 is the resistance at the base temperature of the sensor. From eq. (2.21) and Ohm's law, the thermal conductance noise can be expressed as:

$$V_{TCN}^2 = \frac{4k_B T^2 I^2 R_0^2 \alpha^2}{G_{th}}\Delta f \tag{2.22}$$

In addition to the two fundamental noise sources described above, 1/f noise (also called flicker noise or pink noise) is a noise also present in thermal detectors. In metals, it stems from random hopping motion of scattering centers, i.e. impurities and defects (Kogan 1996). It is a low-frequency, non-equilibrium phenomenon related to DC current. Hooge's empirical law describes it as:

$$V_{1/f}^2 = \frac{V^2\beta}{Nf^\alpha} \tag{2.23}$$

where N is the numbers of carriers in the thermo-sensitive layer of the bolometers, α is a dimensionless constant and β is the Hooge constant for the given material. In the case of platinum films, the Hooge constant typically used is $\beta = 0.002$ (Fleetwood et al. 1983). The number of carriers N depends on the active layer volume, therefore it is defined as $N = N_0 \times V$, where N_0 is the free carrier density and V the volume. The free carrier density N_0 is a sensitive parameter to determine, and it is discussed in section 2.4.1 below.

There has been a thorough discussion on 1/f noise in platinum films over the past decades, especially with regards to whether this noise contribution is of an intrinsic or extrinsic nature. Numerous experiments and models have been designed and attempted, to no definite conclusion. Hooge and co-workers have defined the 1/f noise as an intrinsic noise of bulk origin, coming from lattice scattering (i.e. electron/phonon scattering). However, Fleetwood (Fleetwood et al. 1983) and Scofield (Scofield et al. 1985) claimed that it is a noise of extrinsic origin, caused by conduction electrons scattered by impurities or defects in the film, or even defect motion. Some experiments with antimony and indium films even suggested that the substrate or the nature of the surface layer between the film and the substrate could influence greatly the 1/f noise. Although both works agree on the extrinsic nature of the noise, a model that could fit all cases could not be defined. 1/f noise is therefore hard to predict and to understand. In nominally identical metallic samples, it has been found that it can vary as much as a factor of 10 (Fleetwood et al. 1983).

It is widely accepted that the 1/f noise in metal films at room temperature is in order-of-magnitude agreement with the Hooge formula. However, it has been questioned whether this law is the most appropriate model for metals. As an example, the Hooge constant for platinum thin-films has been found to be ranging from $\beta = 10^{-5}$ to $\beta = 10^{-3}$ (Scofield et al. 1985). It comes from the fact that in such films, as introduced before, most of the noise arises from elastic scattering as opposed to phonon scattering. Therefore it depends strongly on the quality of the film, leading to variations in the measured Hooge constant. Also, Pt films usually exhibit a lower 1/f noise than other metals due to their higher resistivity.

Several factors play a major role on the amplitude of the 1/f noise in metallic films. As it is influenced by the number of defects and impurities, the quality and method of deposition are of importance. A smooth and continuous film is likely to present a lower noise than a rougher one, due to less carrier scattering. Ideally, a metal film of sufficient quality should be dominated by lattice scattering; hence in this case the Hooge law shall be applicable.

Also, as it is evident from either eq. (2.23) or eq. (2.24), 1/f noise is greatly reduced when the device is operated with an AC bias. The name itself indicates that 1/f noise drops considerably as the frequency increases. This means that 1/f noise can be as dominant as the Johnson-Nyquist noise in small resistors biased by a DC current. Resistivity affects the Hooge constant, as it decreases for highly resistive films. In this

case, ultra-thin (3 nm-thick maximum) and thin-films are likely to have a lower Hooge constant than literature values.

It is therefore quite complex to find the best model for each specific experimental case. Fleetwood et al. (Fleetwood et al. 1983) assert that for a given metal, the minimum level of 1/f noise can be fairly well-defined. As this minimum level is exhibiting a dependence on resistivity, they proposed a revised Hooge law expressed as:

$$V^2_{1/f,revised} = \frac{\rho_0}{\rho}\frac{V^2}{Nf^\alpha} \tag{2.24}$$

where ρ_0 is a constant with a value of around 6×10^{-3} $\mu\Omega$cm. This formula omits the Hooge constant while incorporating the resistivity of the film. Which formula to use depends upon the experimental conditions and properties of the samples under study.

Usually the thermal detectors are Johnson-Nyquist-noise limited, with the thermal conductance noise being negligible. The 1/f noise depends on operating conditions such as the bias current: from eq. (2.23) one can see that $V^2_{1/f} \propto I^2_{bias}$. It can also be reduced with higher operating frequencies. Thus, 1/f noise can sometimes be the dominant noise source. Rahman et al. (1996) reports a niobium bolometer coupled with gold antennas where 1/f noise is dominant below 3 kHz. Above this frequency, the device is Johnson-Nyquist limited.

2.3.4. Thermal conductance and heat capacity

Thermal conductance G_{th} is a crucial factor, conveying the quality of thermal and electrical insulation of the sensing part from the substrate. Heat capacity C_{th} shows the amount of heat needed to change the temperature of an object by one degree, expressed in J/K. When an external radiation hits the detector, the rise in temperature can be found by solving the following heat balance equation:

$$C_{th}\frac{dT}{dt} + G_{th}(T - T_0) = W_h + \Delta W \tag{2.25}$$

with T the steady temperature of the bolometer, higher than T_0 the temperature of the surroundings. W_h is the heating due to DC biasing and ΔW the power absorbed from the external source of radiation. $G_{th}(T - T_0)$ is the rate of flow of heat from the element, by conduction and radiation. Conduction loss is dominant in our case, and

G_{th} can be expressed as (Smith et al. 1957):

$$G_{th} = \frac{W_h}{T - T_0} = \frac{RI^2}{T - T_0} \tag{2.26}$$

This equation was used for thermal conductance noise calculation (eq. (2.22)) and time response (eq. (2.28)). Concerning the heat capacity, it is evident that the amount of required heat will be proportional to the mass to be heated. Hence C_{th} is proportional to volume and can be expressed as:

$$C_{th} = C_p \rho V \tag{2.27}$$

where C_p is the specific heat, ρ the density and V the volume of the object of interest. For metals, the difference between C_p and C_v can be neglected. The specific heat capacity for most metals, gases or other materials is available in tables. To our knowledge, there is no data available for specific heat capacity of thin-films for platinum, therefore the bulk values were used. Commonly, C_p^{Pt} varies from 130 J.kg^{-1}K^{-1} to 150 J.kg^{-1}K^{-1} as temperature increases from 300 K to 900 K.

2.3.5. Time response

The time response of infrared detectors relates to the speed at which the sensor reacts to changes in the incoming infrared radiation. Typically photon detectors are faster than thermal detectors, the latter having a time response of some milliseconds (Rogalski 2003).

However, fast-response thermal devices have been fabricated and characterized. During the 70's, such fast thermal detectors were investigated; Block & Gaddy (1973) presents a 60-nm thick bismuth sensor with a time response on the order of tens of nanoseconds. The time response was found to increase with the film's thickness. Similarly, Contreras & Gaddy (1970), Day et al. (1968) introduce metallic thin-films operating at room temperature with time response down to 15 ns. In the 80's, Boragno et al. (1987) studied semiconductor bolometers made of P-doped silicon with response times faster than 60 ns, operating in liquid helium. Recently, Boreman et al. (González et al. 2004, 2000) proposed microbolometers achieving a time response of around 100 ns, but with reduced bolometric performances. Also, Galkina et al. (2007), Klokov et al. (2010) presented a bolometer made of diamond with a time response of 25 ns, although its responsivity is not known.

Time response is strongly linked to the ability of the thin-film to conduct the heat

generated by the incoming IR radiation to the heat sink. It can be written as:

$$\tau = \frac{C_{th}}{G_{th}} = C_{th} R_{th} \tag{2.28}$$

where C_{th} is the thermal capacity of the detectors and G_{th} is the thermal conductance to the surroundings. $R_{th} = 1/G_{th}$ is the thermal resistance, in $\mathrm{K.W^{-1}}$. From this equation, it is straightforward that the thermal conductance must be as high as possible to have a rapid time response. However, G_{th} influences both the responsivity and the thermal conduction noise (see eq. (2.22)). The more the sensing core of the detector is thermally insulated from its surroundings, the greater ΔT will be generated by the infrared. This means that the optimization of the responsivity calls for a small G_{th} value. There is thus a trade-off to be made between sensitivity of the detector and its time response. Also, the thermal capacity is directly proportional to the sensing core volume. Hence a small device will reduce the time constant, although a reduced active area induces a smaller responsivity.

2.4. Optimization of metal bolometers

Some common metals used for bolometers are nickel, bismuth, platinum, titanium or antimony. They have the advantage of a high resistance to corrosion and long-term stability, which is a valuable criterion for quality devices. Usually these types of bolometers are small, in order to limit the heat capacity and thus allow reasonable sensitivity. They typically come as thin-film strips, with a thickness of tens of nanometers. Such structures can be rather fragile, especially when suspended, though platinum can be shaped in fairly strong thin strips (Smith et al. 1957).

2.4.1. Electronic properties of platinum

Platinum is a noble metal, located in the d-block of the periodic table of Mendeleev, group 10, period 6. It is a dense, ductile transition metal with a face-centered cubic (fcc) crystalline structure. Its symbol is Pt and its atomic number is 78. Platinum is the least reactive metal, has an excellent resistance to corrosion and oxidation and has stable electronic properties. This makes platinum a very good choice for open-air engineered devices, compared to other metals that will be quicker to oxidize. The electron configuration of platinum is [Xe] $6s^1 4f^{14} 5d^9$, hence each atom has two incomplete orbitals resulting in 10 valence electrons. Figure 2.5 illustrates the electronic configuration of platinum, with the distribution of electrons on each energy level.

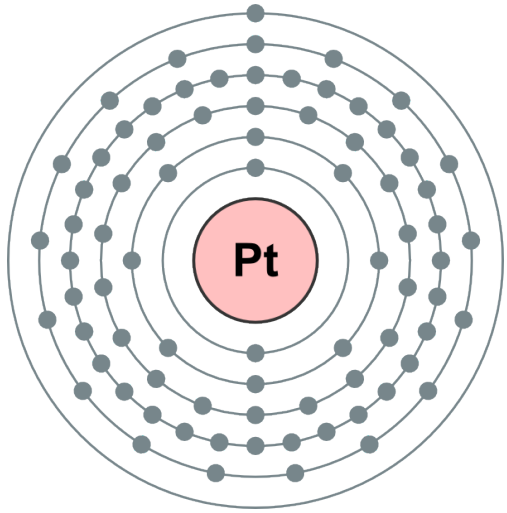

Figure 2.5: Electronic configuration of an atom of platinum (license GFDL). Each circle represents an energy level, from 1 to 6 starting from the circle closer to the nucleus. Each circle bears the total number of electrons in each energy state, e.g. the 4^{th} circle from the nucleus represents the 4^{th} energy level filled with 32 electrons in total ($4s^2 4p^6 4d^{10}$).

In the 1970's and 1980's, a lot of studies were published about mapping and describing the electronic configuration of transition metals, including platinum. Both theoretical methods, such as Andersen (1970) with the RAPW (relativistic-augmented-plane-wave) model, or experimental (de Haas-van Alphen effect, cyclotron resonance, ESCA (electron spectroscopy for chemical analysis), etc.) were used to determine such parameters as for example the density of states or the band diagram. The Fermi energy of platinum has been determined at 8.9 eV. Transition metals have peculiar conduction bands, and platinum is a two-band conductor according to Windmiller et al. (1969). When aggregating to form a bulk, orbitals of platinum atoms split into molecular orbitals and form two conduction bands: one an s-like band and the other an s-d hybridized band. D-carriers are more strongly linked to the core than s-carriers, and the d-band is lower in energy range than the s-band. This will lead to an almost full d-band while the s-band is only partially filled. Dosdale & Livesey (1974) confirm that d-carriers in platinum films have a low velocity and a high contribution to the electrical conductivity, while Sekiyama et al. (2010) has similar results for Au.

One of the parameters that are important for our study is the free electron density of platinum. As presented in eq. (2.23), it is necessary to know as precisely as possible the fraction of carriers that participate in the electrical conduction in platinum films. In one of his paper, Andersen (Andersen 1970) states that there are 0.405 free electrons per atom in bulk platinum. This is confirmed by Ketterson & Windmiller (1970) who experimentally find a value of 0.426. However, experiments by Fischer et al.

(1980) indicate that for ultra thin films (3 nm-thick maximum) this ratio falls to 0.24 free electrons per platinum atom. In ultra thin films, one of the two bands gets either filled up or emptied, leading to a one-band conduction mechanism. In other words, the effective free electron density is affected by the thickness of the film below a certain thickness value (Vancea et al. 1984). Below this value, the free electron density decreases with the thickness. This comes from the fact that as the grain size reduces, more electrons are elastically reflected from the grain boundaries. Thus, the number of charge carriers that pass over all the boundaries and then contribute to the electrical conduction reduces. As the grain size generally reduces with the thickness of a metallic film (Xin et al. 2010), so does the free electron density.

During this Ph.D. project, we have been fabricating bolometers made of metallic films of different thicknesses. While usual samples have a thickness of 50 nm of platinum plus 5 nm of adhesion layer (chromium or titanium), samples as thin as 3 nm have been fabricated and measured. The question then arises as to how to determine the free electron density in our samples? Are the thinnest samples one-band conductors? One way to look at it is to check the evolution of the electrical resistivity as a function of the film thickness. Figure 2.6 displays the resistivity of samples as a function of the inverse of their thickness. Data is from **Paper 4**.

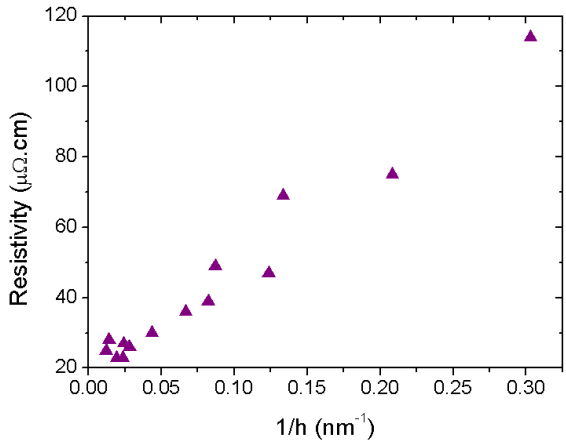

Figure 2.6: Electronic resistivity of bolometers as a function of the inverse of the film thickness. Thickness ranges from 82 nm to 3 nm.

From eq. (2.30), one can see that the resistance of samples with the same lateral dimensions is expected to be proportional to the inverse of film thickness h. Figure 2.6 shows that for the range of film thickness studied in this work, this is the case. We believe that as there is no disruption in the resistivity, we can assume that there is no severe change in the conduction properties of the platinum films from 82 nm to 3 nm thickness. Hence it is realistic to use the value of 0.405 electron per atom of

platinum participating in the electrical conduction. The atomic density of platinum is $n = 6.62 \times 10^{22}$ /cm^3. Therefore, its free electron density, or in other words the density of carriers in the film $N_0 = 0.405 \times n$, thus $N_0 = 2.68 \times 10^{22}$ /cm^3. This value is used in our calculations for 1/f noise.

2.4.2. Temperature coefficient of resistance

The change in electrical resistance upon heating depends on the quantity α, as discussed above. It is measured in K^{-1} and defined by:

$$\alpha = \frac{1}{R}\frac{dR}{dT} \tag{2.29}$$

where R is the resistance of the element at a temperature T. Typical TCR for metals used as bolometric materials is around 0.003 K^{-1}, which is much smaller than other materials used for infrared detection (see section 3.2.5). For most thicknesses of platinum, the TCR value was measured as $\alpha = 0.002$ K^{-1}. Typically TCR values of thin-films are drastically smaller than bulk ones; as an example the TCR value of bulk platinum is 0.0039 K^{-1}, thus twice the thin-film value (Serway 1998). The TCR is a function of the resistivity and of the micro-structure of the film (e.g. grain size), therefore the deposition method will affect it. For our films, we measured a consistent drop in TCR when the thickness was below a threshold value of 40 nm. Thus, the thickness of the sensing layer can affect the TCR value of thin films, as developed in section 4.3.

2.4.3. Optimization of performance

The incoming radiant power produces heat within the bolometric material, which leads to a change in resistance. There is no direct photon-electron interaction, unlike in photon detectors. The general conceptualization of a thermal detector is as presented in fig. 2.7.

The incoming radiation is absorbed by the detector, causing a change in temperature ΔT. This temperature rise is dissipated from the metallic core to the heat sinks, coupled to the detector by G_{th}. By definition, heat sinks stay at a constant temperature T_s. Therefore, the time response can be defined as the time it takes for the metal core to come back to its initial temperature, i.e. time for ΔT to dissipated through the heat sinks.

There are two main factors to improve, in order to increase the performance of bolome-

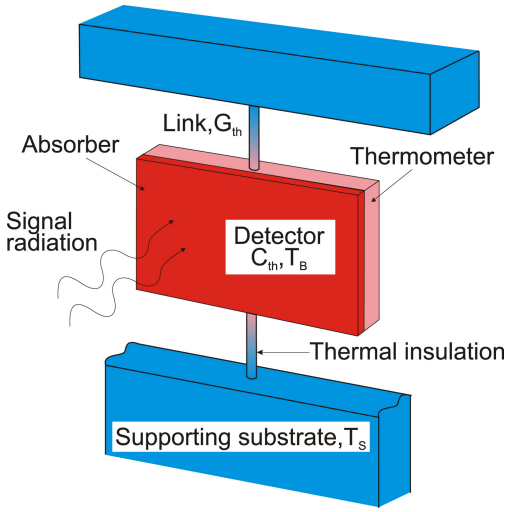

Figure 2.7: Schematic of thermal detectors, from Rogalski (2012).

ter. The key to high sensitivity is high temperature coefficient of resistance α and a low thermal conduction G_{th} insuring good thermal insulation. A low heat capacity C_{th} is also preferable.

These requirements often lead to complicated structures made of multiple layers, though with today's advances in micro/nano-fabrication, building such structures has become easier. A straightforward way to increase the thermal insulation is to suspend the detector. The bolometric material is then supported, e.g. by a suspended membrane over an etched substrate (Chen et al. 2007, Eriksson et al. 1997, Shie et al. 1996, Zhang et al. 2005). However, in the work presented here, the bolometric material is directly sputtered on top of a Si/SiO_2 substrate. We also looked for other means to improve the sensitivity. Chapter 4 summarizes the outcome of optimizing the performance of our bolometers.

2.4.4. Si/SiO_2 as substrate for bolometers

Silicon wafers topped with native oxide SiO_2 are the most common device substrates in the semiconductor industry. Reasons for its extensive use are that silicon remains a semiconductor below 300°C, is relatively inexpensive, and silicon dioxide is easily grown in furnaces. Figure 2.8 presents the transmittance of silicon to infrared radiation.

Although silicon is transparent to infrared, there is a loss in transmittance due to reflection from two interfaces (air/SiO_2 and SiO_2/Si). This results in a transmittance of silicon is around 0.5 for wavelengths in the range of [1.5 - 6] μm. For longer

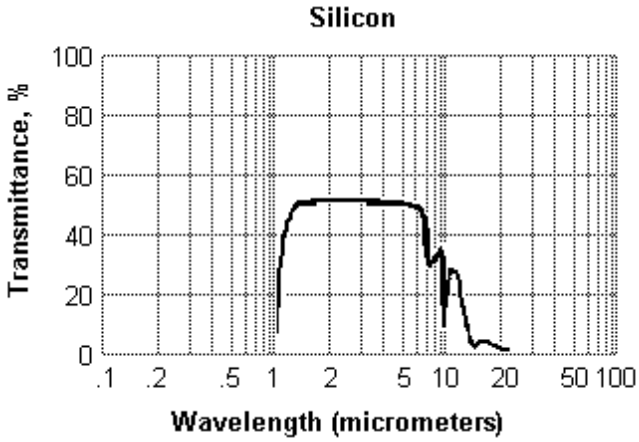

Figure 2.8: Transmittance through a slab of silicon in the infrared range, from Almaz Optics.

wavelengths, transmittance is lower than 0.5, which leads to a high interaction of the substrate with the incoming radiation. Ideally the substrate would have a transmittance close to 1, i.e. without any interface reflections. Silicon can be made conductive or resistive through doping; but in general, silicon is a good thermal conductor. However, the bolometric material is rarely in direct contact with the silicon. It is the layer of silicon dioxide SiO_2 that plays the role of electrical and thermal insulation layer.

Silicon has a native oxide thickness of around 10 Å, which can be increased by different oxidation techniques (see section 3.2.3 for our method). It is an essential layer in our detector as it provides both electrical and thermal insulation from the silicon substrate. The electrical resistivity of SiO_2 can vary depending on the growth methods. Its electrical resistivity is many orders of magnitude larger than that of the silicon. Hence it provides a very good electrical and thermal insulation. Figure 2.9 and fig. 2.10 display the transmittance of two types of SiO_2 to infrared radiation.

Figure 2.9 presents the transmittance of a slab of SiO_2 tailored for maximum transmittance to optical wavelengths, while fig. 2.10 is for silica optimized for infrared wavelengths. In both cases SiO_2 is mostly transparent for wavelengths smaller than 2.5 μm, while for wavelengths longer than $3 - 3.5$ μm transmission drops. The silicon dioxide will absorb and emit infrared in this range, even for the infrared-tailored silica. The quality of the thermal insulation is then lowered. This is not desirable, as ideally all the heat produced by the incoming radiation should be confined in the bolometric material.

One could think that Si/SiO_2 wafers may not be the best suited as substrate for bolometers as it interacts with infrared radiation with wavelengths above 4 μm. A

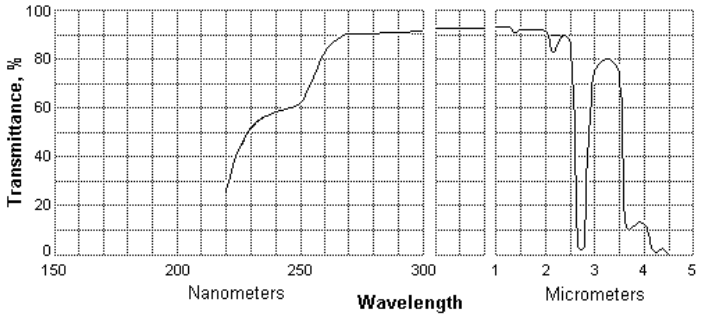

Figure 2.9: Transmittance through a slab of optical grade fused SiO_2 in the infrared range, from Almaz Optics.

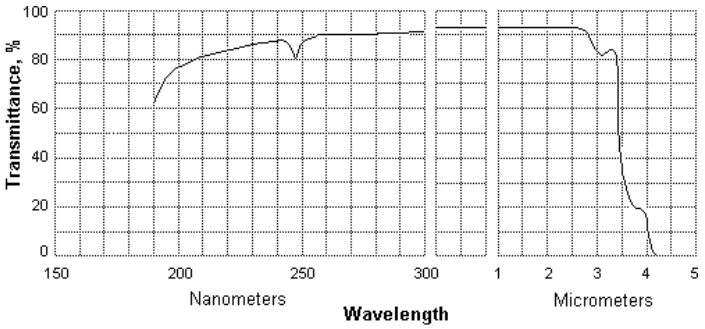

Figure 2.10: Transmittance through a slab of infrared grade fused SiO_2 in the infrared range, from Almaz Optics.

lot of different types of substrates have been used for bolometric applications, such as silica aerogel. The thermal conductance of aerogel can be tailored by varying its porosity, and can even be lower than the thermal conductance of air (Fricke & Tillotson 1997). Such material has been used as a very insulating thermal substrate, leading to improved bolometric performances (González et al. 2004, Ruffner et al. 1998). However, aerogel generated more noise in the sample, due to surface roughness and its low thermal conductance. Since 2005 the interest in using aerogel as a substrate for infrared sensors seems to have waned. Silicon nitride (SiN) can be used to improve the TCR of metallic films (Tsutsumi et al. 2002), or mechanical stability (Eriksson et al. 1997, González 2006*b*) when fabricating suspended structures. Quartz provides high thermal insulation and can be used as a substrate (Bumble & LeDuc 1997). Sapphire is often used for super-conducting THz bolometers for its high Debye temperature and mechanical strength (Karasik & Cantor 2011, Verghese et al. 1991). Some other works include BeO substrates (Contreras & Gaddy 1970), NaCl (Gehrer & Hayek 1984), or even KCl, ZnSe or CdTe (Jónsson 2009).

2.4.5. Evolution of performance with dimension

In this work, we present a study of the performance of metallic bolometers, depending on several characteristics. Among those, the dimensions of the sensing core (the "wire") were modified. It was shown that α is independent of the wire size within our size range. However, it affects directly the two figures of merit characterizing the bolometric performance. First, the wire resistance can be written as:

$$R = \rho_0 \alpha \frac{L}{hW} \tag{2.30}$$

where ρ_0 is the resistivity, α the TCR and L, W and h respectively the length, width and thickness of the wire. Thus, combining eq. (2.21) and eq. (2.30) gives a change in resistance as:

$$\Delta R \propto \frac{\rho_0 \alpha L}{hW} \Delta T \tag{2.31}$$

We chose to include the film resistivity and the TCR in the model. However, ρ_0 and α are only expected to change with the film thickness. Even in our smallest samples, the wire width is at least two orders of magnitude larger than the electron mean free path. Thus we do not expect to see contribution from sidewall scattering in the resistance. We take into account that the irradiance is constant, that $\mathcal{A} = L \times W$ and $\Delta V = \Delta R \times I$, for a fixed bias current. Entering eq. (2.31) into eq. (2.17), one obtains:

$$\Re \propto \frac{\rho_0 \alpha I}{hW^2} \Delta T \tag{2.32}$$

for the responsivity. One can note that the energy absorbed from the incoming radiation is expected to be proportional to the sample area $L \times W$. Also, the thermal conduction to the surrounding scales in the same way, hence it is reasonable to assume ΔT is constant for samples of different area. The previous equation can be rewritten as:

$$\Re \propto \frac{\rho_0 \alpha I}{hW^2} \tag{2.33}$$

Metal film resistors like our bolometers are affected by several noise sources, as described in section 2.3.3. Depending on the dominant noise source in the sample, the detectivity may or may not be affected by its dimensions.

If the bolometers are Johnson-noise limited, by combining eq. (2.18) and eq. (2.19), the detectivity can be expressed as:

$$D^* \propto \Re \times \sqrt{LW} \times \sqrt{\frac{hW}{\rho_0 \alpha L}} \tag{2.34}$$

This leads to:

$$D^* \propto \frac{I\sqrt{\rho_0 \alpha}}{\sqrt{hW}} \tag{2.35}$$

However, if 1/f noise is the dominant source, by combining eq. (2.18) and eq. (2.23), the detectivity can be expressed as:

$$D^* \propto \Re \times \sqrt{LW} \times \frac{1}{I\rho_0 \alpha}\sqrt{\frac{W^3 h^3}{L}} \tag{2.36}$$

This leads to:

$$D^* \propto \sqrt{h} \tag{2.37}$$

Responsivity is directly proportional to the bias current and is affected by the thin-film thickness, the resistivity, the TCR and the width. Detectivity can be affected or not by such parameters depending on the nature of the dominant noise source. In case of Johnson-Nyquist dominant noise, D^* shares the same dependence to bias current, resistivity, TCR, width and thickness as $\Re$. However if 1/f noise is dominant, D^* is only affected by the film thickness. It is interesting to note that neither $\Re$ nor D^* is dependent on the length of the wire. The evolution in performance as a function of the samples' lateral dimensions has been characterized (see section 4.2). The influence of film thickness on resistivity and bolometric performance is presented in section 4.3. The evolution of performance with bias current is presented in section 4.5.

3. Fabrication and characterization

Our samples were fabricated in the class 100 cleanroom of the University of Iceland. We used standard fabrication techniques, such as e-beam lithography, DC magnetron sputtering and rapid thermal annealing. In this section we describe the process of fabrication, from design to metal deposition and lift-off. The electrical characteristics of the samples are also presented, as well as the setup used to measure them.

3.1. Sample design

There are several conditions that must be met in order to fabricate a high-sensitivity bolometer. First, it is important that the sensing film's resistance has the largest possible TCR value. The higher the TCR is, the bigger the output amplitude will be, leading to high responsivity and detectivity (see section 2.4.2). Another critical parameter is the quality of the thermal insulation of the sensing layer to the surroundings. The better the insulation is, the more heat will be confined in the sensing layer, hence increasing the output signal amplitude. However the quality of the thermal insulation also plays a direct role on the time response of the bolometers, see eq. (2.28). It is also important to think about fabrication costs and device size in order to later realize low-cost, high-quality devices. This is why the perfect bolometer would have a simple design, but also be small, sensitive and easy to use. We worked on our samples with these desiderata in mind.

In the literature, bolometers are based on different designs, often depending on the material used. Different shapes and structures can improve sensitivity or change absorption properties. It is common to suspend the absorbing film, in order to improve the thermal insulation to the substrate or the microcircuit underneath. This configuration is found in microbridge structures, where the detector is supported by side legs connecting it to the read-out circuit, and in pellicle-supported detectors, where the absorbing layer rests on a thin dielectric film coplanar to the substrate, but with an etched volume underneath (Saxena, Bhan, Jalwania, Rana & Lomash 2008, Shie et al. 1996). In Yoneoka et al. (2011)the platinum is deposited on an aluminum oxide membrane, whereas in Tanaka et al. (1996) the titanium membrane stands by itself and even supports a dielectric diaphragm. Other bolometers include a small sensing core coupled to antennas. In this case, the antennas help collect and transfer IR ra-

diation to the sensing core. They can also be tailored to make the detector selective in wavelength or polarization (González & Boreman 2005). We chose to work with a thin-film of platinum acting as a sensing layer, on top of SiO_2 to ensure thermal and electrical insulation from the substrate.

As noted previously, the idea behind this doctoral project stemmed from previous experiments on thermal emitters. Hence we kept the same design as a basis for our experiments, later improving it to increase its sensitivity to infrared light. We used the software ELPHY Plus developed by RAITH to design the samples. Each structure is defined within a square of 1 mm^2, and is composed of a rectangular core part, usually called the wire. This rectangular core of various dimensions is attached to four connecting lines that broaden to contact pads, as shown in fig. 3.1.

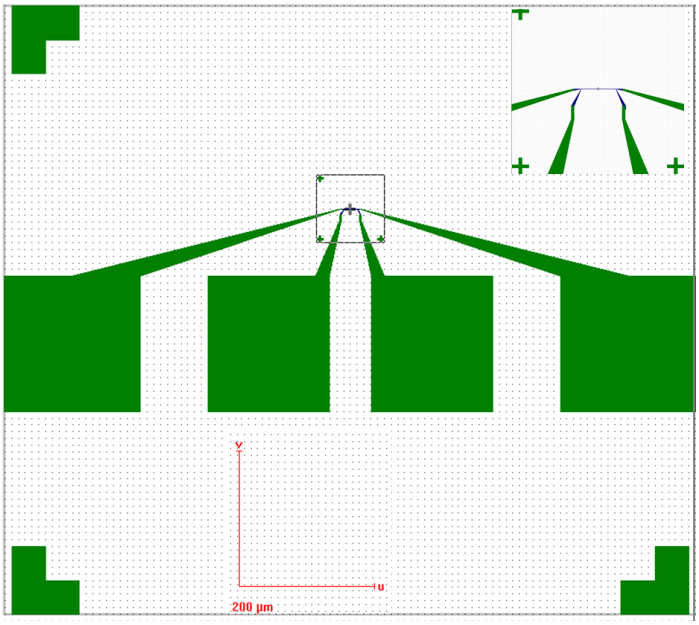

Figure 3.1: General structure of the bolometers and zoom on a 20 μm-long wire. The core part (blue) is a rectangle of variable dimensions attached to four lines broadening to contact pads (green) for 4-point measurements.

The idea is to use the two external pads to bias the wire with a DC or AC current, while measuring the voltage drop across it through the two internal pads in a 4-point measurement technique. In this way the measurement of the wire resistance doesn't include the contact resistance of the points used to connect and bias the sample. Throughout the doctoral project, we used this design as a template for our samples. The pads have constant lateral dimensions of 180-200 μm.

As this design is kept simple, it does not require complicated fabrication processes

in the cleanroom. Typically one day and a half would be needed to make a chip of samples. This is one of the advantages of our approach. Figure 3.2 below describes the general fabrication process of our samples.

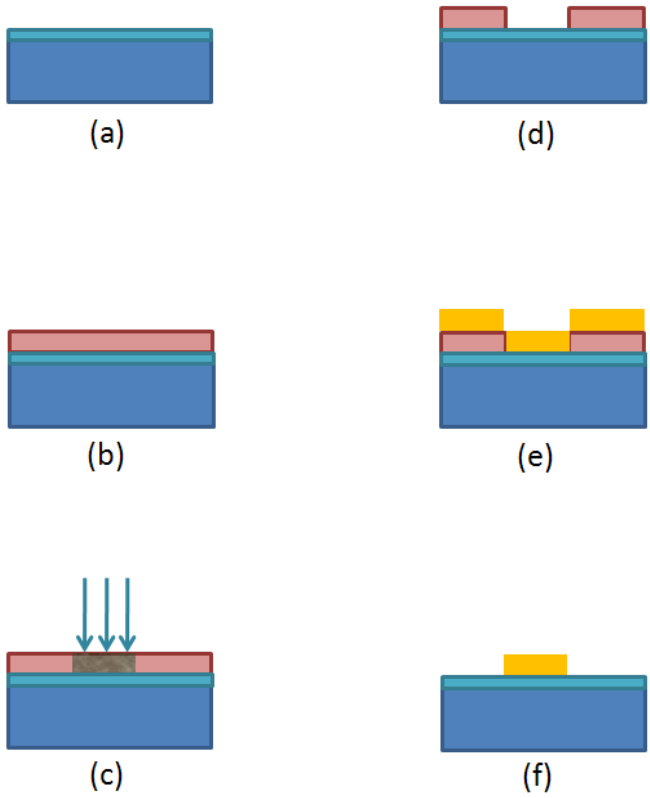

Figure 3.2: Step by step schematic of the lithography process: (a) clean Si/SiO_2 substrate, (b) spin-coat with PMMA resist, (c) e-beam lithography patterning of the sample, (d) development of the resist, (e) DC sputtering of adhesion layer and platinum, (f) lift-off with acetone.

3.2. Fabrication process

3.2.1. E-beam lithography

Given that our structures contain features smaller than a micron, patterning by 365-nm photolithography was ruled out. We used state-of-the-art e-beam lithography

techniques during our fabrication process.

Standard polished Si(100) commercial wafers with a typical thickness of 0.5 mm were used as substrates. We mostly used thermally oxidized wafers with a thickness of SiO_2 of 100 nm, but for some specific experiments we used SiO_2 of 1 μm or SiO_2 of 10 Å i.e. just native oxide. Several other SiO_2 thicknesses were grown by RTA. Since silicon wafers are used extensively in optical and semi-conductor research and industry; they have been well characterized and are both relatively inexpensive and easy to manipulate during the different cleanroom processes.

The first step is to get the wafer surface as clean as possible. In most cases we used fresh wafers from the box; in this case a pre-bake for 5 minutes on a 170°C hotplate is enough to eliminate any water or other loosely bound contaminants. If the wafer had been used before, we usually left it in acetone for 2 to 3 minutes in an ultra-sonic bath. It is then followed by a rinse in methanol and isopropanol and blow drying with N_2. As a resist for e-beam lithography, we commonly used a 4% solution of 496K poly-methyl-methacrylate (PMMA) spun on the wafer at a maximum speed of 4000 rounds per minutes for 40 seconds. Following this, the wafer is post-baked at 170°C for 5 minutes and ready for e-beam lithography.

Electron beam lithography opens up a new range of possibilities in lithography by overcoming the Rayleigh criterion that limits the traditional photolithography, and most importantly as the wavelength of electrons (in the pm range) is much smaller than the wavelength of UV photons (around 400 nm). The use of a focused beam of electrons reduces the writing limit to 10 nm or smaller compared to around 1μm with photolithography available in our cleanroom (the current industrial state-of-the-art is down to 32 nm). However, this is a serial/raster way of patterning, while photolithography is parallel. Using this machine also calls for a sometimes painstaking optimization of exposure parameters. As a consequence, it takes much longer time to write patterns and hence is quite a costly tool. It is not suited for large-scale production and its use is currently limited to research and development labs, as well as specific uses like photomask-making for photolithography.

The University of Iceland co-owns a SEM machine equipped with an e-beam lithography module, located at Nýsköpunarmiðstöð Íslands. It is a Supra 25 SEM from Carl Zeiss AG, with a Schottky emitter made of tungsten tip coated by zirconium. The system is equipped with an ELPHY Plus e-beam writing module from RAITH. Thanks to this module, the beam motion can be controlled to scan the surface of the wafer in desired patterns. There, at the surface of the resist-coated wafer, the high-energy electrons will break the PMMA polymer chains, making them more soluble.

As mentioned above, the minimum dimension of our structures is down to 300 nm. This calls for a careful focusing of the beam, achieved by adjusting the alignment aperture, stigmation and focus wobble to correct the aberrations caused by the different electronic lenses inside the SEM. This focus optimization is done on a dummy sample

covered by gold nanoparticles with a diameter of 50 nm. . This correction step is done for each beam aperture used during writing. Figure 3.1 presents the general design of our samples. The contact pads and connecting lines (in green) have dimensions almost a factor of 100 larger than those of the sensing core (in blue). It was then necessary to use different apertures for the writing. Using a smaller aperture improves the pattern resolution, but increases the writing time. It is therefore used for writing small structures with high precision, like the sensing part of our bolometers. For this we used a 30 μm beam aperture. For the pads and connecting lines, we made a compromise between writing time and resolution using a bigger aperture of 120 μm. We usually wrote several series of samples on a single chip to save time. In this case, shifts are likely to occur when writing multiple samples, resulting in disconnected and useless structures. To avoid this, we designed the structures with an overlap between the connecting points between the blue and green parts. Also, we wrote the structures line by line, starting writing the wires from the left to the right with aperture 30 μm and then, from the right to the left writing the pads with aperture 120 μm. This method proved to be the most successful one to have a maximum writing yield.

After writing, exposed areas were removed as the sample was immersed in an organic solvent mixture of Methyl-Isobutyl-Ketone and isopropanol (MIBK:IPA – 1 : 3) for 45 seconds. The sample was rinsed in isopropanol for 30 seconds to stop the development and blow-dried with nitrogen. The quality of the written structures was then checked under optical microscope and SEM.

3.2.2. DC sputtering

Direct current (DC) sputtering is a material deposition process used to coat substrates with thin films of one or different materials of choice. This process is done by bombarding plasma ions on a target. Noble gases are used to form the plasma. Argon is often used as it has high sputter yields for most metals, is relatively inexpensive compared to krypton or xenon, and is chemically inert and non-toxic. To trigger the deposition process, a high DC voltage (from hundreds to thousands of volts) is applied to the target (cathode). This causes the ionization of the argon gas molecules, creating plasma between the target and the sample substrate. Ar^+ ions are accelerated towards the target and strike its surface, displacing the target atoms and creating secondary electrons. The freed target atoms move in every direction in the chamber, some striking the sample and forming a thin-film at its surface. Figure 3.3 displays the general physical process of DC sputtering.

The secondary electrons released around the target surface will sustain the plasma, ionizing argon atoms as they approach the target. This is possible only if their density is high enough. Magnets around the target help confine these electrons so that the stability of the plasma is increased as well as the process efficiency.

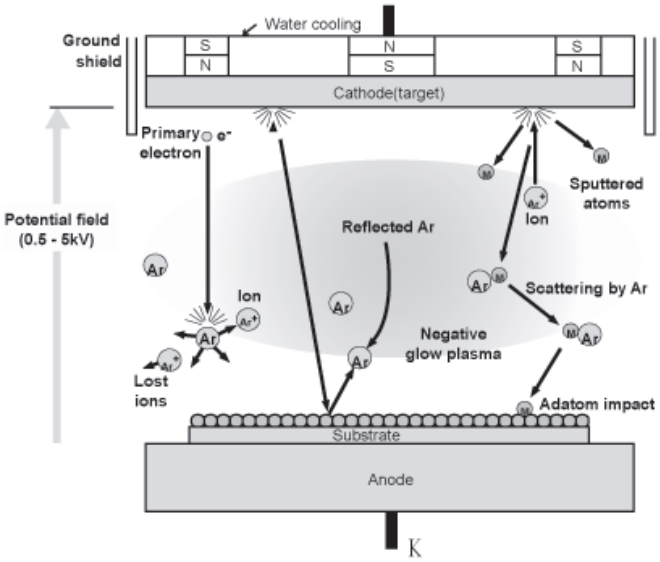

Figure 3.3: Diagram of DC sputtering process. The argon plasma hit the cathode, displacing atoms. Some of them will strike the sample and form an even thin-film on its surface (license GFDL).

Many parameters influence the deposition, such as the argon pressure, the voltage applied to the cathode, and the current passed through the plasma by the ions. In our case, we typically applied 50 W to the targets. Base pressure of the chamber was around 1.0×10^{-7} mbar, provided by a cryopump. Depositions were made with an argon pressure of 3.3×10^{-3} mbar.

Our bolometers are made of films of platinum (Pt), typically with a thickness between 10 nm and 100 nm. This range of thicknesses ranks our samples in the ultra-thin to thin-film categories. We chose platinum as bolometric material for several reasons. Firstly, it proved reasonably effective in terms of infrared thermal emission, as seen in previous works from our group (Au et al. 2008, Ingvarsson et al. 2007). By Kirchoff's principle, we expect platinum to also be effective as an infrared sensing material. Also, platinum has a high absorptivity compared to gold, silver or copper. It is resistive to corrosion and oxidation, making it reliable for long-term uses. Also, it has a lower 1/f noise than other bolometric materials (Yoneoka et al. 2011).

An adhesion layer needs to be deposited before the platinum to avoid any delamination during the lift off process and subsequent measurements. For this purpose we deposited 5 nm of chromium before platinum. After deposition, the chamber is vented to atmospheric pressure and the samples are immersed in acetone to do the lift-off.

After all sacrificial resist is removed, the sample is rinsed in isopropanol and deionized water, then checked under the optical microscope. The final structure is as displayed in fig. 3.4 and fig. 3.5.

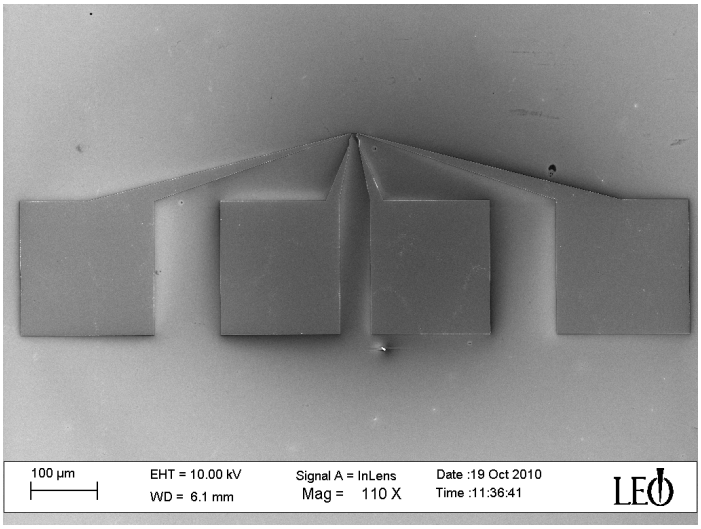

Figure 3.4: SEM picture of the whole structure after fabrication. The sensing part is attached to four lines broadening to contact pads for 4-points measurement.

3.2.3. RTA furnace

RTA machines (Rapid Thermal Annealing) are ovens with monitored gas flow, either to anneal samples or to grow oxides on top of them. The cleanroom at the University of Iceland is equipped with a RTA furnace (Jipelec Jet First 100C) which can reach a maximum temperature of 1200°C, using heating by halogen lamps. Among others, gas inputs are N_2 and O_2. We mainly used the furnace to grow silicon dioxide up to a desired thickness on top of native oxide wafers. During the dry-oxidation process, the thickness of SiO_2 is increasing logarithmically with time: at the beginning the growth is very fast (e.g. 2 minutes are needed to achieve 50 nm of oxide at 1100°C) and slows down with increasing thickness (e.g. 60 minutes for 220 nm). Special care had to be taken in the ramping of temperature to protect the halogen lamps from failure. After the process, the SiO_2 thickness was measured by ellipsometry.

This oxidation process usually creates a gradient of thickness on the substrate, as the temperature of the sample tends to be lower at the edges, where cooling is more efficient. In our case we oxidized small pieces of wafers. Experimentally, we measured a difference of thickness from edge to center of less than 10%. Therefore, the SiO_2 thickness variation underneath the samples is much less than 10%, as they are patterned

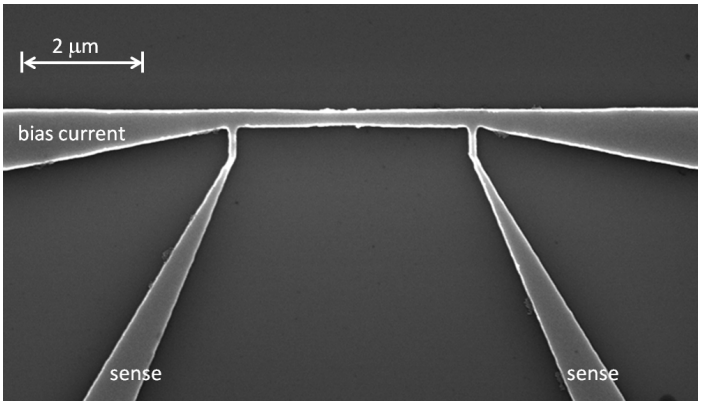

Figure 3.5: SEM image of the sensing core of our samples. Here the wire is 4 μm long and 300 nm wide, and attached to four connecting leads. During measurements, the outer lines are used for biasing the wire while the inner ones for sensing the voltage across it.

in a small area of the oxidized wafers.

3.2.4. Thickness and quality assessment

Knowing the microstructure of our samples precisely is of prime importance for our experiments. Several tools are available through the labs to characterize physical parameters such as thin-film thickness, lateral dimensions, etc.

The ellipsometer is a versatile tool widely used to find dielectric properties of thin films. It is also often used as a fast and easy way to measure SiO_2 thickness. Our ellipsometry system is composed of a monochromated light from a Xenon lamp that strikes the surface of the sample and a detector that senses the reflected beam. The reflected beam will have a polarization state different from the original one. Through the analysis of the polarization of the reflected light, it is possible to find the thickness of the studied layer. Our ellipsometer is reliable for measuring SiO_2 thicknesses down to a few nanometers, although it is preferable to double-check the result with X-ray measurements for thicknesses below 50 nm. X-ray characterization technique uses a similar physical phenomenon. In this case, the incoming beam is an electromagnetic radiation with wavelength on the order of Ångström. The beam is reflected from the air-metal and the metal-oxide interfaces, and the interference of the waves creates a pattern that contains information about the film structure. We used the PANalytical X'Pert Pro machine to measure the roughness and thickness of our Cr and Pt thin-films.

We also used scanning electron microscopy tools to check the structural properties of our samples. With the Supra 25 SEM we measured the final dimensions of our structures and checked their quality. We also measured the thickness of our metallic layers with a XEI AFM (Atomic Force Microscopy) from Park Systems. In this case we used optically patterned structures instead of e-beam-patterned ones. Through this method we have larger structures, making it easier to align the AFM head onto them, but also with edges sharp enough to ensure reliable results.

3.2.5. Physical properties of our samples

During this Ph.D., close to 50 chips were fabricated. They all have the same basic design presented in fig. 3.1, fabricated with Pt on top of Si/SiO_2. The adhesion layer between the oxide and the metal thin-film is either made of titanium or chromium, always having a thickness of several nanometers. We varied the size of the sensing part (the so-called "wire") and the thicknesses of some layers (results of these experiments are detailed in chapter 4). The resistance of our samples, that is to say of the sensing part, varies between several ohms to hundreds of ohms. This is quite modest compared to most of the bolometers that have a resistance in the kΩ range (e.g. Kosarev et al. (2008) or Mei et al. (2002).) Our bolometers had a measured TCR value of 0.002 K^{-1}. This value is within range of typical metallic thin-film TCR values (Mei et al. 2002). However oxides like VO_x or semiconductors have higher TCR values, usually around 0.03 K^{-1}.

In case of metal bolometers, ohmic loss is the predominant heat dissipation mechanism. During illumination, the heat caused by the infrared light will be concentrated in the wire, dissipating quickly out of the wire through the substrate but also with lines and pads acting as heat sinks. This is supported by numerical calculations as presented in Ingvarsson et al. (2007) and Jónsson (2009).

3.3. Characterization of bolometers

In this section we will provide a description of our measurement setup, as well as the choices we made concerning the techniques used. As platinum is extremely resistant to corrosion or oxidation, and our samples sensitive enough to infrared radiation at room temperature, it was not necessary to use any kind of cooling nor encapsulation.

Figure 3.6 below gives a schematic of our measurement bench. The chip of samples (1) is on a probe station (2) with four probes connected to a Keithley 2400 source-meter (3). This source-meter biases the sample with DC current through its outer probes, while monitoring its voltage across the wire through the inner pads. The Keithley

itself is connected through GPIB connection to a laptop (4) running a Labview program specially designed for our measurements. This program records the change in resistance in the sample's wire when illuminated by the ceramic heater (5) used as a blackbody source. From this experimental setup we are able to characterize the performance of our samples. Risks of damage due to static electricity or vibrations are minimized by installing the measurement bench on an air-cushioned optical table and carefully programming the instruments to avoid current peaks.

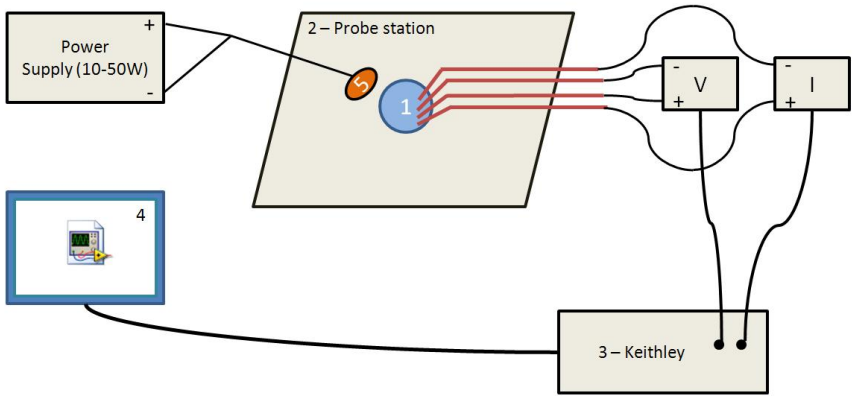

Figure 3.6: Schematic of the bolometer characterization setup. Detailed explanation is found in the text.

3.3.1. Probe station and source-meter

The sample is installed on a Signatone H100 probe station. It is equipped with a standard optical 10x microscope that allows us to precisely lower each of the four tungsten probes onto the sample's contact pads. We moved up and down the sample platform to connect or disconnect all the probes simultaneously, hence minimizing the risk of damage by static electricity, as compared to lowering the probes one by one. The probes are connected to a Keithley 2400 source-meter, in a 4-wire sensing setup. This allows us to electrically characterize the central part ("wire") of our samples without any contribution of the wiring and contact resistances. The sampling rate of the Keithley is 1 second. This will allow us to precisely measure the change in the bolometer's electronic properties under IR illumination.

3.3.2. Infrared source

We use a commercial radiator as an infrared source, as shown in fig. 3.7. The heating part is made of ceramic and coated black to increase its radiative power. This device can reach a temperature between 900°C and 90°C with the proper power supply. Thus the maximum wavelength of its infrared radiation can be tuned between 2 μm and 8 μm. It radiates a continuous infrared thermal spectrum, and is a good approximation to a blackbody source. Its irradiance was carefully characterized for different operating powers.

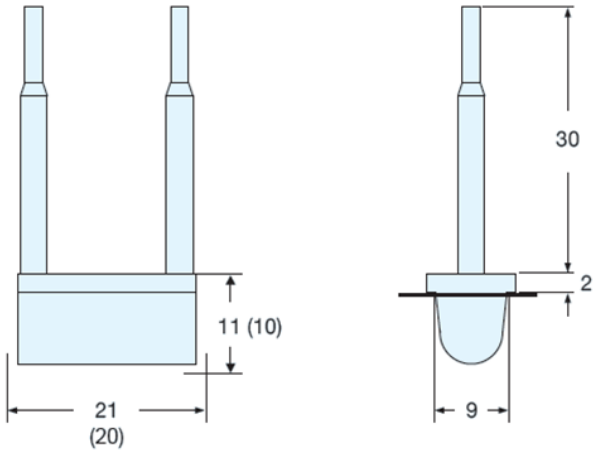

Figure 3.7: Schematic of the ceramic radiator used as an infrared source, with its dimensions (mm).

3.3.3. Labview program and data process

The Keithley multimeter is connected via GPIB to a laptop running Labview. We designed a special Labview program to control and automize our measurements. Before any infrared illumination, the IV characteristics of the sample are taken. This will give information on its integrity and base resistance. If the sample is sound and behaving properly, a DC current (from hundreds of μA to several A) is run through the sample. The live monitoring of the voltage allows us to record the change in voltage when the sample is exposed to the IR lamp. Later, the data is used to determine the responsivity and detectivity of our bolometers.

Thus, our measurement setup records the increase in resistance of the bolometers under infrared illumination, provided by a lamp with characterized irradiance. This will

allow us to calculate the related responsivity, as expressed by eq. (2.17). The area $\mathcal{A}$ is defined with the sensing wire's lateral dimensions. As stated before, the sensing wire is attached to DC leads and contact pads. These are heat sinks where heat dissipates quickly to the substrate due to their large dimension. Hence the temperature rise is strongly localized in the wire part of our samples. Moreover, when recording the rise in temperature due to IR illumination, the 4-point measurement setup allows us to record the rise in resistance in the wire part alone.

In order to further determine the detectivity of our wires, the noise sources in our samples need to be characterized. As introduced in section 2.3.3, there are three relevant noise sources: Johnson-Nyquist noise (eq. (2.19)), thermal conductance noise (eq. (2.22)) and 1/f noise (eq. (2.23)). We chose to numerically calculate the contribution from these noise sources as the resistance of our samples is low (maximum hundreds of Ohms and typically less than 50 Ω).

While it is technically possible to measure directly the noise contribution, it calls for specialized setup and careful measurements. As an example, commercial low-noise preamplifiers typically have noise floors in the vicinity of 4 nV.Hz$^{-1/2}$ (e.g. the Signal Recovery 5113), which is too high to measure Johnson noise of 300 Ω resistors directly. Yet we expect our Pt wire samples to be Johnson-Nyquist noise limited, except at very low frequency where 1/f noise becomes important. One is forced to employ more involved techniques, such as cross-correlation with two identical amplifiers or a bridge technique (Ingvarsson 2001, Scofield 1987). González (2006*a*) used a special circuit with an ultra-low-noise op-amp TL1028, useful down to resistance of about 200 Ω. However as the electrical resistance of our samples is typically under 50 Ω, this solution is not feasible. We believe it is fair to expect the wires to be Johnson noise limited over most of the spectrum of interest, and chose to base our arguments on calculation of the noise level rather than direct measurement.

3.3.4. Effects of the bias current on the film microscopic structure

Before starting any study of the bolometric performance of our samples, their electrical properties had to be characterized. As they are biased with a DC current, special attention was given to microscopic phenomena that occur inside the thin-films due to self-heating. Self-heating is inherent to any conductor submitted to an electric current, and is also known as Joule heating. This internal rise in temperature is due to the increase of collisions between charge carriers and atomic ions with bias current. This well-known phenomenon is harmless for our work if its intensity is kept under a certain threshold. If the self-heating becomes too high, it influences significantly the resistivity of the films and can even change their microscopic structure.

First, there is an annealing effect, due to the diffusion of atoms. The increased temperature caused by self-heating increases the rate of diffusion, augmenting the grain

size and thus lowering the resistance of the wire. Annealing is sometimes witnessed the first time we bias our samples. After a second bias, the resistance is lower but constant, and experiments can start. One could post-bake the samples to avoid this first current-induced annealing. In any case, it is important to avoid further annealing when the bias current is too high, as this leads to a permanent change in the resistivity of the film, which can disrupt our measurements.

The second effect occurring in the samples is electromigration. This is caused by the movements of ions when the sample is biased, resulting in displacement of material. Eventually, this leads to the physical destruction of the sample, as illustrated by fig. 3.8. Both of these phenomena lower the lifetime of the samples. They must be avoided by limiting the self-heating and choosing an adapted bias current value. Experiments (Elíasson & Ingvarsson , to be submitted) have shown that both phenomena are avoided if the current density in the wire is kept under 10^7 A.cm^{-2}. Saxena, Bhan, Jalwania & Khurana (2008) presents the effect of excessive bias current on titanium bolometers, and the conclusions are similar to what we have witnessed in our samples when the current density is high.

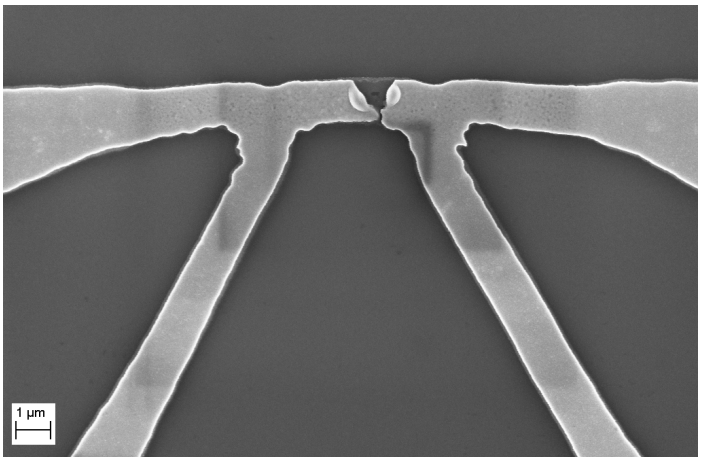

Figure 3.8: SEM picture of a metallic sample, destroyed after excessive bias current. The electromigration phenomena led to the transport of metal ions, eventually causing device failure.

It is possible to reduce the electromigration effect by biasing the sample with an AC square-wave current instead of DC. This idea was introduced in Jónsson (2009) and developed in Elíasson & Ingvarsson. Concerning our samples, extensive studies have shown that their thermal resistance remains constant, despite changes in electrical resistivity due to the aforementioned effects. This is also in agreement with numerical simulations that showed a weak dependence of the thermal resistance on the thermal conductance G_{th} of the wire. This is because the heat dissipation away from the wire is governed by the thermal properties of the surroundings and not by the properties

of the wire itself.

4. Optimization of performance for metallic thin-film bolometers

This chapter presents the experimental results on bolometer performance obtained during this doctoral work. Each section of this chapter presents an evaluation of the performance of our bolometers as we vary a specific parameter. We have focused on physical parameters, such as the dimensions of the sample, as well as on driving parameters, such as the bias current. For each experiment, we first present its aim and expectations, based on a scaling model from the theoretical equations of figures of merit. We then introduce experimental results and discussions, summarized from our published papers. The full papers (Renoux et al. 2012, 2013, Renoux & Ingvarsson 2013, Renoux et al. 2011) can be found at the end of this thesis.

In section 2.4 several factors influencing the performance of bolometers were discussed. In this chapter, we present the results of experiments pertaining to these arguments. Section 4.2 summarizes the results on changing the length and width of the bolometer's sensing area. Deviations from models derived from macroscopic formulas presented in section 2.4.5 are shown, hinting that at some dimensions the absorption is enhanced in our wavelength sensing range. The results in section 4.3 present the influence of the thickness of the metallic sensing layer on the bolometers' electronic properties and sensitivity. It reveals that there is a local peak of responsivity for a certain thickness, although more generally a trade-off has to be made between high responsivity and detectivity. As detectivity is affected by noise in the sample, we carry out a discussion on several noise sources. The influence of the SiO_2 layer on performance and time response is discussed in section 4.4. Section 4.5 presents the effect of the bias current. This parameter is of great importance, as it influences the responsivity, noise and detectivity of bolometers, but also potentially affects their microstructure. Finally, section 4.6 introduces the evaluation of the time response of our samples as a function of several parameters, and gives a general picture of what is expected from such samples in terms of detection speed.

4.1. Notes on the measurement protocol

We adopted a measurement protocol using DC current to bias our samples. As explained before in section 3.3.4, biasing the samples with current induces some amount of self-heating, due to the Joule effect. This resistive heating increases with the bias current value, and can lead to important modifications of the microscopic structure of the sample, and even to its total destruction. In order to avoid these phenomena, it is necessary to choose a bias level causing an acceptable power dissipation so as not to cause annealing or electromigration. With this in mind, we chose to operate with a constant Joule dissipation power P_J in all our samples. Referring to earlier studies (Jónsson (2009)), $P_J = 24\ \mu$W was chosen as a reference value, where it is certain to limit the self-heating to an acceptable value, usually less than several K.

With this in mind, we set the bias current for each sample to be:

$$I = \sqrt{\frac{P_J}{R_0}} \tag{4.1}$$

with P_J the Joule dissipation power and R_0 the base resistance of the sample, obtained after the initial IV characterization. This leads to different bias current values when the samples have different dimensions or thicknesses. By using this method we are sure to limit the effect of the resistive heating. However, a wide range of bias current values could bring some difficulty in comparing bolometric performances, as the responsivity is directly proportional to I_b. Hence there is a choice to be made between choosing a constant Joule dissipation power (thus controlling the amount of self-heating) and choosing a constant bias current value (easier for comparison but different degree of self-heating among the samples). In this last configuration, depending on the selected current value, the self-heating induced could go up to tens of kelvins for the smallest samples.

In our papers we have used both methods, and the reader should be aware of this fact. In this chapter where our work is summarized, we will sometimes replot the published data in order to facilitate the comparison between samples and the discussion of results.

4.2. Optimizing the performance by tailoring the sensing area

This section summarizes the work presented in **Paper 1** and **Paper 3**, on how the size of the sensing core of the bolometer could influence its performance. Also, it was interesting to see if there could be a relation between the sensed IR wavelengths

and the dimension of our bolometers' active area. Several samples with a central part of various dimensions were fabricated and studied. Since only the central metal constriction was modified, the overall size of our devices (including the contact pads) was not changed.

The central part of our devices is the active area, where the metal constriction undergoes a change in temperature upon IR illumination. This change in temperature triggers a jump in resistance that is proportional to the intensity of the incoming IR radiation. As described earlier in this thesis (section 3.2.5), the area heated up is limited to the central constriction. As the heat quickly dissipates from the leads to the heat sinks, the sensing core of our bolometers is truly defined by the central wire. It was therefore interesting to investigate how the geometry of the wires could affect the sensing performance.

4.2.1. Influence of bolometer length on sensing performance

For this study, samples with an active area of a fixed width but different lengths were made in two different laboratories, with a similar process. Both sets of samples were measured and their performance was compared to study the influence of the core dimensions on bolometric performance. Specifications of fabrication are summarized in table 4.1.

Table 4.1: Fabrication details of samples used for the study of the effect of samples' core dimension on bolometric properties.

	Set A	**Set B**
Place of fabrication	IBM Research Yorktown Heights	University of Iceland
Width	300 nm	300 nm
Length range	300 nm - 17μm	300 nm - 19μm
Pt thickness	50 nm	50 nm
Adh. material	Titanium (5 nm)	Chromium (5 nm)
Substrate	$Si/SiO_2(100)$	$Si/SiO_2(70)$
Presented in	Paper 1 and Paper 3	Paper 2 and Paper 3

At the University of Iceland, we measured the responsivity and detectivity of both sets of samples using the same setup. All the samples were biased with DC current in order to keep a constant Joule dissipation power ($P_J = 24\ \mu$W), as explained in section 4.1. Our results indicate an effect of the length on the bolometric performance, with an increase of the responsivity as the length of the active area is reduced. However, these results need to be put in perspective. A constant Joule dissipation power leads to increasing bias current values as the sample's length is reduced. As the bias current directly affects the responsivity, the results ought to be compared in order of *bias current*, instead of *bias power*. Figure 4.1 displays the responsivity of **Set A** samples

as a function of their active core's length.

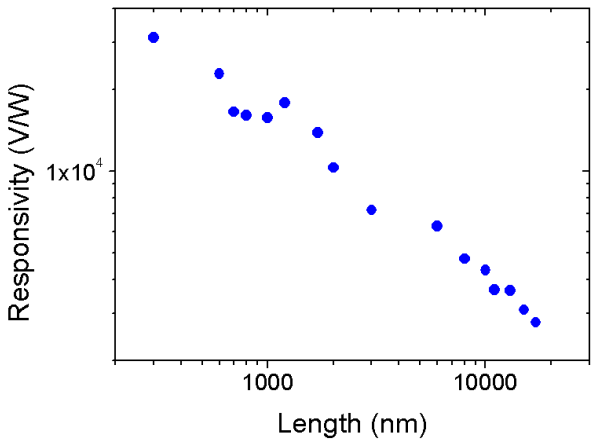

Figure 4.1: Responsivity of platinum bolometers as a function of their active parts' length. Samples are from **Set A**, with lengths ranging from 300 nm to 17μm. Joule dissipation power is constant at 24 μW and the SiO_2 thickness is 100 nm. Log-log scale is used for visualization purposes only.

As illustrated by this figure, shorter samples reach a better responsivity than longer ones. The sample with a dimension of 300 nm $\times$ 300 nm displays a responsivity of 3.1×10^4 V/W. The longer one has a responsivity of 2.8×10^3 V/W and has a collection area of 17 μm $\times$ 300 nm.

Keeping a constant Joule dissipation power of 24 μW in all samples limits the self-heating between 0.3K and 8.6K, depending on the electrical resistance of the sample (hence its length). As the IR source is providing a rise in temperature of around 1K, bolometers are actually detecting a change in temperature that is down to a tenth of their own self-heating temperature rise. However, by using a constant Joule dissipation power, the samples have been biased by different current values. As the current value to apply was calculated with eq. (4.1), and knowing the relation between electrical resistance and sample dimension eq. (2.30), the current follows:

$$I \propto \sqrt{\frac{1}{L}} \tag{4.2}$$

for samples with varied length (L), but same width and resistivity. Hence, larger current values were applied to shorter samples. Bias current value ranges from 1.9 mA to 0.3 mA. Therefore it is also interesting to plot the resistivity as a function of the bias current. From eq. (2.33), the responsivity is expected to increase linearly with

the bias current for samples which have the same width and thickness. In attempt to account for bias current affect, Figure 4.2 shows the responsivity of **Set A** this time as a function of the inverse of the sample length.

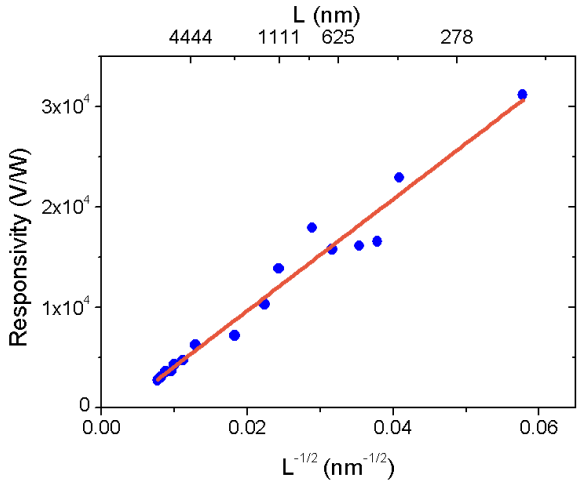

Figure 4.2: Responsivity of platinum bolometers as a function of the square root of the inverse of their length. The orange line is a linear fit representing the expected responsivity from the scaling model. Samples are from **Set A**, with lengths ranging from 300 nm to 17 μm. Joule dissipation power is constant at 24 μW and the SiO_2 thickness is 100 nm.

The responsivity is thus increasing with the square root of the inverse of the samples' length. Longer samples with a width between 17 μm and 8 μm have their responsivity increasing linearly with the applied current. Due to their macroscopic size, they are more likely to adhere to the simple scaling model introduced above. With these data points, we build the linear fit represented by the orange line, and extend it to find the responsivity expected for samples with smaller lengths. From fig. 4.2, it is clear that the measured responsivity of our samples agrees with the theoretical scaling. This means that the high responsivity displayed by shorter samples is mainly due to their higher bias current. However, one can see that the experimental results are not always fitting closely the scaling predictions. There are visible deviations of measured responsivity for samples whose length is between 800 nm and 2 μm. A local maximum responsivity is reached by the sample with a length of 1.2 μm, as seen also in fig. 4.1.

The same phenomenon was found in another set of samples made at the University of Iceland, **Set B**. The only differences between the two sets are a different material for adhesion layer and a slightly thinner silicon dioxide layer. Like **Set A**, the samples of **Set B** have been biased with different current values depending on their length. Figure 4.3 displays the responsivity of **Set A** samples as a function of the square root of the inverse of their length.

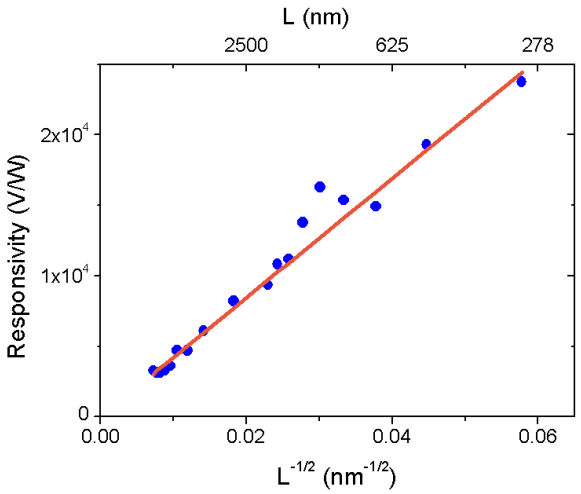

Figure 4.3: Responsivity of platinum bolometers as a function of the square root of the inverse of their length. The orange line is a linear fit representing the expected responsivity from the scaling model. Samples are from **Set B**, with lengths ranging from 300 nm to 19 μm. Joule dissipation power is constant at 24 μW and the SiO_2 thickness is 70 nm.

As in fig. 4.2, we build a scaling model from longest samples representing the expected responsivity from eq. (2.33). The same conclusions can be drawn from the evolution of responsivity with the device length for the two sets of samples, confirming the scaling arguments. There is also a deviation of experimental data from the linear fit for samples, with a local maximum in responsivity centered at 1.1 μm. This local maximum of responsivity for **Set A** and **Set B** represents an increase of 29% and 36% respectively, compared to the expected responsivity value given by the linear fit.

From the deviations displayed in fig. 4.2 and fig. 4.3, it can be deduced that the length of the active area has an impact on bolometers' responsivity, when this length is roughly between 600 nm and 2 μm. We believe these local enhancements to be related to an antenna resonance. The infrared lamp used in our setup is a blackbody with a $\lambda_{peak} = 2.74$ μm, meaning that we are at the threshold between optical and near-infrared frequencies. Following the classical antenna theory (Novotny & van Hulst 2011), the half-wavelength resonance would occur at $L = \lambda/2 = 1.37$ μm. However, our experimental resonant lengths, 1.1 μm and 1.2 μm, are respectively 20% and 12% shorter. Some recent experimental studies show that antenna resonances in metallic antennas occur at lengths 20% shorter than predicted by the classical antenna theory (Bryant et al. 2008, Codreanu & Boreman 2002, Mühlschlegel et al. 2005, Neubrech et al. 2006). Novotny (Novotny 2007) introduces a new model for a revised effective wavelength scaling that takes into account these latest experimental results. This revised scaling is for metallic rod antennas in the optical frequency regime, and our

experimental results seem to be in agreement with it. However, this model is defined for ended antennas, whereas our samples are "open-ended". This could result in a slightly longer effective "optical length" compared to the physical length we identify them by. Also, one has to take into account the optical properties of the surroundings, as it was demonstrated in both experimental and theoretical work (Au et al. 2008, Fumeaux et al. 2000). In our case, the metallic films are deposited on a thin SiO_2 layer (100 nm or less) which will affect the antenna resonance condition. The presented experimental results, backed up by a revised antenna resonance theory, suggest that the incoming IR radiation gives rise to plasma oscillations in our samples. This leads to an additional contribution to the absorption within a specific bandwidth. The detectivity of **Set A** was also calculated from the measured responsivity. Figure 4.4 displays the evolution of detectivity as a function of the sample's length.

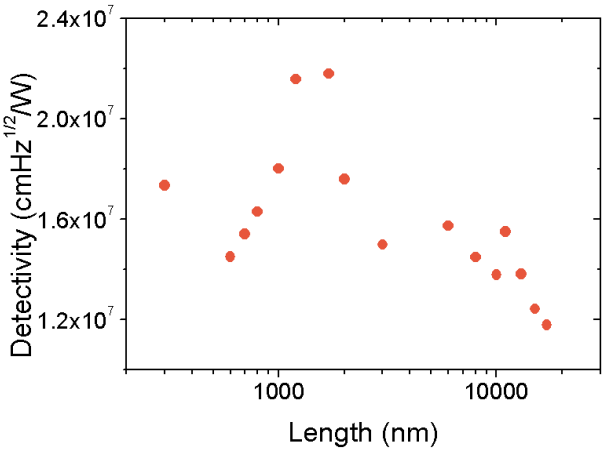

Figure 4.4: Detectivity of samples as a function of their active area's length. Samples are from **Set A**, with lengths ranging from 300 nm to 17 μm. Joule dissipation power is constant at 24 μW and the SiO_2 thickness is 100 nm.

Although theoretically, the detectivity should not be influenced by the sample length when the 1/f noise is dominant (see eq. (2.37)), there is some visible effect of the length on the detectivity of the samples displayed in fig. 4.4. One can see that shorter samples display a relatively higher detectivity than others. Samples with a length of 1.3 μm and 1.7 μm almost reach a detectivity of 2.2×10^7 cmHz$^{1/2}$/W, when longer ones see their detectivity dropping from 1.6×10^7 cmHz$^{1/2}$/W to 1.2×10^7 cmHz$^{1/2}$/W. Detectivity is the ratio between responsivity and the noise, and usually when the 1/f noise is dominant, it flattens out all the features displayed by the responsivity. In this case, the 1/f noise is certainly dominant, but it is constant for all sample lengths. This could be the reason why the detectivity displays here some influence by the sample length.

4.2.2. Influence of bolometer width on sensing performance

Secondly, we studied the possible influence of the bolometer's active part's width on its performance. Several samples with active parts of different widths and lengths were designed and fabricated at the University of Iceland. Lengths were ranging from 300 nm to 15 μm and widths from 300 nm to 4 μm. The samples are made of a thin-film of platinum with a thickness of 50 nm and 5 nm of chromium on top of commercial Si/SiO_2(100 nm) wafers. The length values were specifically chosen in order to avoid the resonant range, presented in the previous section section 4.2.1. Between fabrication and measurement steps, the physical dimensions of the samples were measured by SEM imaging. On average, there was a slight deviation of measured dimensions from nominal values, due to aberrations or other e-beam lithography error sources. In our calculations, we used the measured values. However in this summary, as well as in **Paper 3** where these results were reported, we refer to the samples by their nominal values.

Previously, the influence of the width of similar samples on their *thermal emission properties* was studied by our group, in particular by Dr. Yat-Yin Au. Several papers describing the impact of the active area dimensions on the thermal emission properties have been published (Au et al. 2008, Ingvarsson et al. 2007, Jónsson 2009, Klein et al. 2008). The samples studied are also made of platinum, usually 50 nm thick, with a chromium adhesion layer, and their design has the same concept as ours: a central metallic constriction that will emit infrared radiation as it is biased with DC current via contact pads. In Au et al. (2008), the infrared radiation spectra of such samples (usually referred to as "heaters") as a function of their active parts width was studied. Samples had a constant length of 8 μm and a width between 200 nm and 8 μm. Their infrared spectrum was detected and analyzed by FTIR for two polarizations: one oriented parallel to the active part's long axis and the other perpendicular to it. These polarizations are thus called respectively "parallel" and "perpendicular". Figure 4.5 displays the evolution of the emitted infrared spectra with the width of the samples. There is a spectra cutoff below 2000 cm^{-1} due to the spectral response of the InSb detector.

In fig. 4.5, the emitted spectra along the parallel polarization for each width have been normalized so they will have the same intensity. The normalization coefficients have then been applied to the corresponding perpendicularly polarized spectra. Several interesting conclusions can be drawn from this figure. Mainly, there is a visible effect of the width on the thermal emission of platinum heaters. Albeit the shapes of the spectra of the parallel-polarized emission seem unaffected as the width of the heater is reduced, the perpendicularly-polarized emission shows drastic changes both in frequency and relative intensity. With decreasing width, the peak wavelength of emission shifts towards shorter values. It is well-known that Stephan-Boltzmann law can hold only for macroscopic samples. Therefore, in the case of thermal emitters, 1 μm seems to be the threshold between macroscopic and sub-macroscopic regime.

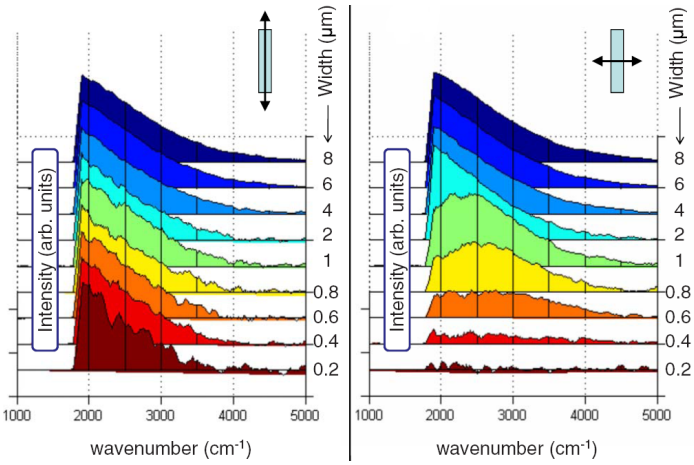

Figure 4.5: Evolution of emitted infrared spectra with active area's width of platinum samples, from Au et al. (2008). (a) For polarization parallel to heater long axis and (b) perpendicular to it. For each width, the intensity for both polarizations has been normalized with a same factor, in order for the parallel polarized peaks to have the same height. Reprinted figure with permission from Au, Y.-Y., Skulason, H. S., Ingvarsson, S., Klein, L. J. & Hamann, H. F., Physics Review B 78, 085402, 2008. Copyright 2013 by the American Physical Society.

Also, the general intensity decreases, finally fading away to below the detector limit. This suggests that samples with a width narrower than 600 nm emit mostly infrared light with a polarization parallel to their long axis. It would be very interesting to verify this by measuring the absorption of the samples for different IR polarizations. However, we do not possess such IR polarized source at the lab.

This study gave us an insight into what could be expected when reducing the width of bolometers' active areas. By Kirchoff's law of thermal radiation (Smith et al. 1957), a link can be made between emission and absorption properties. One can then expect to find an influence of the width on bolometric performance. We measured change in electrical resistance (ΔR) of each sample under IR illumination. This time, we chose to bias each of them with fixed DC currents, several times, from 0.5 mA to 4 mA with a step of 0.5 mA. The responsivity is then calculated. Figure 4.6 displays the evolution of the responsivity of samples with a fixed length of 9 μm and various widths, as a function of bias current. From eq. (2.33), we expect a linear increase in $\Re \times W^2$ with bias current, as the samples have the same thickness, and assuming the resistivity is constant. However, this model is not expected to hold below a certain width value, as for the thermal emitters exhibiting a shift in emitted spectra when their width is below 1 μm.

The responsivity displayed in fig. 4.6 seems to adhere to the scaling, with a linear

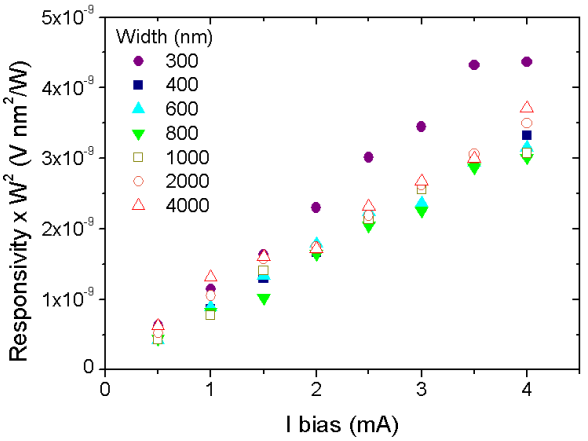

Figure 4.6: Responsivity $\times$ W^2 of 9 μm-long samples as a function of their width and bias current. The samples' width ranges between 300 nm and 4 μm.

dependence on bias current. There is an increase in responsivity with the bias current, and also with decreasing width. At 4 mA, samples with a width of 300 nm reach a responsivity of 4.9×10^4 V/W, while ones with a width of 4 μm have a responsivity of only 230 V/W. Thus there is a drop of more than two orders of magnitude for the responsivity when the bolometer's width varies from 300 nm to 4 μm. It is therefore clear that width plays a major role in the bolometers' performance. This could be expected, as responsivity is directly proportional to active area dimension, see eq. (2.17). But as fig. 4.6 shows, there is something more than this. Samples that have a width of 300 nm stand out compared to broader ones, that tend to have the same evolution of $\Re \times W^2$. This suggests that the higher responsivity displayed by these narrow samples is not only due to their reduced active area value when using eq. (2.17). From this figure, there are two important conclusions to be made: first, an overall higher responsivity of samples with a width of 300 nm, and second, a departure from the scaling theory in this width range. In other words, the area is not the only factor influencing the responsivity for such reduced dimensions.

The same measurements were carried out for all the samples, with various lengths and widths. The different lengths of our samples are out of the resonant range presented previously in section 4.2.1. From eq. (2.33) one can see that the responsivity is independent of the sample's length, for a fixed bias current. Also, from our experimental data we do not see any dependence. Therefore, for each specific width and bias current value, the experimental results of all lengths were averaged in order to reduce fluctuations. Figure 4.7 shows the product of averaged $\Re \times W^2$ as a function of bias current, therefore encompassing data for all samples.

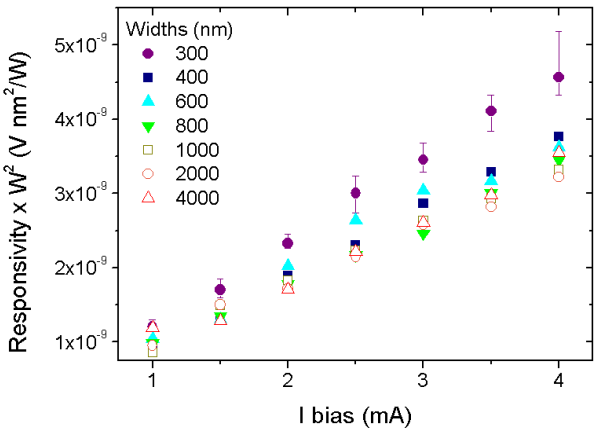

Figure 4.7: Responsivity $\times$ W^2 of samples with various lengths, as a function of their width and bias current. Length ranges between 900 nm and 15 μm, and width between 300 nm and 4 μm. Data from samples with various lengths but same width and bias current was averaged. Plot for the 300 nm width has error bars representing maximum and minimum values of the data averaged.

In fig. 4.7, one would expect to see the same linear increase for all samples and all widths. Albeit the product $\Re \times W^2$ of all widths tend to increase linearly with the bias current, some narrow width increase faster than the main trend. As in fig. 4.6, samples with a width of 300 nm are obviously apart from the main trend. Thus, the width effect seen previously with the samples with a length of 9 μm is confirmed in samples with different lengths. Also, samples with widths of 400 nm and 600 nm are slightly breaking away from the main cluster. Samples of width more than 800 nm or more, are intertwined together in a same trend. This suggests that samples of width superior or equal to 600 nm do not have the same behavior as narrower ones, the responsivity of which is enhanced beyond the scaling predictions.

If samples with a width of 600 nm or less are breaking away from the expected scaling model, one has to understand what makes their responsivity better. When looking at the data, we see that the change in electrical resistance (ΔR) triggered by the IR illumination is higher for 300 nm-wide samples than for broader samples. As responsivity is directly proportional to ΔR, it leads to a higher responsivity for such samples. There can be two main reasons for such a difference in ΔR: either from a difference in electrical resistance between narrow and wide samples, or a difference in absorption properties. According to eq. (2.30), electrical resistance of samples is proportional to ρ/W. Indeed, our samples have an electrical resistance spanning from hundreds of ohms for samples with a width of 300 nm to tens of ohms for those with a width of 4 μm. To better understand this difference in resistance, one must look at

the effective resistivity. The calculated resistivity of samples with a length of 9 μm and various width is displayed by fig. 4.8.

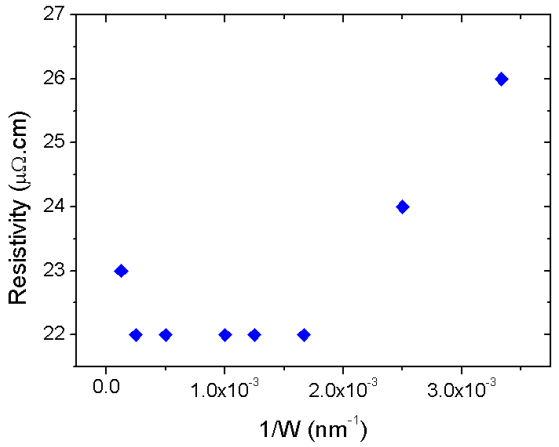

Figure 4.8: Effective electrical resistivity of 9 μm-long samples as a function of the inverse of their width.

The resistivity is constant for samples with a width higher than 600 nm, and then is increasing linearly for widths from 600 nm to 300 nm. The slightly higher resistivity value displayed by the wider sample (4 μm) can come from its low aspect ratio, creating non uniform current distribution in the device, hence a higher resistivity. From eq. (2.33) we know that responsivity depends on the resistivity. Therefore, samples with a width higher than 600 nm, which have a constant resistivity, will see their responsivity only influenced by width. From eq. (2.33) we can express this as:

$$\Re \times W^2 \propto I \tag{4.3}$$

However, samples with a width smaller than 600 nm have their effective resistivity vary linearly with 1/W. This extra dependence on W for samples with a width smaller than 600 nm explains why they stand out of the main trend in fig. 4.7. A higher value of ΔR can also come from better absorption from the sample. In this case, samples with a width smaller than 600 nm may absorb more infrared radiation than their wider counterparts. However, if both higher film resistivity and enhanced absorption contribute to a higher ΔR in narrow samples, the influence of each is not clearly defined yet.

As discussed above, a similar study has been carried on by our group about the effect of samples' width on the infrared emission. Figure 4.5 shows that the width

has an impact on the emission polarization. We saw that the width also has an impact on the responsivity of similar samples. Also, in terms of infrared emission, its total intensity should scale with the sample's surface area, according to the Stefan-Boltzmann law. The work done by Au et al. (2008) measured the intensity evolution of the emitted spectra for both polarizations, and reveals that the law does not apply for smallest samples. Actually, larger samples adhere to the Stefan-Boltzmann law as the emitted intensity for both polarizations decreases with the width, from 8 μm to 1 μm. But for narrow samples, the intensity along the perpendicular polarization drastically decreases, while the intensity along the parallel one stabilizes at a constant value. This is an indication that at this dimension scale, the sample's active area is not the only factor influencing the radiation intensity. A connection can be made between our two studies, as Dr. Au's work show that at subwavelength widths, the emission properties are modified, whereas here we demonstrate the same thing for the responsivity of similar samples. However, the threshold width below which samples depart from theory, is different in the two experiments. In our case, bolometers depart from the model when their width is smaller than 800 nm. For thermal emitters, the threshold width is 1 μm. This difference can come from the different temperature of the samples. Bolometers are picking up IR radiation from a blackbody-like source at 1064 K when the thermal emitters have a temperature of 750 K. Therefore, bolometers are picking up an IR radiation with a peak wavelength of 2.74 μm, while the thermal emitters spectra have a peak wavelength of 3.86 μm. This longer peak wavelength could explain why thermal emitters depart from theory when their width is smaller than 1 μm when bolometers do when width is smaller than 800 nm.

In this study the polarization of the incoming infrared light is not taken into account, but the earlier study by Dr. Au sheds a light on how the absorption properties of our samples are modified by their width. We believe that bolometers studied here get more and more selective in the polarization of infrared light they absorb as their width is reduced. For samples with a width equal or larger than 800 nm, the same amount of perpendicular- or parallel-polarized infrared light would be absorbed. However as the width is reduced, the amount of absorbed perpendicular-polarized light is expected to remain constant, despite the fact that the sensing area is getting smaller. For samples with a width of 300 nm, very little or no infrared radiation with a polarization parallel to the long axis of the bolometer would be absorbed. If this is verified, that makes the enhanced responsivity of 300 nm-wide samples quite remarkable as they absorb only part of the incoming radiation.

The detectivity of these bolometers was also studied. Figure 4.9 displays the detectivity of all samples, following the same method as for fig. 4.7. For each bias current value and width, detectivity for samples with various lengths was averaged.

The detectivity does not show any clear dependence on the bias current or on the width of the samples. The average detectivity is around 1.7×10^7 cmHz$^{1/2}$/W. Wider samples exhibit a somewhat higher detectivity for low bias current values; this comes from less data points to include in the averaging and their low aspect ratio. From the scaling

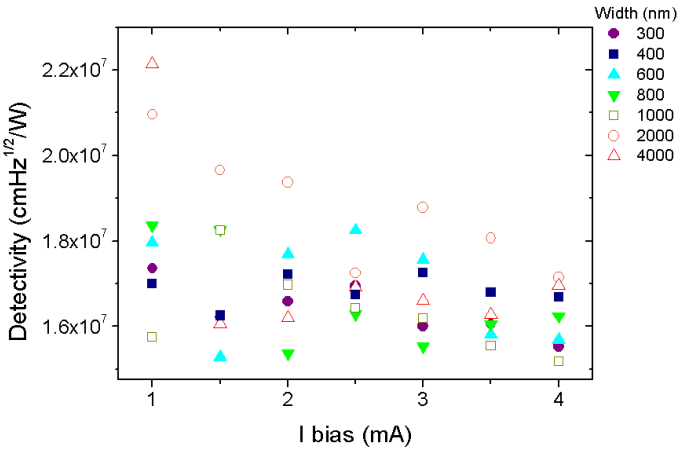

Figure 4.9: Detectivity of samples with various lengths, as a function of their width and bias current. Length ranges between 900 nm and 15 μm, and width between 300 nm and 4 μm. Data from samples with various lengths but same width and bias current was averaged.

model of detectivity presented in section 2.4.5, we do not expect any influence of the width on the specific detectivity (see eq. (2.37)). This is confirmed by our experimental data. However, if 1/f noise could be reduced to the point where the samples would be Johnson-Nyquist limited, the detectivity would be affected by sample width (see eq. (2.35)).

4.2.3. Conclusion on the effect of the active area's lateral dimensions on bolometric performances

The bolometric performance (responsivity and specific detectivity) of several samples made of 50 nm-thick platinum films was studied, as a function of the dimension of their active area. The study shows that both length and width have an impact on the performance. However with our measurement protocol, this effect has been demonstrated only on the responsivity. From macroscopic models, we defined expectations for the evolution of responsivity along bias current, lengths and widths. Our measurements suggest a range of lengths to be more sensitive to infrared illumination. Samples with a length between 600 nm and 2 μm show enhanced IR absorption attributed to antenna-like resonances. This is in accordance with relatively recent experimental findings (Bryant et al. 2008, Neubrech et al. 2006) and subsequent theoretical modeling (Novotny 2007). The width is also playing a strong role on the responsivity. Indeed, responsivity increases as the width is reduced from 4 μm to 300 nm. Also, bolometers

with a width below 800 nm departs from the macroscopic scaling relations, meaning that the area is not anymore the dominant factor on sensitivity. Narrow samples see their responsivity amplified due to increased resistivity and enhanced absorption. Based on an emissivity analogy, it is also believed that as the width is reduced, only a certain polarization of the IR irradiation is picked-up by the bolometer. However, such small samples display a responsivity of 10^4 V/W and a specific detectivity of 10^7 cmHz$^{1/2}$/W.

4.3. Influence of the Pt thickness on electronic properties and sensitivity of bolometers

Thin films are defined as sheets of material that have a thickness ranging from an atomic layer to a few micrometers. They have been extensively studied as they exhibit peculiar properties as the thickness is reduced. The thickness of a metal film changes its electronic properties, specifically its resistivity and TCR. As these two parameters have an influence on the responsivity and detectivity of our bolometers, it is interesting to study samples with a varying thickness. Contreras & Gaddy (1970) and other studies have shown an impact of film thickness on the device bolometric performance. In our case, we have studied samples with a total thickness (adding the platinum film and the chromium adhesion layer) of less than 100 nm. The experiments described so far were carried on samples with an average total thickness of 55 nm. As platinum possesses a skin depth of 50 nm for $\lambda = 2.5$ μm (Cuadrado et al. 2013), a film thickness of 55 nm is considered optimum: the incoming IR radiation penetrates through all the film, leading to a better coupling between the IR radiation to the metal. Later, we fabricated and measured samples with a total thickness ranging from around 3 nm up to 80 nm. In this case, the IR radiation either penetrates through all the film and into the silicon dioxide, or through only a part of the film.

Paper 4 presents the results of the study on the influence of the metal film thickness on bolometric performance. Up to 70 samples were fabricated during 18 deposition rounds in order to have sufficient data. As the focus was on the thickness effect, all samples had the same dimension, i.e. 300 nm by 1000 nm. A first batch of samples was fabricated with a constant thickness of 5 nm for the chromium adhesion layer, with a platinum thickness varying from 10 to 77 nm. Measurements hinted that as the thickness is decreasing, the responsivity is increasing. A second batch of samples was therefore fabricated, this time with platinum thicknesses from 2 nm to 12 nm. Because of such low thickness values, we decided to use only 1 nm of chromium as adhesion layer, to keep platinum dominant in the metallic layer. The thinnest sample studied is composed of 1 nm of chromium and 2.3 nm of Pt, hence in this case the metallic layer is at minimum constituted by more than 60% platinum. Preliminary experiments showed that using only a nanometer of chromium was enough to ensure adhesion of platinum on the substrate. During the deposition of metal on patterned

substrates, we also deposited unpatterned wafers for X-ray evaluation of the platinum thickness. In the following summary of our results, as well as in **Paper 4**, we refer to a sample's thickness as its total thickness, i.e. the measured platinum thickness of the sample plus its chromium layer (either 1 nm or 5 nm).

4.3.1. Temperature coefficient of resistance and resistivity dependence on thin film thickness

As the film thickness is reduced, the ratio between surface and volume increases. This implies a growing significance of surface effects compared to bulk ones, and changes the electronic properties of films. In our study, we specifically investigated the evolution of the temperature coefficient of resistance (TCR, see section 2.4.2) and resistivity with decreasing thickness.

TCR directly affects the sensitivity of bolometers, as it conveys the amplitude of resistance change upon IR illumination. From eq. (2.17) it is evident that a large ΔR is desirable to obtain a maximized responsivity. The TCR of patterned samples with various thicknesses was measured using a hot plate and our usual 4-probe setup. The increase in resistance caused by the change in temperature was measured, from which we could extract the TCR value proper to each thickness, according to eq. (2.21). Results are displayed in fig. 4.10.

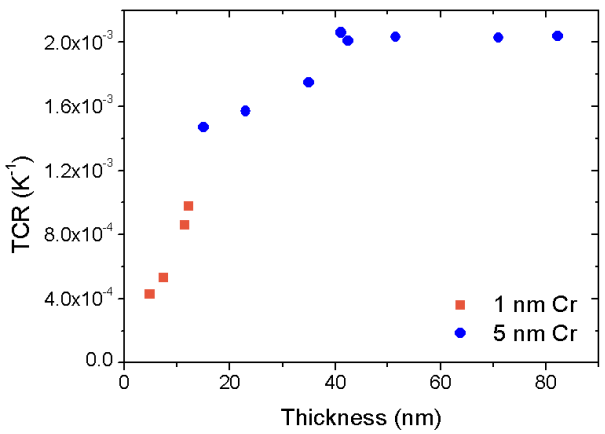

Figure 4.10: Evolution of the temperature coefficient of resistance of bolometers with thickness of the metallic thin film. Red squares and blue circles corresponds to samples with a chromium adhesion layer of 1 nm and 5 nm, respectively.

Figure 4.10 shows that the TCR of our samples is greatly affected when the film

thickness decreases below 40 nm. Samples that are 40 nm-thick or more display a constant TCR value of 2×10^{-3} K^{-1}. This experimental result is consistent with values found in literature concerning platinum thin films (Tsutsumi et al. 2002). Our thin film value is also half of the platinum bulk one, reported as 3.85×10^{-3} K^{-1} (Iniewski 2013). For films having a thickness below 40 nm, the TCR value decreases substantially. The thinnest sample that could be measured (4.8 nm thick) displays a TCR of 4×10^{-4} K^{-1}. This is lower by a factor of 5 compared to the constant value reach by samples with a thickness of 40 nm or higher. There is also a change in the resistivity of our samples, which increases considerably when the thickness is lower than 40 nm. We calculated the resistivity after performing I-V measurements, measuring lateral dimensions and film thickness of samples with various thicknesses, and using eq. (2.30). Figure 4.11 displays the resistivity as a function of the inverse of sample thickness.

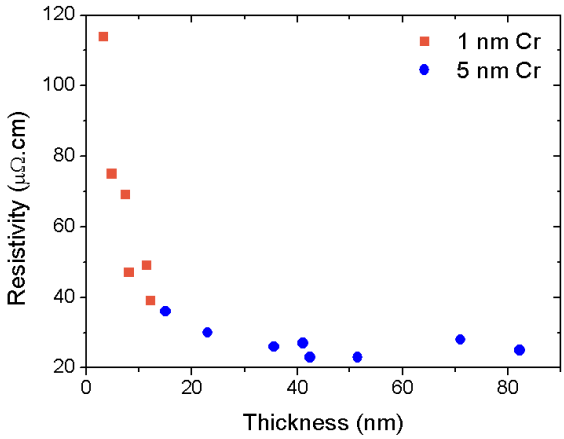

Figure 4.11: Resistivity of bolometers' thin films as a function of their thickness. Red squares and blue circles corresponds to samples with a chromium adhesion layer of 1 nm and 5 nm, respectively.

Just as for the TCR, the measured resistivity of thin films is strongly affected by their thickness. It is well known that resistivity increases as the film thickness decreases, and fig. 4.11 illustrates this. Again, 40 nm represents a threshold in the evolution of electronic properties of our samples. Thin films with a thickness of 40 nm or above presents a constant resistivity of 23 $\mu\Omega$.cm, which is about twice the bulk value of platinum (10 $\mu\Omega$.cm). The resistivity increases rapidly as the thickness decreases below 40 nm, up to 114 $\mu\Omega$.cm for the thinnest sample at 3.3 nm.

As a result, our samples display a large range of electrical resistance; from 10Ω for the thickest to 1 kΩ for the thinnest. This increase in resistivity, and thus resistance, for thin samples is linked to the reduction of the grain size with the thickness decreasing.

In a previous work done in our lab, the grain size of similar samples but of different series with a thickness of 55 nm was estimated to be around 14 nm (Elíasson & Ingvarsson , to be submitted). As the thickness is reduced, the grain size decreases. This leads to an increased contribution of grain boundary scattering to the overall electron scattering rate.

As the resistivity and TCR are constant for samples of thickness 40 nm or above, it is plausible to say that below 40 nm surface effects are becoming important compared to bulk ones. As the film gets thinner, the ratio between surface effect and bulk effect increases, leading to an increase/decrease of resistivity/TCR. This threshold thickness value of 40 nm is specific to our samples. A similar pattern in TCR and resistivity was found in Zhang et al. (2006), where they study the influence of the thickness of platinum thin films on their electronic properties. It is interesting to see that in their case, the thickness threshold value is 30 nm, below which the TCR is decreasing and resistivity is increasing. Also, their samples display a higher resistivity of about 100 $\mu\Omega$.cm while their TCR is around 1×10^{-3} K$-$1. This difference can be attributed from the different coating method, as they use e-beam physical vapour deposition, which produces denser films.

4.3.2. Influence of the thin film thickness on bolometric properties

The responsivity was calculated for our samples with different thicknesses. From eq. (2.17) it is evident that DC bias current directly influences the responsivity value. Hence it is desirable to bias the samples with the same current. However, the current must also be kept under a certain value to avoid any excessive Joule dissipation-induced self-heating. We used a maximum current density value of 10^7 A/cm^2 as a reference to prevent electromigration. Thus most of the samples were biased with 1 mA, except the two thinnest. As they have an electrical resistance higher than 500 Ω, we biased them at 0.5 mA (thickness 4.8 nm) and 0.3 mA (thickness 3.3 nm) instead of 1 mA to avoid any self heating.

It is useful to define an expected evolution of responsivity with decreasing thin film thickness. From eq. (2.33) one can see that as the width is constant, and for the same bias current, the responsivity is expected to be directly proportional to the inverse of the film thickness. Figure 4.12 displays the measured responsivity as a function of the inverse of sample thickness.

For samples that have a thickness higher or equal to 12.2 nm, the responsivity increases linearly as their thickness is decreasing. However, as the thickness is further decreased, there is a large increase of responsivity, with the 7.5 nm-thick sample reaching a peak responsivity of 2×10^5 V.W^{-1}. Then, the two thinnest samples display a lower responsivity compared to the peak one, even when considering that they were biased by a current at least half lower than their thicker counterparts. If they were biased

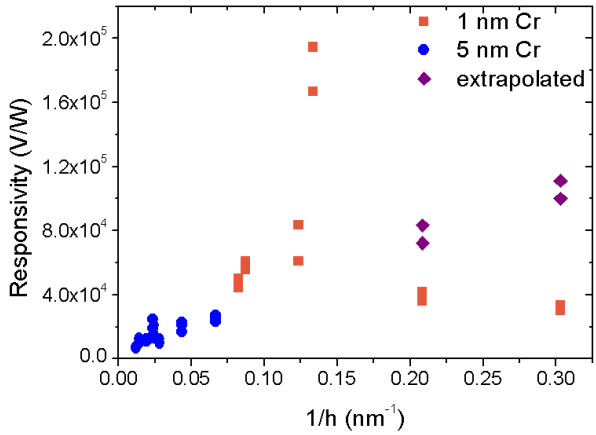

Figure 4.12: Responsivity of bolometers as a function of the inverse of the thin-film thickness. Red squares and blue circles are for samples with a chromium adhesion layer of 1 nm and 5 nm respectively. Bias current is set at 1 mA for all samples, except the two thinnest samples (4.8 nm and 3.3 nm) that were biased with 0.5 and 0.3 mA respectively. Responsivity of these samples if biased with 1 mA is displayed by the purple diamonds.

with 1 mA, we expect that they would display a larger responsivity, but not exceeding 1.2×10^5 V.W^{-1}, and also the samples would be subjected to high current density (see section 3.3.4). Through this result it is interesting to see a global improvement of responsivity when the thickness is decreased from 77.3 nm to 7.5 nm. For lower thicknesses, it is likely that the responsivity deteriorates. This would indicate that 7.5 nm is an optimum thickness for our bolometers' responsivity. Block & Gaddy (1973) similarly reports an optimum thickness below 10 nm bolometers made of various metals. Also, this peak responsivity at a thickness of 7.5 nm of oxide could be due to a plasmon resonance, although numerical calculations are needed to confirm it.

Detectivity is calculated from responsivity and the calculated noise contribution. As the studied samples presented a wide range of resistivity, it calls for a revised Hooge formula when calculating the 1/f noise. How to calculate the 1/f noise contribution is discussed in section 2.3.3, where we present a revised Hooge formula taking into account the resistivity of the thin film. To calculate the effect of thickness on detectivity, we have been using eq. (2.24). From eq. (2.37) the detectivity is expected to be proportional to the square root of the film thickness. Figure 4.13 thus displays the specific detectivity as a function of the square root of thin film thickness.

The results present a general increase of detectivity with the thin film thickness. Although the detectivity values are quite scattered for certain thickness values, the evo-

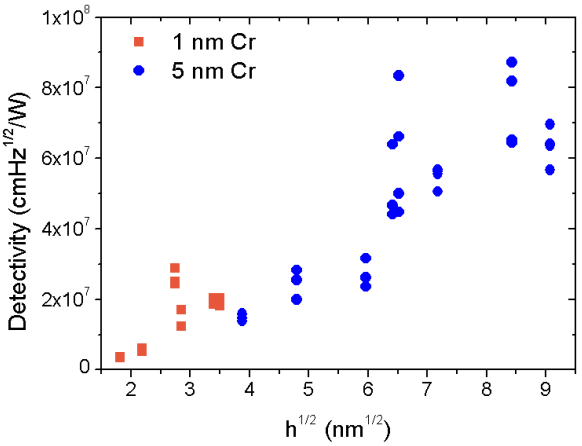

Figure 4.13: Evolution of detectivity with bolometer film thickness as a function of the square root of film thickness. Red squares and blue circles are for samples with a chromium adhesion layer of 1 nm and 5 nm respectively. Bias current is set at 1 mA for all samples, except the two thinnest samples (4.8 nm and 3.3 nm) that were biased with 0.5 and 0.3 mA respectively.

lution of detectivity with film thickness seems to agree roughly with eq. (2.37). Maximum detectivity is reached by the thickest samples, around 6×10^7 cmHz$^{1/2}$/W. As the thickness decreases, detectivity is deteriorating. Thinnest samples display the lowest detectivity, at 3×10^6 cmHz$^{1/2}$/W, despite large electrical resistance and responsivity values. Between the two extremes of the studied thickness range, namely 2.3 nm and 82.3 nm, there is an increase of a factor 20 in detectivity.

This conclusion can be quite surprising at first glance, bearing in mind our previous study on responsivity and knowing that detectivity is directly proportional to it. The answer lies in the noise behavior of our samples. This loss in detectivity with low thicknesses comes from a large increase of the 1/f noise as the thickness is reduced. The 1/f noise contribution is larger than the Johnson-Nyquist one for all thicknesses. For the thickest sample, the 1/f noise contribution is 10^2 higher than its Johnson counterpart. This factor is up to 10^5 in the thinnest ones. Hence the 1/f noise is the dominant factor noise in such samples, partly because of their increased resistivity.

It would be useful to reduce the 1/f noise contribution, and one simple way to do so would be to reduce the bias current. However, using 0.1 mA instead of 1 mA would only reduce the 1/f noise by a factor of 10^2. In this case, 1/f noise and Johnson noise will have an equal contribution in thick samples, but in thin samples the 1/f noise will still be dominant. A more efficient way to reduce 1/f noise would be to use AC current instead of DC current.

4.4. Effect of the silicon dioxide layer on bolometer performance

The properties of Si/SiO_2 substrates are detailed in section 2.4.4. While silicon is a good thermal conductor, SiO_2 provides both electrical and thermal insulation for the metallic film deposited on top of it. Also, as illustrated by fig. 2.9 and fig. 2.10, SiO_2 has a varied transmittance over optical to mid-IR wavelengths. It is transparent to wavelengths shorter than 2 μm, the transmittance drops for wavelengths between 2 μm and 4 μm. Finally, the transmittance is almost none for wavelengths longer than 4 μm, making SiO_2 absorbing and emitting infrared in this spectral range. In our experimental protocol, the blackbody lamp has temperature of 1064 K, thus a peak wavelength of 2.74 μm. Therefore the IR emission spectra ranges mainly from 1 μm to 12 μm. The spectra of a blackbody with a temperature of 1064 K is displayed in fig. 4.14. The thickness of SiO_2 also influences the bolometric properties of the device through constructive or destructive interference between the reflected infrared radiation at the Si/SiO_2 interface. Depending on several distinct parameters, such as the incoming IR peak wavelength or its angle of incidence, there is an optimum SiO_2 thickness that improves the absorption of the sensor (Cuadrado et al. 2013).

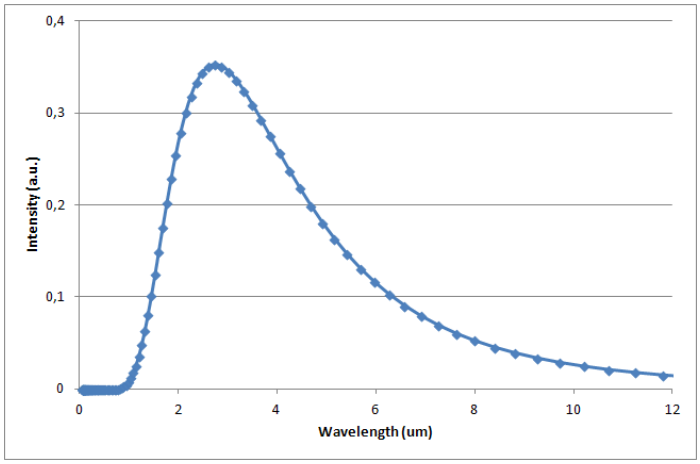

Figure 4.14: Blackbody spectrum at a temperature of T = 1064 K. The maximum intensity will be at wavelength $\lambda_{peak} = 2.74$ μm.

As SiO_2 defines the thermal insulation of the metallic film to the substrate, it is directly influencing the bolometer's thermal conductance G_{th}. In turn, G_{th} affects the time response of the bolometer, τ (see section 2.3.5 and section 2.3.4). Thus, SiO_2 is an essential layer in our bolometers, as was already pointed out in section 4.2.1. We have been further studying the influence of its thickness on the bolometric properties of our samples and some of the results have been published in **Paper 2**.

Several thicknesses of SiO_2 have been grown in an RTA furnace at the University of Iceland (see section 3.2.3) from Si wafers with native oxide. After each SiO_2 growth, the actual thickness of the oxide layer was measured via ellipsometry (see section 3.2.4). Six wafers with SiO_2 thicknesses ranging from 50 nm to 600 nm were compared, as well as commercial wafers made of Si/SiO_2(100 nm) and Si/SiO_2(1 μm). Platinum bolometers made of 50 nm of platinum and 5 nm of chromium were patterned on top of these wafers. Their active part has a fixed width of 300 nm, and lengths ranging from 300 nm to 19 μm. All samples were biased by a DC current corresponding to a constant Joule dissipation power of 24 μW, as introduced in section 4.1. The responsivity of several samples with various lengths, as a function of the SiO_2 thickness is displayed in fig. 4.15.

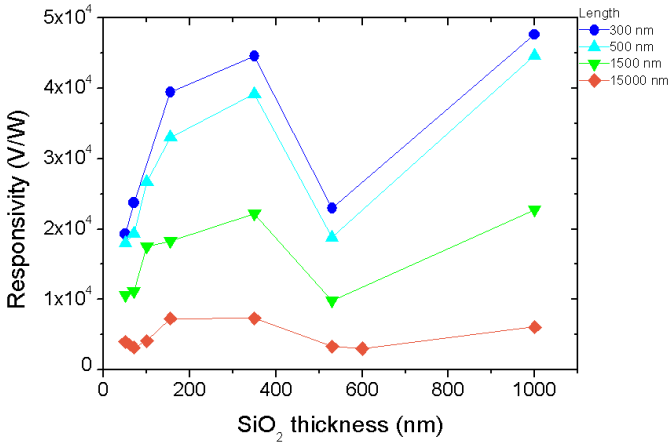

Figure 4.15: Responsivity of several samples as a function of the SiO_2 layer thickness. Measurements were made on four samples with various active part's length, from 300 nm to 15 μm. Solid lines are guides to the eye.

Figure 4.15 shows the same data as presented in **Paper 2**, with the addition of some new data. The way of plotting responsivity values is also different: responsivity is plotted as a function of the SiO_2 thickness instead of length. From this figure, one can see that increasing the SiO_2 layer from 50 nm to 350 nm increase the responsivity. However, a strong decrease in responsivity is observed for samples with a SiO_2 layer thicker than 350 nm. Finally, samples with a SiO_2 thickness of 1 μm display a responsivity comparable to when the SiO_2 layer is 350 nm thick. Responsivity is also higher for shorter samples. This comes mainly from the fact that in these experiments we used a constant bias power. Therefore, shorter samples have been biased with a higher current value. For all lengths, however, it seems that there is an optimum SiO_2 thickness value between 155 nm and 530 nm, and another maximum at 1 μm. For the four samples displayed on fig. 4.15, there is a factor of 2.3 between the maximum (i.e. either for a SiO_2 thickness of 350 nm or 1 μm) and minimum (i.e. either for a SiO_2

thickness of 50 nm or 600 nm) value. A maximum responsivity of 4.8×10^4 V/W is achieved by the shortest sample, patterned on a 1 μm thick SiO_2 substrate.

An increased thickness of SiO_2 provides better thermal and electrical insulation of the metallic film from the silicon substrate. In other words, the heat produced by the absorption of the incoming IR radiation conducts more slowly to the substrate. This heat confinement in the active area leads to an increase of ΔT, hence of ΔR. Therefore, the electrical output of the bolometer is larger, and so becomes its responsivity. Our experimental data confirms this, as ΔR displays the same evolution with SiO_2 as the responsivity does. However, it is interesting to see that both ΔR and responsivity drop when the SiO_2 layer is thicker than 350 nm. The detectivity of all these samples was calculated, and fig. 4.16 displays its evolution with the thickness of SiO_2 for four samples with different lengths.

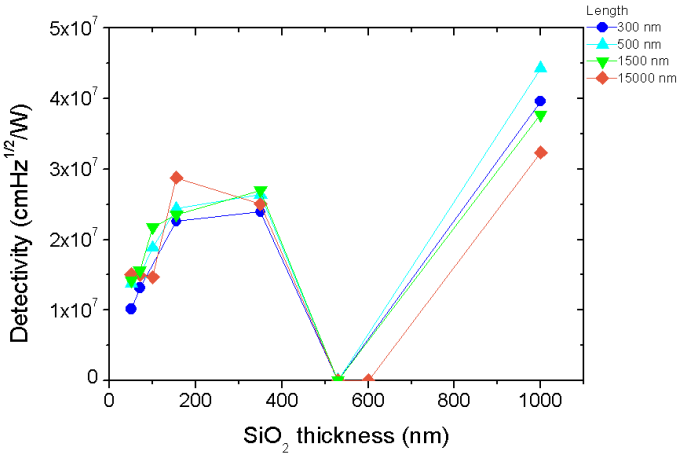

Figure 4.16: Detectivity of several samples as a function of the SiO_2 layer thickness. Measurements were made on four samples with various active part's length, from 300 nm to 15 μm. Solid lines are guides to the eye.

Detectivity shows the same evolution with SiO_2 thickness as the responsivity. From 50 nm to 350 nm of SiO_2, the detectivity increases, but samples with a SiO_2 thickness of 530 nm or 600 nm display an extremely reduced value of detectivity. However, the specific detectivity for samples with a SiO_2 thickness of 1 μm is high, almost 2 times higher than for SiO_2(350 nm). Overall, there is a factor of 10^3 between the maximum and minimum detectivity values. Finally, the detectivity appears to be independent of the sample length. This is in accordance to eq. (2.37), when the 1/f noise is dominant in the samples. Maximum detectivity is reached by samples on a 1 μm thick SiO_2 substrate, with $D^* = 4 \times 10^7$ cmHz$^{1/2}$/W.

This oscillating pattern in both responsivity and detectivity could come from two

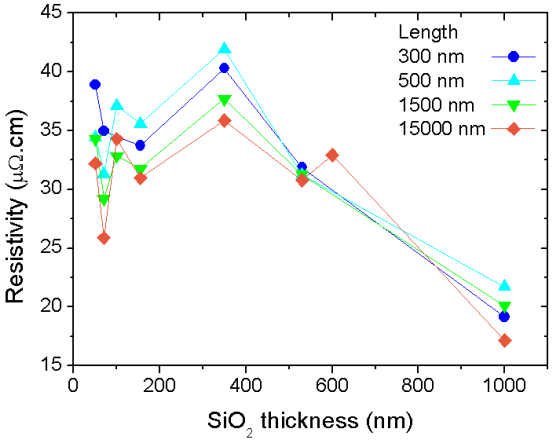

Figure 4.17: Resistivity of several samples as a function of the SiO_2 substrate thickness. Measurement were made on four samples with various lengths of the active part. Solid lines are guides for the eye.

reasons. First, the resistivity of the samples varies with film thicknesses, due to the fact samples have been fabricated in several deposition rounds. The resistivity ranges between 16 and 42 $\mu\Omega$.cm, with a maximum for the SiO_2(350), as displayed in fig. 4.17. The resistivity plotted against the SiO_2 thickness shows a maximum for 300 nm oxide thickness, as seen for the responsivity and detectivity. This fluctuation in resistivity is also found in the evolution of $\Delta R/R$ with SiO_2, shown in fig. 4.18.

Samples with higher base resistance will display higher ΔR compared to samples with lower base resistance, under the same IR illumination. Plotting the ratio $\Delta R/R$ allows to see the relative increase in resistance ΔR due to IR light, whatever the base resistance of the sample. As ΔR directly influences the responsivity, its variation might explain the oscillation in fig. 4.15 and fig. 4.16. However, one can see in fig. 4.17 that if the resistivity is dropping for samples patterned on a 1 μm-thick SiO_2 substrate, the respective $\Delta R/R$ value do increase (or stay the same for the 15 μm-long sample). This means that another phenomenon is influencing the absorption of IR in the bolometer in this case. This could come from the interference effects of IR light reflected at the interface between silicon and SiO_2, affecting the total amount of absorbed IR. Taking into account the refractive index of silicon oxide at $\lambda = 2.74$ μm, the IR light inside the SiO_2 has an effective wavelength of $\lambda_{eff} = 2.74/1.5 = 1.81$ μm. The first two interference minima can be expected to occur around $\lambda_{eff}/4$ and $3\lambda_{eff}/4$, which are around 500 nm and 1500 nm respectively. Such values are consistent with our observations. Also, preliminary FDTD calculations also support our experimental results. However, a more detailed calculation taking into account e.g. the internal reflectivity at the Pt/SiO_2 interface would be needed to obtain more precise values.

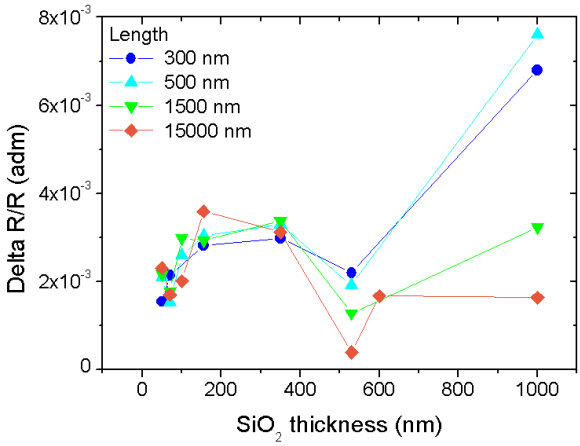

Figure 4.18: Increase in resistance (ΔR) over base resistance of several samples under IR illumination, as a function of the SiO_2 substrate thickness. Measurements were made on four samples with various lengths of the active part. Solid lines are guides for the eye.

As a conclusion, there is choice to be made about the optimal thickness of SiO_2 for our samples. Thicknesses around 350 nm and 1 μm are linked to a maximum in responsivity and detectivity. However, a thicker SiO_2 layer implies a slower device in terms of time response. Therefore, it can be wiser to choose a thickness around 350 nm. Samples patterned on a SiO_2 layer of 350 nm exhibit a fairly good performance, with a responsivity of 4.5×10^4 V/W and a detectivity of 2.7×10^7 cmHz$^{1/2}$/W.

4.5. Changing the bias current to optimize performance

The bias current is a crucial factor in the operation of our bolometers. It directly influences the responsivity, but also affects the detectivity via the noise sources. Moreover, it can have in extreme cases a significant effect on the microscopic structure of the device through Joule dissipation, leading to annealing and/or electromigration. Therefore, it is important to study the evolution of both figures of merit as well as the noise with bias current/bias power. Some conclusions have been presented in **Paper 2**. We used samples made of 50 nm of platinum on top of a 5 nm of titanium for adhesion, on a commercial $Si/SiO_2(100)$ wafer. Bolometers with an active area of width of 300 nm and various lengths ranging from 600 nm to 10 μm were fabricated and measured.

Four samples were biased with increasing DC current values, until their eventual destruction. The DC bias current values have been calculated to correspond to Joule dissipation power values ranging from 20 μW to 2 mW. Naturally, the intrinsic self-heating also increases with the bias current. As an example, a sample with a length of 600 nm was biased up to 9.7 mA, which corresponds to a temperature of 700 K. However, even with such a self-heating contribution, the bolometer was able to sense a change of 3 K brought by the external IR source. Figure 4.19 below displays the responsivity of four samples as a function of their bias power and length.

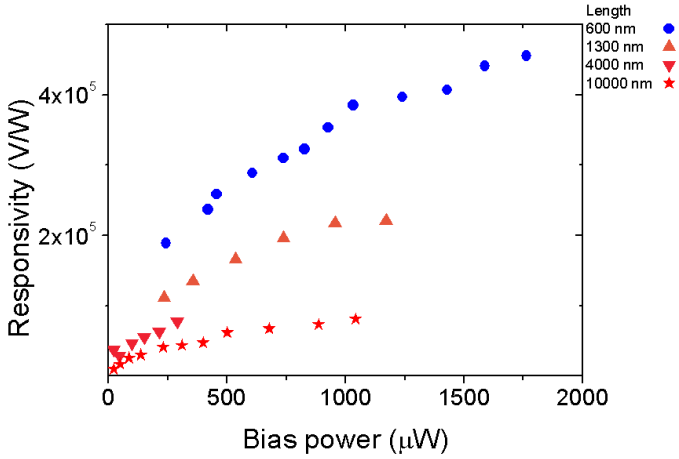

Figure 4.19: Responsivity of four samples as a function of the bias power and length, from 600 nm to 10 μm.

For all sample lengths, the responsivity is increasing sublinearly with the bias power. As here we deal with bias power, we can express the responsivity as follows:

$$\Re \propto \sqrt{\frac{P_J}{R}} \tag{4.4}$$

with P_J the Joule dissipation power and R the resistance of the sample. This explains the sublinear increase of responsivity displayed in fig. 4.19. For the same bias power, samples display a higher responsivity as their length is shortened. This comes from the fact that shorter samples have a smaller resistance, hence they are biased with a higher current. As a consequence, the shortest sample studied (with a length of 600 nm), displays a maximum responsivity of 4.5×10^5 V/W when reaching a Joule dissipation power of 1.7 mW (corresponding to a bias current of 9.7 mA).

It is also important to look at the evolution of the current density J when increasing the sample bias. It reaches a maximum of 6.5×10^7 A/cm^2 for the 600 nm-long sample

when biased at 9.7 mA. This is a rather high current density value, likely to induce annealing and electromigration. Eventually, samples broke down around this current density value, as noted before (see section 3.3.4). In a comparable study, Saxena, Bhan, Jalwania & Khurana (2008) present the effect of excessive bias current on titanium bolometers, and the conclusions are similar to what we have witnessed in our samples when the current density is high.

Noise calculations for our samples suggest that the dominant noise source is 1/f noise. Moreover, the 1/f noise becomes more important as the bias power increases. The difference between Johnson-Nyquist noise and 1/f noise depends on the length of the sample: shorter samples have stronger 1/f noise compared to longer ones due to their larger bias current. This leads to the 1/f noise being between 10^3 and 10^6 larger than the Johnson-Nyquist noise contribution. The detectivity of the four samples previously studied is displayed in fig. 4.20.

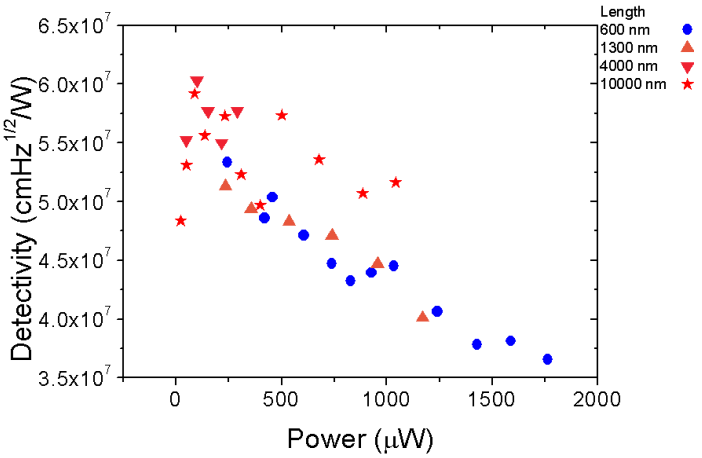

Figure 4.20: Detectivity of four samples as a function of the bias power and length, from 600 nm to 10 μm

In fig. 4.20, the detectivity is not affected by the length of the sample, as all detectivities show the same decrease with the increasing bias power. This corroborates eq. (2.37), which states that specific detectivity does not depend on length. As the bias power (or bias current) increases, 1/f noise in the samples increases, leading to a decrease in the specific detectivity. Thus detectivity is affected by the bias power, albeit not tremendously within our studied power bias range (factor 1.6). In any case, it is preferable to keep a moderate bias power in order to minimize the 1/f noise and therefore maximizing the detectivity. However, as seen previously in fig. 4.19, the responsivity is increasing with the bias power. Therefore, a compromise has to be made between responsivity and detectivity, while keeping the current density below

10^7 A/cm^2. Consequently, the maximum bias power or current must be adapted considering the geometry of the sample's active part. It should be noted that over the range of studied bias power, the responsivity can be increased by an order of magnitude, while the specific detectivity decreases by a factor smaller than 2.

4.6. Time constant of Pt thin-film bolometers

One of the drawbacks of thermal detectors is their rather slow time response compared to their photodetector counterparts. Typically, thermal detectors show a response time in the millisecond range, while photodetectors react within microseconds (see section 2.2). Section 2.3.5 presents the theory behind time response of infrared detectors, and introduces the idea that a trade-off needs to be made between sensitivity and time response. In eq. (2.28) one can see that the time response can be improved (i.e. made shorter) if the thermal conductance G_{th} is maximized. However, a larger thermal conductance means more heat transferred from the metallic film to the substrate, leading to a loss in ΔR created from the incoming infrared radiation. As the size of the active area directly influences the thermal conductance, it is then of great interest to study the time response of our microscopic bolometers.

Measuring the time response of thermal sensors can be straightforward when using an AC-bias setup combined with lock-in amplifiers (Chen et al. 2001, Codreanu et al. 2003, Gawarikar et al. 2013, González et al. 2004). However, we used a DC-bias setup, therefore other solutions have been considered. An ultra-fast oscilloscope (Agilent Technologies Infiniium DSO9404A) was used to build a new setup, combining DC and high-frequency apparatus. Samples were redesigned in order to incorporate new contact pads for the high-frequency probe. An 80 MHz pulsed super-continuum laser was used as an IR source, and its internal trigger linked to the oscilloscope. So far, several attempts to measure the time constant of bolometers have been made without conclusive results. A bias tee was used to filter out the DC part of the output voltage signal, but the signal amplitude brought by the external laser illumination is still too low for the oscilloscope to detect. Given that the sensitivity limit of the high-speed oscilloscope is 1 mV, the sample signal has to be electronically amplified.

It is also insightful to study the time response theoretically. Jónsson (2009) presents a model of samples made of platinum with a design similar to ours, but used as thermal sources instead of bolometers. Through finite element simulation, the time response of thermal emitters was studied as a function of their width. From this study, it appears that samples with a length of 8 μm and a width below 1 μm have a time response equal to or shorter than 40 nanoseconds. The time response becomes quicker as the width is reduced. This suggests that our samples could also possess a very short time response to IR radiation, which would be a great advantage.

We have calculated the time response of bolometers as a function of the metallic film thickness. According to eq. (2.28), time response depends on both C_{th}, the thermal capacity, and G_{th}, the thermal conductance. In order to calculate the heat capacity, we used eq. (2.27), with $C_p = 130$ J.kg^{-1}K^{-1} and $\rho = 21450$ kg.m^{-3}. Thermal conductivity is calculated with eq. (2.26). For each thickness value, parameters from several nominally identical samples were used. There are two sources of heat affecting the bolometer: an external one, brought by the IR radiation, and an internal one, caused by self-heating. However, the infrared radiation is a perturbation of our system. It is then preferable to calculate the time response without taking into account this perturbation. Therefore, G_{th} will be calculated with only taking into account self-heating induced changes in temperature. Thus, G_{th} is the inverse of the dT/dP value that is extracted from IV measurements of each sample.

The time response of samples of same width and length has been calculated, for different metal film thickness and bias current. Each sample's dT/dP value has been extracted from IV measurements so the temperature elevation due to Joule heating (ΔT_{sh}) can be also calculated. Overall, dT/dP does not vary much with the film thickness. The design of our samples leads to a stronger effect of the lateral area (length and width) on dT/dP, while the influence of the film thickness is negligible. This means that by calculating G_{th} as the inverse of dT/dP, it will also be independent of the thickness. This makes physical sense: as G_{th} described the amount of heat transferred from the film to the substrate via the interface between the two, it is not expected to be influenced by the film thickness. On the other hand, with our sample design, C_{th} depends only on sample film thickness. Finally, the time response should not be affected by the bias current fed to the sample. This means that we expect the time response τ to be directly proportional to the film thickness. Figure 4.21 displays the calculated time response of several samples with different film thicknesses, with a bias current of 0.5 mA.

Generally, our samples have a thermal conductance value around 2×10^{-5} W/K, and a heat capacity between 8×10^{-15} and 6×10^{-14} J/K depending on the sample thickness. This leads to a time response increasing with the thickness, as expected from theory and previous experiments (Block & Gaddy 1973). As the thickness ranges between 10 nm to 77 nm, the time response is increased by roughly a factor of 10. It is also interesting to see that the time response is in the nanosecond range, as hinted from previous modeling works. Figure 4.21 shows that the longer response time is obtained by the thickest sample at around 4 ns, and the fastest time response by the thinnest one at around 0.4 ns. Relaxation time of electrons in metals is typically of 10^{-15} s, therefore it is physically realistic. In any case, this nanosecond range for the time response of bolometers is very promising, and would represent a huge improvement of performance. This short response time would also allow spreading the use of bolometers in applications such as thermal vision, or any application that requires a fast frame rate.

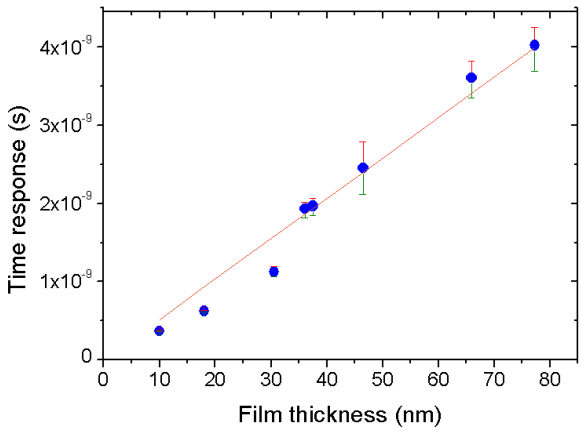

Figure 4.21: Time response calculated for samples with various film thickness, from 10 nm to 77.3 nm. Samples are biased with a DC current of 0.5 nm and are patterned on a Si/SiO2(100 nm)substrate. Full blue circles represent the average time response of samples with the same thickness, red and green ticks are error bars related to the maximum and minimum time response value of the set respectively. The orange line is a linear fit of the averaged data.

5. Summary and conclusions

Bolometers made of platinum thin-films have been designed and fabricated at the University of Iceland. They are active infrared sensors and their performance has been characterized for blackbody radiation at 1060K. At this temperature, the infrared spectrum has a peak wavelength of 2.74 μm, which corresponds to the near- to mid-infrared range. Bolometers are designed as a central active part attached to four contact pads. As the central part is biased by DC current, the electric resistance change brought by incoming infrared radiation is measured. Thus, the bolometric performance of the device is assessed by calculating its responsivity and specific detectivity. Typical lateral dimensions of the active area are between 300 nm and 17 μm in length and between 300 nm and 19 μm in width, and the thickness of the thin-film between 3 and 80 nm.

The main aim of this project was to study how multiple factors, such as fabrication, geometry and also driving parameters impact the sensitivity of our bolometers. Therefore, we have fabricated and measured samples with an active area of different length and width, and various thicknesses of the metallic thin-film. Also, samples with different silicon dioxide thickness have been characterized. Finally, the DC current bias value has been varied to study its effect on both bolometers' microscopic structure and sensitivity.

Lateral dimensions of the central part play a decisive role on the infrared absorption. When the size is reduced below 2 μm, samples stop following classical models and the absorbed infrared light does not scale with the sensing area. Responsivity is locally enhanced when the length of the central part is around 1.1 μm. This can be explained by the revised theory of antenna resonance applied to open-ended metallic antennas at optical frequencies. Also, when the width is reduced below 600 nm, the area ceases to be the main factor influencing the sensitivity. From boundary scattering and enhanced absorption, narrow bolometers display higher responsivity compared to their wider counterparts. Interestingly, it also appears that as the width is reduced, they may become more polarization selective, to the point where only 50% of the incoming unpolarized IR is picked-up.

Bolometers with a thin-film thickness lower than 40 nm have degraded electronic properties, such as reduced TCR and a large resistivity. Detectivity is also maximized for thicknesses equal to or larger than 40 nm. However, the responsivity increases by a factor of 3 for samples with a thickness of 7.5 nm compared to other thicknesses.

Infrared sensitivity is also maximized when the silicon dioxide has a thickness of 350 nm and 1 μm, presumably because of interference effects due to infrared reflected at the interface between silicon dioxide and silicon. Increasing the DC bias current causes the responsivity to increase linearly. However, it also leads to a quick decrease of the detectivity, as the 1/f noise is increasing. Therefore a trade-off has to be found between responsivity and detectivity when the bias current is increased, considering the device requirements. Finally, the expected time response of our thin-film bolometers has been calculated to be less than 4 ns, which represents a great improvement compared to the general time response of thermal detectors. This value can even be further reduced by reducing the metallic film thickness.

Table 5.1 summarizes the sensitivity values reached by our bolometers, as well as their physical properties. It appears that our samples are limited by 1/f noise, due to the use of a rather large DC bias (on the order of mA). As the metallic thin-film is a good electrical conductor, bolometers have a small resistance value. This prompts the need for a large bias current to be able to have a measurable change in voltage upon IR exposure.

Table 5.1: Summary of bolometer sensitivity and both thermal and electronic properties. Values are from experiments and theoretical calculations and models. Bolometers were exposed to blackbody spectra with a peak wavelength of 2.74 μm.

Responsivity	10^4 - 10^5 V/W
Specific detectivity	10^7 and 10^8 cmHz$^{1/2}$/W
Response time	< 4 ns
TCR	2×10^{-3} K^{-1}
Resitivity	23 μm.cm
Electrical resistance	5 Ω - 500 Ω
Thermal conductivity	10^5 W/K
Heat capacity	10^{-15} - 10^{-14} J/K

Such bolometric performance is comparable to what is found nowadays in the literature. Furthermore, our devices present additional advantages: a reduced size, ease of use, simple fabrication and a very fast time response to infrared illumination. Sub-wavelength platinum thin-film bolometers are promising infrared sensors that ought to be further developed in terms of sensitivity. This could be achieved by reducing intrinsic noise. It would be also very interesting to work on their integration on ROIC (Read Out Integrated Circuit) towards a commercial device. Due to their microscopic size, they are a good candidate for integration with other platforms, such as coupling them to optical waveguides.

To further improve sensitivity, the 1/f noise should be reduced, therefore rendering the Johnson-Nyquist noise dominant (as it is the case for most bolometers). Detectivity would be improved, and would most probably show the same features as responsivity (local maxima, improvement with reduced width, etc.). A first approach should be

taken by biasing the bolometers with AC current, and using lock-in amplifiers to pick-up the voltage signal across the active part. Also, the bolometric performance should be characterized for longer wavelengths. As an example, a CO_2 laser could provide coherent IR radiation at $\lambda = 10.6$ μm and could also be used to characterize the bolometers' absorption as a function of IR polarization.

A. Publications, presentations and posters

A.1. Publications

A.1.1. Published papers

Pauline Renoux, Sigurdur Ægir Jónsson, Levente J. Klein, Hendrik F. Hamann and Snorri Ingvarsson. *Sub-wavelength bolometers: Uncooled platinum wires as infrared sensors.* Optics express **19**, no. 9 (2011): 8721-8727.

Pauline Renoux and Snorri Ingvarsson. *Sample size effects on performance of sub-wavelength metallic thin-film bolometers.* Journal of Optics **15** (2013): 114011

A.1.2. Conference proceedings

Pauline Renoux, Alice Beauny, Levente J. Klein, Hendrik F. Hamann and Snorri Ingvarsson. *Thin-film platinum nanowires as sub-wavelength bolometers.* In Proc. SPIE, **8261** (2012): 82610I

Pauline Renoux, Dorine Charpentier, Sylvain Augé and Snorri Ingvarsson. *Optimization of performance for platinum nanowires as sub-wavelength bolometers.* In SPIE Optical Engineering + Applications, International Society for Optics and Photonics (2013): 88680C-88680C

Floria Ottonello Briano, Snorri Ingvarsson, **Pauline Renoux**, Göran Stemme, Hans Sohlström and Kristinn B. Gylfason. *High-Frequency, sub-wavelength thermal IR source.* Abstract submitted to SPIE Photonics Europe (2014)

A.1.3. Short communications

Pauline Renoux. *New infrared sensors are small, simple, and sensitive.* SPIE Newsroom (March 5, 2012). doi: 10.1117/2.1201202.004114

Pauline Renoux. *Sub-wavelength metallic bolometers with improved sensitivity.* IOP Science LabTalk (October, 2013).

A.2. Conference presentations

SPIE Photonics West, San Francisco, USA
Thin-film nanowires as sub-wavelength bolometers. January 25, 2012

Graphene Nanophotonics, Benasque, Spain
Sample size effects on performance of sub-wavelength bolometers. March 8, 2013

SPIE Optics + Photonics, San Diego, USA
Optimization of performance for platinum nanowires as sub-wavelength bolometers. August 27, 2013

A.3. Seminars

5th NTT-BRL School, Atsugi, Japan
Poster: *Nanoheaters for data storage and near-field microscopy.* November 25, 2009

R-VON 2010, Reykjavík, Iceland
Oral presentation: *Nanobolometers: uncooled platinum thin-film wires as infrared sensors.* October 2010

6th NTT-BRL School, Atsugi, Japan
Poster: *Performance optimization of sub-wavelength platinum nanobolometers.* November 26, 2013

B. Included Papers

Paper I

Sub-wavelength bolometers: Uncooled platinum wires as infrared sensors

P. Renoux
S. Æ. Jónsson
L. J. Klein
H. F. Hamann
S. Ingvarsson

Optics express **19**, 8721 (2011).

Sub-wavelength bolometers: Uncooled platinum wires as infrared sensors

Pauline Renoux,[1,3] Sigurdur Ægir Jónsson,[1] Levente J. Klein,[2] Hendrik F. Hamann,[2] and Snorri Ingvarsson[1,*]

[1]*Science Institute, University of Iceland, Dunhaga 3, Reykjavík IS-107, Iceland*
[2]*IBM T.J. Watson Research Center, Yorktown Heights, New York 10598, USA*

[3]*pauline@raunvis.hi.is*

[*]*sthi@hi.is*

Abstract: We present characterization results of microscopic platinum wires as bolometers. The wire lengths range from 16 μm down to 300 nm. Thus they are in many cases significantly smaller in size than the wavelength of the radiation from the 1200 K blackbody source they were exposed to. We observe a steep rise in both responsivity $\Re$ and detectivity $D^\star$ with decreasing wire size, reaching $\Re = 3.1 \times 10^4$ V/W and $D^\star = 2.7 \times 10^9$ cmHz$^{1/2}$/W at room temperature for a 300×300 nm^2 device. Two significant advantages of such small wires as bolometers are their low power requirement and fast response time. Our numerical estimations suggest response times in the order of nanoseconds for the smallest samples. They could help improve resolution and response of thermal imaging devices, for example. We believe the performance may be further improved by optimizing the design and operating parameters.

OCIS codes: (310.6845) Thin film devices and applications; (040.6808) Thermal (uncooled) IR detectors, arrays and imaging.

References and links

1. A. Rogalski, "Infrared detectors: status and trends," Prog. Quantum Electron. **27**, 59–210 (2003).
2. E. N. Grossman, J. A. Koch, C. D. Reintsema, and A. Green, "Lithographic dipole antenna properties at 10 μm wavelength: comparison of methods-of-moments predictions with experiment," Int. J. Infrared Millim. Waves **19**, 817–825 (1998).
3. I. Codreanu, F. J. González, and G. D. Boreman, "Detection mechanisms in microstrip dipole antenna-coupled infrared detectors," Infrared Phys. Technol. **44**, 155–163 (2003).
4. F. J. González and G. D. Boreman, "Comparison of dipole, bowtie, spiral and log-periodic IR antennas," Infrared Phys. Technol. **46**, 418–428 (2005).
5. F. J. González, B. Illic, and G. D. Boreman, "Antenna-coupled microbolometers on a silicon-nitride membrane," Microwave Opt. Technol. Lett. **47**, 546–548 (2005).
6. F. J. González, C. S. Ashley, P. G. Clem, and G. D. Boreman, "Antenna-coupled microbolometer arrays with aerogel thermal isolation," Infrared Phys. Technol. **45**, 47–51 (2004).
7. S. Ingvarsson, L. J. Klein, Y.-Y. Au, J. A. Lacey, and H. F. Hamann, "Enhanced thermal emission from individual antenna-like nanoheaters," Opt. Express **15**, 11249–11254 (2007).
8. Y.-Y. Au, H. S. Skulason, S. Ingvarsson, L. J. Klein, and H. F. Hamann, "Thermal radiation spectra of individual subwavelength microheaters," Phys. Rev. B **78**, 085402 (2008).
9. A. Kosarev, M. Moreno, A. Torres, and C. Zuniga, "IR sensors based on silicon-germanium-boron alloys deposited by plasma: fabrication and characterization," J. Non-Cryst. Solids **354**, 2561–2564 (2008).
10. C. Chen, X. Yi, X. Zhao, and B. Xiong, "Characterizations of VO_2-based uncooled microbolometer linear array," Sens. Actuators, A **90**, 212–214 (2001).

#143876 - $15.00 USD Received 9 Mar 2011; revised 3 Apr 2011; accepted 9 Apr 2011; published 19 Apr 2011

11. R. Smith, F. Jones, and R. Chasmar, *The Detection and Measurement of Infra-red Radiation* (Oxford Univ. Press, 1957).
12. S. Kogan, *Electronic Noise and Fluctuations in Solids* (Cambridge Univ. Press, 1996).
13. D. Fleetwood, J. Masden, and N. Giordano, "1/f Noise in platinum films and ultrathin platinum wires: evidence for a common, bulk origin," Phys. Rev. Lett. **50**, 450–453 (1983).
14. S. Sedky, P. Fiorini, K. Baert, L. Hermans, and R. Mertens, "Characterization and optimization of infrared poly SiGe bolometers," IEEE Trans. Electron Devices **46**, 675–681 (1999).
15. R. Lu, Z. Li, G. Xu, and J. Wu, "Suspending single-wall carbon nanotube thin film infrared bolometers," Appl. Phys. Lett. **94**, 163110 (2009).
16. S. Æ. Jónsson, "Nonlinear thermal electric analysis of platinum microheaters," Master's thesis, University of Iceland (2009).
17. H. F. Hamann, J. A. Lacey, and S. Ingvarsson, "Progress towards a thermally driven, infra-red near-field source using nanoheaters," J. Microsc. **229**, 512–516 (2008).
18. L. J. Klein, S. Ingvarsson, and H. F. Hamann, "Changing the emission of polarized thermal radiation from metallic nanoheaters," Opt. Express **17**, 17963–17969 (2009).

1. Introduction

Microbolometers are widely integrated in various technologies for both military and civilian applications. These include surveillance, security, and thermal imaging. They are made from different materials, e.g. metals or semiconductors [1]. The basic operating principle relies on the change of electrical properties of the device upon absorption of infrared (IR) radiation. Two highly desirable technical attributes for many applications are good sensitivity and fast response. Ease of use and cost can also play an important role for the end user. Semiconductor detectors that rely on excitation of electrons across a small band gap by IR photons usually have a high signal-to-noise ratio and a fast response time, but are selective in wavelength. Also such detectors often depend on complicated fabrication processes. Further, due to the small band gap they are operated at low temperature in vacuum, adding to inconvenience in use and price. Thermal detectors however, make use of the heating effect of the IR radiation. These can be as simple as a thin metallic strip or wire, thus quite straightforward to fabricate, low cost and reliable. They also operate at room-temperature but usually have a slower response (in the millisecond range) and a lower overall performance [1]. A great deal of work has been done on antenna-coupled microbolometers (see e.g. [2–5]) with time constants approaching 100 ns [6]. In this paper we present results of our study on thermal bolometers from lithographically patterned platinum micro- and nanowires. The smallest elements have dimensions significantly smaller than the wavelength of IR radiation being detected. They exhibit detectivity comparable with or higher than other bolometers and we argue that their response time is in the order of ten nanoseconds. Previously, we have studied thermal emission properties of such wires during resistive heating by a DC current. We observed a significant increase in the radiated signal for our narrowest wires [7, 8]. With Kirchoff's law of thermal radiation in mind the question naturally arose whether they would serve well as bolometers.

2. Characterization of responsivity, noise, detectivity and time response

2.1. Samples and experiment

We have fabricated two sets of platinum wires with different dimensions. Set A has widths ranging from 8 μm to 2 μm and lengths from 16 μm to 2 μm. Set B has lengths ranging from 300 nm to 20 μm with a fixed width of 300 nm. Both sets were fabricated on Si/SiO_2 (105 nm) substrates using photolithography and e-beam lithography respectively, then DC sputtering and lift-off techniques. The SiO_2 layer acts as thermal insulation between the wire and the Si substrate. Below the platinum we deposited 5 nm of chromium and titanium for set A and set B respectively, in order to improve adhesion. The thickness of the platinum layer was 50 nm for both sets. A typical sample is displayed in Fig. 1. It is designed with fine voltage sense leads,

#143876 - $15.00 USD Received 9 Mar 2011; revised 3 Apr 2011; accepted 9 Apr 2011; published 19 Apr 2011

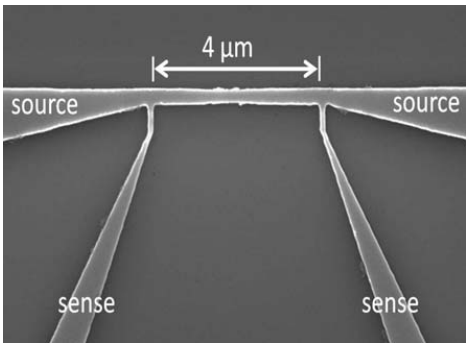

Fig. 1. Scanning electron microscope image of a 4 μm long by 300 nm wide wire showing the four-lead sample structure.

and source leads that broaden at the heater ends. This allows us to bias the wire by passing an electrical current through the outer source leads, and at the same time we monitor the resistance through the two inner sensing leads. We carefully characterize the current-voltage properties of our samples and record both their electrical and thermal resistance. The electrical resistance is approximated by:

$$R = R_0(1 + \alpha\Delta T), \tag{1}$$

where R_0 is a constant and α is the temperature coefficient of resistance (TCR) of the material. The resistance of our wires ranges from 6 to 300 Ω and their TCR is 0.002 K^{-1}. Extensive studies have revealed that the thermal resistance remains constant, despite changes in resistance caused by e.g. changes in grain size if the wire is exposed to high temperatures. This is in agreement with our numerical modeling that shows a very weak dependence of the thermal resistance on the thermal conductance of the wire. Essentially this is because the heat dissipation away from the wire is governed by thermal properties of the surroundings, but not by the properties of the wire itself. Thus, after careful characterization, we can tell the temperature of the wire quite accurately by measuring its resistance. To characterize our bolometers we bias them at room temperature with a DC current source and we monitor their resistance. Samples were biased within the range of 300 μA to 1.9 mA. As a reference we chose to keep the Joule dissipation power constant at 24 μW, in order to limit the self-heating contribution to the temperature change, in comparison with the IR-heating. The self-heating contribution was in most cases limited to within 2 K (for samples longer than 2 μm), but rose gradually up to 9K with decreasing sample length. With a fixed bias current and with the resistance in a steady state the bolometer is suddenly exposed to a NiCr-Ni blackbody source at a temperature of 1200 K. The corresponding blackbody emission spectrum is in the near-IR and has a maximum at a wavelength of 2.4 μm. The irradiance of the source was 1 W/cm^2. Exposure to the light source causes an abrupt resistance change in the wire that is easily detected with a four-point measurement without resorting to building the wire into a resistance bridge.

2.2. Responsivity

The performance of bolometers is characterized in terms of responsivity $\Re$ and noise. Responsivity is defined as the ratio of the output signal generated to the incident power [1], hence can

#143876 - $15.00 USD Received 9 Mar 2011; revised 3 Apr 2011; accepted 9 Apr 2011; published 19 Apr 2011

be expressed as:

$$\Re = \frac{V}{P_{\text{inc}}}, \tag{2}$$

where V is the voltage along the wire and P_{inc} is the incident IR power. In our case this can be expressed as [9]:

$$\Re = \frac{\Delta R \times I}{\mathscr{A} \times \text{Irr}}, \tag{3}$$

where I is the bias current, ΔR is the resistance change, Irr is the irradiance of the blackbody IR source and $\mathscr{A}$ is the area of the wire. Figure 2 displays the responsivity as a function of the

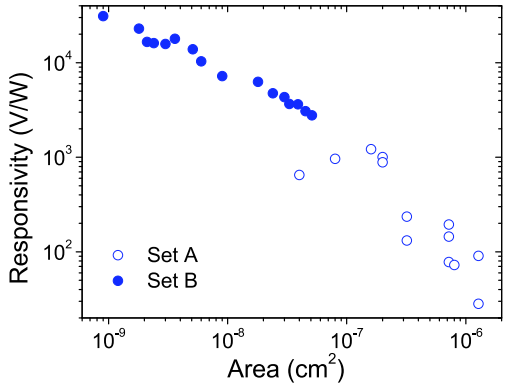

Fig. 2. Responsivity dependence on the area for the two sets of platinum nano- and microbolometers. Empty circles are samples from set A and filled ones are from set B.

surface area of the wire. From these results it is clear that as the dimensions of the wires are reduced, responsivity increases. This is to be expected from Eq. (3). A maximum responsivity of 3.1×10^4 V/W is reached for the 300 nm long sample. The larger, micron-scale, photolithographically defined samples from set A yield a more modest responsivity of around 10^3 V/W or below.

2.3. *Noise and detectivity*

A standard figure of merit to evaluate the performance of bolometers is the specific detectivity $D^\star$, expressed as [10]:

$$D^\star = \frac{\Re \times \sqrt{\mathscr{A}}}{V_n}, \tag{4}$$

where V_n is the root mean square (RMS) voltage fluctuation per unit bandwidth corresponding to the total voltage noise power spectral density S_n in the sample. It is evident from Eq. (4) that noise can severely limit the performance of the device. As it is quite challenging to measure noise in low resistance devices such as ours we estimate the contribution of the main sources: Resistance noise (i.e. Johnson-Nyquist noise), thermal conductance noise (TCN) and $1/f$ noise. We use the results to calculate a detectivity for our bolometers. The resistance noise can be expressed as:

$$S_{V,\text{JN}} = 4k_{\text{B}}RT, \tag{5}$$

#143876 - $15.00 USD Received 9 Mar 2011; revised 3 Apr 2011; accepted 9 Apr 2011; published 19 Apr 2011

where $S_{V,\mathrm{JN}}$ is the voltage power spectral density due to the resistance fluctuations, k_B is the Boltzmann constant and T is absolute temperature. Thermal conductance noise arises from temperature variations in the detector caused by heat conductance fluctuations between the wire bolometer and its surroundings (mainly the substrate). The power spectral density of voltage fluctuations caused by this is expressed as [11]:

$$S_{V,\mathrm{TCN}} = \frac{4k_B T^2 I^2 R_0^2 \alpha^2}{G}, \tag{6}$$

where we have used $G = \frac{RI^2}{T-T_0}$ for the thermal conductance to the surroundings. Excess, or $1/f$ noise in metals is usually attributed to random hopping motion of scattering centers, i.e. impurities and defects [12]. It is a low-frequency, non-equilibrium phenomenon related to DC bias current. It can be expressed by Hooge's empirical law [12]:

$$S_{V,1/f} = \frac{V^2 \beta}{N_0 f}, \tag{7}$$

where β is the Hooge constant for platinum films ($\beta = 0.002$, see Ref. [13]) and N_0 the numbers of carriers in the thermo-sensitive layer of the bolometer. Usually, the thermal conductance noise is negligible, and the preponderant noise between the Johnson noise and the $1/f$ noise depends on material properties and operating conditions. When evaluating noise according to equations (5), (6) and (7), we chose $f = 1$ Hz in Eq.(7) as our measurements are done at DC and 1 Hz is a commonly chosen reference point for frequency dependent noise. Figure 3

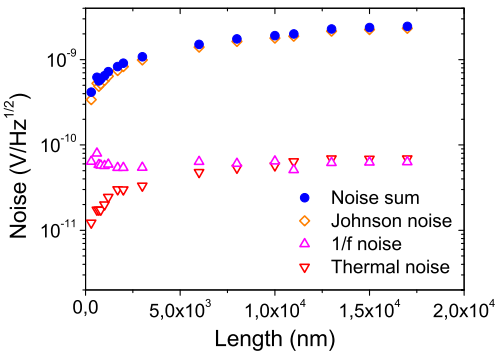

Fig. 3. RMS noise voltage components and total noise dependence on length for set B samples (constant width of 300 nm).

displays the total noise voltage dependence on length for set B samples. The results indicate that under our measurement conditions the predominant noise source in our platinum thin film bolometers is resistance noise, i.e. Johnson-Nyquist noise. Increase in wire temperature and electrical resistance contribute to the increase in TCN with length. Even at the low frequency of $f = 1$ Hz the $1/f$ noise is an order of magnitude weaker than the resistance noise. Combining these results with our data for responsivity gives a measure of detectivity according to Eq. (4). The results are displayed in figure 4. It can be seen that the detectivity increases significantly as area decreases. A maximum detectivity of around 2.7×10^9 cmHz$^{1/2}$/W was

#143876 - $15.00 USD Received 9 Mar 2011; revised 3 Apr 2011; accepted 9 Apr 2011; published 19 Apr 2011

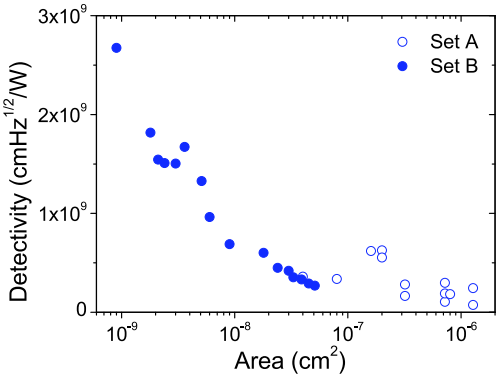

Fig. 4. Detectivity dependence on the area for the two sets of platinum nano- and microbolometers. Empty circles are samples from set A and full ones from set B.

reached for the square 300 nm long sample. Our platinum bolometers show high responsivity, low noise, and thus high detectivity compared to other reported values, such as a VO_2 bolometer (1.94×10^8 cm$\,$Hz$^{1/2}$/W) [10], poly SiGe (2.3×10^9 cm$\,$Hz$^{1/2}$/W) [14] or even carbon nanotubes (4.5×10^5 cm$\,$Hz$^{1/2}$/W) [15]. They also have a smaller size and a smaller resistance than most typical bolometers.

2.4. Time response

Another important advantage of using small bolometers is their short response time. A simple estimation of the thermal *RC* time constant τ is obtained by taking the ratio of thermal capacitance C to the thermal conductance to the surroundings G [11],

$$\tau = \frac{C}{G} \quad . \tag{8}$$

As an example, an estimation based on $c_p = 140$ J/(kg K) and a sample with lateral dimensions 300×600 nm^2 gives $C = 2.7 \times 10^{-14}$ J/K. With the measured value of thermal resistance $Z_{\mathrm{th}} = G^{-1} = 150$ K/mW this results in a response time of $\tau = 4$ ns. This estimation agrees very well with our time dependent finite element simulation results [16]. Our previous results have shown that emission spectra from heated wires in the size range of the smaller samples reported here differs appreciably from the blackbody spectrum [8]. (Wires wider than $\sim 1\mu$m do however appear to emit like blackbodies.) Nevertheless our smallest devices do emit very strongly in the energy range of interest, although this is limited to light polarized along the wire axis [7, 8, 17, 18]. Therefore it is not surprising that they are sensitive as radiation detectors in the same regime although this may indicate that they are wavelength selective. Consequently we expect our devices to act as polarization sensitive bolometers. We are presently investigating the detectivity as a function of polarization, the results of which shall be published shortly. We believe that the performance can be improved by optimizing the bias current and the thermal insulation of the wires. Increasing the thermal impedance of the bolometers can be achieved by raising the thickness of the SiO_2, using suspended structures or using substrates of low thermal conductivity, e.g. silica aerogel [6] or Si_3N_4 [5].

#143876 - $15.00 USD Received 9 Mar 2011; revised 3 Apr 2011; accepted 9 Apr 2011; published 19 Apr 2011

3. Conclusion

In summary we have investigated bolometric properties of Pt wires with dimensions in the order of and smaller than the IR wavelength being detected. These are uncooled devices that exhibit responsivity of 3.1×10^4 V/W and detectivity of 2.7×10^9 cm$\mathrm{Hz}^{1/2}$/W. The design and fabrication of these devices is very simple and can be achieved with state-of-the-art photolithography. The resistance of our devices ranges from several Ω's to a few hundred Ω. They display comparable detectivity to many more complex bolometers. We estimate numerically their time response in order of nanoseconds. This, together with their smallness should help improve e.g. imaging devices such as scanning thermal microscopes or thermal cameras. Further improvement in their detectivity could be made by optimizing the bias current and the thermal insulation of the wires.

Acknowledgments

This research was funded in part by the Icelandic Research Fund and the University of Iceland Research Fund.

#143876 - $15.00 USD Received 9 Mar 2011; revised 3 Apr 2011; accepted 9 Apr 2011; published 19 Apr 2011

Paper II

Thin-film platinum nanowires as sub-wavelength bolometers

P. Renoux
A. Beauny
L. J. Klein
H. F. Hamann
S. Ingvarsson

Proceedings of SPIE, **8261**, 82610I (2012).

Thin-film platinum nanowires as sub-wavelength bolometers

Pauline Renoux[a†], Alice Beauny[b], Levente J. Klein[c], Hendrik F. Hamann[c] and Snorri Ingvarsson[a‡]
[a]Science Institute, University of Iceland, Dunhaga 3, Reykjavík IS-107, Iceland
[b]INSA Toulouse, Department of Physics, 135 avenue de Rangueil, 31077 Toulouse, France
[c]IBM T.J. Watson Research Center, Yorktown Heights, NY 10598, USA

ABSTRACT

We present novel nanoscale bolometers made of lithographically defined platinum wires. The cores of our structures are narrow wires with fixed width of 300 nm and length ranging from 300 nm to 17 μm. Some are significantly smaller in size than the wavelengths they are exposed to from a 1200 K blackbody source. The response of the wire's resistance to the external radiation reflects its temperature and can be monitored in real-time. Previously, we have reported a steep rise in responsivity and detectivity with decreasing wire length under such infrared exposure, for a constant Joule power dissipation in the wire (drive power). In this work, we aim to enhance the performance of the bolometers by changing physical and driving parameters, i.e. the insulating layer thickness or the external bias. We find that after such optimization, structures can reach a responsivity $\Re$ of 4.5×10^5 V/W and a detectivity D* of 2.3×10^{10} cmHz$^{1/2}$/W. With a reduced size and a high performance, these devices could improve the infrared sensors technology.

Keywords: Bolometers, Infrared sensors, Optoelectronic nanotechnology, Thin film devices and applications.

1. INTRODUCTION

Infrared detectors are widely used in infrared detection for various purposes in research and everyday life. Their basic operating principle relies on the change of electrical properties of the device upon absorption of infrared (IR) radiation. Two highly desirable technical attributes for many applications are good sensitivity and fast response. For the user and the industry, ease of use and low cost are also essential. Within the classification of infrared sensors, bolometer devices fall under the class of thermal detectors, with their resistance changing under IR absorption. Compared to photon detectors, they have slower response times and lower overall performances, but are low-cost and reliable, due to simpler design and use[1]. In a previous paper[2] we presented results of a study on bolometers whose sensitive cores are lithographically patterned platinum nanowires of different lengths. The smallest elements have dimensions significantly smaller than the wavelength of IR radiation being detected. They proved to exhibit detectivities comparable with or higher than other bolometers. Also, our numerical simulations suggest that their response time is in the order of ten nanoseconds[2,3]. In this article, after developing our previous results, we present an optimization of the bolometers performance by tuning their current bias and the thickness of the silicon dioxide layer.

2. FABRICATION AND DEVICE PHYSICS

We have fabricated 300 nm-wide platinum wires with lengths ranging from several hundreds of nanometers to several micrometers. They are made by writing patterns in e-beam resist on Si/SiO_2 followed by a 50 nm thick DC-sputtering platinum deposition and lift-off. A typical sample is displayed in Fig. 1.

† pauline@raunvis.hi.is
‡ sthi@hi.is

Terahertz Technology and Applications V, edited by Laurence P. Sadwick, Créidhe M. O'Sullivan,
Proc. of SPIE Vol. 8261, 82610I · © 2012 SPIE · CCC code: 0277-786X/12/$18 · doi: 10.1117/12.904965

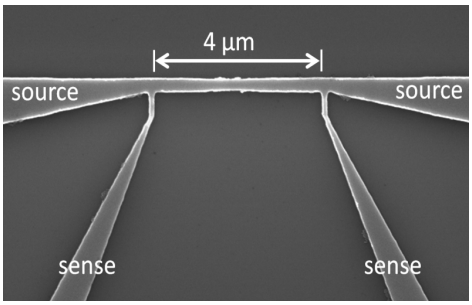

Fig. 1. Scanning electron microscope image of a 4 μm long by 300 nm wide wire (close-up of the center).

The SiO_2 layer acts as thermal and electrical insulation between the metallic film and the Si substrate and is a key factor for the performance of the device. For the first part of this study we used commercial wafers with a SiO_2 thickness of 100 nm. Later, when investigating the influence of the silicon dioxide thickness on the performance of the samples, we grew manually the desired oxide thickness at 1150°C in a RTA furnace from Si wafers with native oxide. We chose to use platinum as bolometric material as it is non-reactive, has a rather low thermal conductance G compared to other metals and a low 1/f noise. It has a temperature coefficient of resistance (TCR) of 0.002 K^{-1}. Below the platinum was deposited 5 nm of titanium or chromium, in order to improve adhesion with the SiO_2. Resistance of the samples ranges from a few ohms to several hundred ohms.

The core function of bolometers is a resistance increase as they are subjected to infrared radiation that heats up the sensitive, or sensing, area. Our samples are designed with a constricted part that we refer to as a "wire", which is bound by DC leads and contact pads at its ends. The pads can be viewed as heat sinks as heat distributes and dissipates quickly to the substrate due to their large surface area. Therefore the temperature rise is strongly localized in the wire part of our samples; this has been confirmed by numerical simulations[3] and thermal imaging[4].

The structure includes fine voltage sense leads, and source leads that broaden at the wire ends. This allows us to bias the wire by passing an electrical current through the outer source leads, and at the same time to monitor its resistance through the two inner sensing leads. To characterize the performance, we bias the samples with a fixed DC current and with the resistance in a steady state (R_0). The bolometer is subsequently suddenly exposed to a NiCr-Ni blackbody source at a temperature of 1200 K. Its corresponding blackbody emission spectrum is in the near-IR with a maximum at a wavelength of 2.4 μm, with an irradiance of 1 W/cm^2. Exposure to the infrared light causes extra heating in the wire and an abrupt resistance change that is easily detected with a four-point measurement, without resorting to building the wire into a resistance bridge. We carefully characterize the current-voltage properties of our samples at room temperature and record both their electrical and thermal resistance with a Keithley 2400 source-meter.

The performance of bolometers is expressed in terms of responsivity $\Re$ and detectivity D*. Responsivity is defined as the ratio of the output signal generated to the incident power[1]. The change in resistance occurring in the bolometer due to the incident radiation is expressed as:

$$\Delta R = R_0 \alpha \Delta T \tag{1}$$

where α is the temperature coefficient of resistance (TCR) of platinum and ΔT the rise in temperature caused by the external IR radiation. Hence the responsivity in our case is:

$$\Re = {\Delta R \times I}/{\mathcal{A} \times Irr} \tag{2}$$

where I is the bias current, ΔR is the resistance change, $\mathcal{A}$ is the area of the wire and Irr is the irradiance of the blackbody IR source.

Detectivity is the ultimate figure of merit to characterize the devices. It is expressed as[5]:

$$D^* = \Re \times \sqrt{\mathcal{A}} / V_n \quad (3)$$

where V_n is the root mean square (RMS) voltage fluctuation per unit bandwidth corresponding to the total voltage noise power spectral density S_n in the sample. It is evident from Eq. (3) that noise can severely limit the performance of the device.

3. RESULTS AND OPTIMIZATION

3.1 On previous wire length dependency study

In early works we have studied the thermal emission properties of wires during resistive heating by a DC current, and observed a significant increase in the radiated signal for our narrowest devices[4,7]. Therefore it was interesting to see if they could as well be efficient bolometers. In a previous paper from our group[2], first bolometer characterization works were carried on to study the influence of the wire length on the overall performance. We studied samples with a constant width of 300 nm and varying length from 300 nm to 17 μm, made on Si/SiO_2 (105nm) wafers. We chose as a reference point to keep the Joule dissipation power constant at 24 μW in all the samples, hence determining the corresponding bias current after measuring the "cold" resistance R_0 by IV characterization. Of course, as small samples have a lower resistance than the larger ones (the resistance is ranging from 7 to 300 ohms), the current through the samples is increased with their size decreasing.

As the Joule dissipation power is kept constant for all samples at 24 μW, the self-heating contribution is in most cases limited to within 2 K (for samples longer than 2 μm), but rise gradually up to 9 K with decreasing sample length. However this does not prevent us from observing large changes in wire resistance upon IR exposure. For all lengths in our study, the noise calculation shows that the predominant noise source in our platinum thin-film bolometers is the Johnson-Nyquist noise. Increase in wire temperature and electrical resistance contribute to the increase of TCN with length. The 1/f noise is an order of magnitude weaker than the resistance noise in these operating conditions.

Generally speaking, the results of our study show both responsivity and detectivity presenting an exponential decrease with the length increasing, meaning a higher performance for smaller samples. And yet, it could be argued that the high performance of smaller bolometers comes from the fact that they are fed with a higher bias current. It is clear that from Eq. (1) that the responsivity is directly proportional to the bias current, and so is the detectivity. Carrying on a simple approximation, stating that ΔT changes little with the length of the sample, we have $\Delta R \propto L$. The same goes for the area, with $\mathcal{A} \propto L$. With the irradiance being constant for all samples, the responsivity can be expressed as $\Re \propto I$. Further, as the bias current is set to keep the Joule dissipation power $P_J = R_0 I^2$ constant, it follows:

$$\Re \propto \sqrt{\frac{1}{L}} \quad (4)$$

The responsivity is then expected to be only dependent on the bias current, which scales with the square root of the inverse of the length. For the detectivity, as Johnson-Nyquist noise is the main noise source in which only the resistance varies, we have $V_{n,JN} \propto R_0 \propto L$. Combining this with Eq. (4) it is possible to express the detectivity as follows:

$$D^* \propto \sqrt{\frac{1}{L}} \quad (5)$$

Fig. 2 below presents the results from our previous paper[2] for different length sample at constant drive power plotted against the square root of the inverse of their length (in this case it is essentially equivalent to plotting versus bias current):

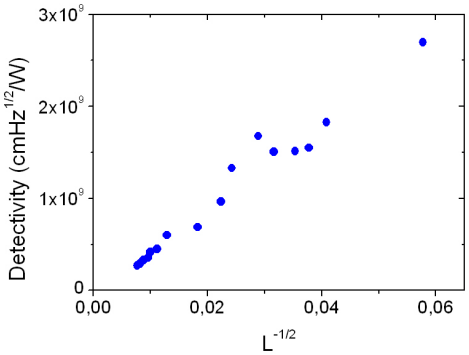

Fig. 2. Detectivity plotted against the square root of the inverse of the length of the samples.

One can see that the detectivity is not totally fitting to the suggested trend line. A strong linear increase is visible; however a deviation is evident for lengths ranging from 800 nm to 2000 nm. If not for this fluctuation, the linearity would be achieved. The center of the deviation is characterized by a peak which occurs for the 1200 nm long bolometer, and comes from a bigger temperature jump occurred in this particular sample. This denotes that even if the performance of the samples is improved when the bias current is increased, it is not the only factor that influences the responsivity and detectivity. Fig. 2 then shows that the responsivity of different length bolometers will be quite different, for a given power value. In the following study, we kept the Joule dissipation power as a reference point.

3.2 Optimization of performance with bias power

From previous experiments, it is clear that our structures can sense a change in temperature of some Kelvin even if the self-heating contribution of the wire lays the same range. Our interest with this study was to characterize the bolometer performance in a higher bias current range and find its limits.

When increasing the bias current, the Joule dissipation power increases, leading to higher self-heating contribution of the wires. As an example, the 600x300 nm^2 sample is almost reaching 700 K when biased by 9.7 mA. Albeit this remarkable rise in temperature, the bolometer is still able to detect a 3 K rise caused by an IR external source. According to Eq. (2) the responsivity is directly proportional to the bias current. The resistance change ΔR caused by the radiation induced temperature jump stays relatively constant as bias increases, resulting in a sublinear increase in responsivity when plotted as function of power. This can be seen in Fig. 3, which displays the results of the characterization of samples of different lengths, with increasing Joule dissipation power:

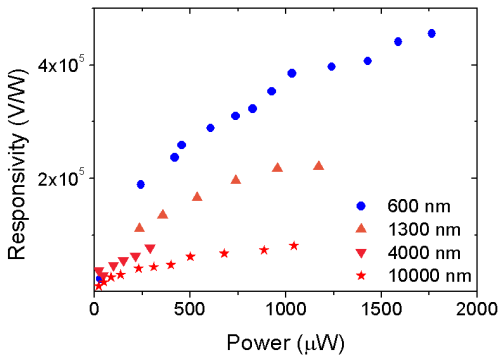

Fig. 3. Responsivity dependence on Joule dissipation power for different lengths of platinum nanobolometers.

As the Joule dissipation power (hence the bias current) increases, the responsivity reaches higher values. But high bias current also leads to stronger electro-migration phenomenon and annealing processes in the nanowires, leading to changes in structural properties and increasing the risks of device failure. The noise is also affected by the bias current, particularly the 1/f noise component. As an example, Fig. 4 displays the evolution of the three main noise components with the bias power for a 1400 nm-long bolometer:

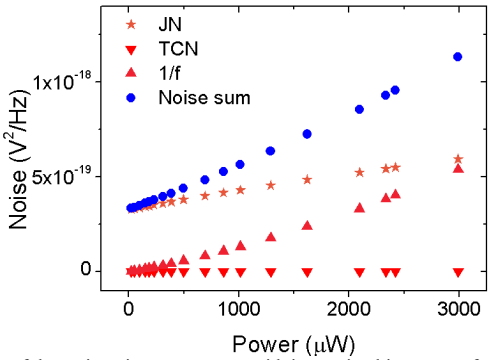

Fig. 4. Evolution of the main noise components with increasing bias power, for a 1400 nm-long sample.

We have not measured noise directly in our devices, as due to their low resistance it calls for specialized setup and careful measurements. It is well known that metallic resistors are Johnson-Nyquist noise limited down to quite low frequencies[6]. At low enough frequency the noise is dominated by 1/f noise (estimated here for 1 Hz, a commonly chosen reference value for DC measurements). The 1/f noise has been well characterized in Pt resistors, but is quite sample specific, so an estimate of noise from calculations will be accurate enough for our purpose. Therefore we estimate numerically the contribution of the major noise components: resistance noise (i.e. Johnson-Nyquist noise), thermal conductance noise (TCN) and 1/f noise, and use the results to calculate the detectivity of our bolometers. More detailed definitions and models of these noise components were presented in our previous paper[2]. In this previous study the bias current was set at a specific value for each sample, to keep the Joule dissipation power constant at 24 μW. This modest power value was chosen to limit the self-heating contribution of the wire in comparison with the external IR heating.

As supposed, the predominant noise source in our platinum wire bolometers is the resistance noise, i.e. Johnson-Nyquist noise. Its power spectral density is linearly proportional to the resistance of the wire, and thus changes slightly as self heating of the wire raises its resistance. For this 1400 nm-long sample, the thermal conductance noise (TCN) stays constant with increasing bias power, with a power spectral density of around 1.8×10^{-21} V^2/Hz. However, the 1/f noise is increasing drastically due to its dependence on bias. For a bias power of 3 mW it is has increased by 2 orders of magnitude, reaching a value of 5×10^{-19} V^2/Hz, when the Johnson-Nyquist noise has a value of 6×10^{-19} V^2/Hz. Therefore for higher bias power values, the 1/f noise would become the main noise component in our devices.

The detectivity, Eq. (3), combines noise and responsivity for each sample. Using the results above, we plot in Fig. 5 the dependence of detectivity on bias power:

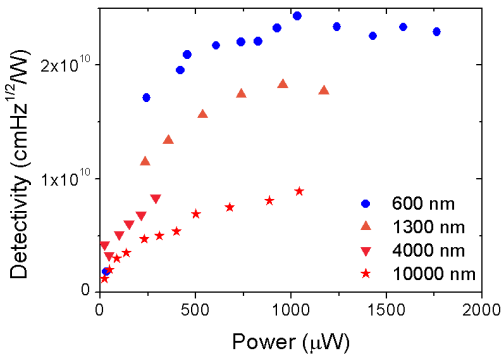

Fig. 5. Detectivity of platinum nanobolometers of different lengths for increasing Joule dissipation power.

One can see that the detectivity is increasing rapidly with the bias power, but levels off to a plateau for power values between 500 and 1000 μW. It is clear that the rise in responsivity for high bias power is balanced by the 1/f noise component, as detectivity is the ratio of responsivity and noise. Fig. 5 shows that smaller samples reach a better performance, as pictured in Fig. 4: the smaller sample 300x600 nm^2 reaches a detectivity of $2.3x10^{10}$ $cmHz^{1/2}/W$ for a bias power of 1 mW, corresponding to a bias current of 7.9 mA. Comparing these optimal performance values to the ones obtained at a fixed Joule dissipation power of 24 μW presented by Fig. 2, we have an increase of at least a factor 10.

3.3 Influence of the SiO_2 thickness on the performance

The SiO_2 layer plays an insulating role that is of major importance in the performance of bolometers. Increasing the insulation between the metal sheet to its surroundings will reduce leakage of heat through the substrate, hence increasing the amplitude of the response signal. Though better insulation increases the sensitivity of the device, it also slows down its response time. This is well depicted by the time response equation:

$$\tau = {}^{C}/_{G} \tag{6}$$

where C is the heat capacity and G is the thermal conductance to the surroundings. As the SiO_2 layer becomes thicker, providing a better thermal insulation, the thermal coupling is decreasing. This will cause the time response of the device to be longer.

As described above, different thicknesses of silicon dioxide were grown on silicon substrate to study its effect on the bolometer properties. Four wafers were fabricated, with SiO_2 thickness ranging from 50 nm to 350 nm, and a commercial wafer with an oxide thickness of 100 nm was also used for this experiment. Platinum structures with wires of fixed width 300 nm and lengths ranging from 300 nm to 19 μm were patterned and fabricated on each of the five wafers. After characterizing their electronic properties (with a constant Joule dissipation power of 24 μW), we calculated the responsivity $\Re$ and detectivity D^* according to Eq. (2) and Eq. (3) respectively. Fig. 6 below displays the responsivity as a function of the sample length and the silicon dioxide thickness:

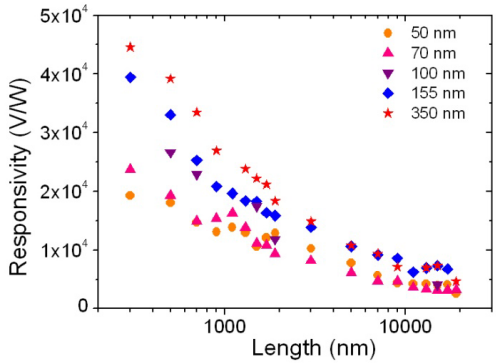

Fig 6. Responsivity of 300 nm-wide platinum wires of different lengths, patterned on Si/SiO_2 wafers with different silicon dioxide thicknesses.

Comparing the responsivity values of our set of samples, one can see that the responsivity increases for wafers with thicker SiO_2 layers. This graph also shows that shorter samples present larger responsivities between oxide thicknesses than longer ones. As an example, with samples of length 300 nm, the responsivity for 350 nm-thick oxide is more than 2 times bigger than its 50 nm-thick counterpart, and reaches a maximum value of $4.5x10^4$ V/W. Longer samples with lengths from 5 to 19 µm show a gain in responsivity of around factor 1,5 over the 50 nm-thick SiO_2. After calculating the corresponding noise components, the detectivity of the samples is presented in Fig. 7:

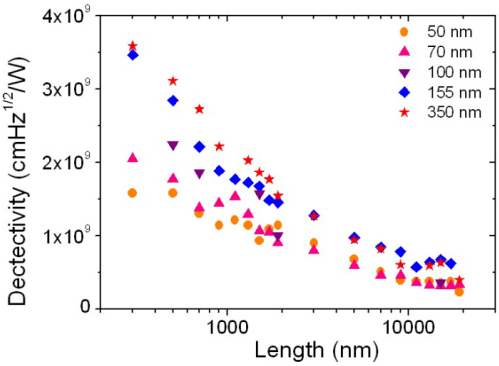

Fig 7. Detectivity of 300nm-wide platinum wires of different lengths, patterned on Si/SiO2 wafers with different silicon dioxide thicknesses.

The detectivity has the same general pattern as the responsivity. Large values of detectivity are obtained for smaller samples on top of thick silicon dioxide wafers. Gain factors between SiO_2 thickness values for same length samples are similar as the responsivity ones. A maximum detectivity of $3.6x10^9$ $cmHz^{1/2}/W$ is reached by 300 nm-long samples. It is also interesting to note that samples on thin layers of silicon dioxide (from 50 nm to 100 nm) and with a length of 3 µm or longer have a similar value for responsivity. The same applies for detectivity. It is only when the sample length is below or equal to 2 µm that we have a significant effect of the SiO_2 thickness on the performance.

Better responsivity and detectivity are achieved for bolometers patterned on top of thick silicon dioxide layer (350 nm). This is caused by an improved electrical and thermal insulation of the metallic wire from the silicon substrate. Consequently the performance is improved: the output signal to the incident power, measured as ΔR, is stronger. This comes from the insulation that prevents the heat produced by the absorption of the incoming IR radiation to dissipate in

the substrate. As the silicon dioxide layer is thicker, the heat is confined in the wire, increasing the corresponding rise in resistance.

4. CONCLUSION

In summary, we presented infrared sensors with two valuable assets: a reduced size of the order of hundreds of nanometers, and a high responsivity and detectivity. In this work, a study of the drive power influence on the performance showed that devices are limited by 1/f noise for higher bias currents. This leads to detectivity reaching a maximum value: for a sample of dimensions 600x300 nm^2, detectivity reaches $2.3x10^{10}$ $cmHz^{1/2}/W$ for a bias power of 1 mW. The sensing performance of the devices can also be improved by thicknening the silicon dioxide layer. This provides better electrical and thermal insulation of the metallic sheet from the substrate. Detectivity is increased by a factor of 2.25 when the SiO_2 thickness is up to 350 nm: the sample 300x300 nm^2 reaches $3.6x10^9$ $cmHz^{1/2}/W$. In the future we plan to continue on improving the performance of our small-size bolometers, to provide new solutions for infrared sensing.

ACKNOWLEDGMENTS

This research was funded in part by the Icelandic Research Fund and the University of Iceland Research Fund.

REFERENCES

[1] Rogalski, A., " Infrared detectors: status and trends," Progress in Quantum Electronics 27, 59-210(2003)
[2] Renoux, P., Jónsson, S. Æ., Klein, L. J., Hamann, H. F. and Ingvarsson, S. " Sub-wavelength bolometers: uncooled platinum wires as infrared sensors," Opt. Express 19, 8721-8727 (2011)
[3] Jónsson, S. Æ., " Nonlinear thermal electric analysis of platinum microheaters," Master's thesis, University of Iceland (2009)
[4] Ingvarsson, S., Klein, L. J., Au, Y.-Y., Lacey, J. A. and Hamann, H. F., " Enhanced thermal emission from individual antenna-like nanoheaters," Opt. Express 15, 11249-11254 (2007)
[5] Chen, C., Yi, X., Zhao, X. and Xiong, B., " Characterizations of VO_2-based uncooled microbolometer linear array," Sensors ans Actuators A 90, 212-214 (2001).
[6] Kogan, S., [Electronic Noise and Fluctuations in Solids], Cambridge University Press, (1996)
[7] Au, Y.-Y., Skulason, H. S., Ingvarsson, S., Klein, L. J. and Hamann, H. F., " Thermal radiation spectra of individual subwavelength microheaters," Physical Review B 78, 085402 (2008).

Paper III

Sample size effects on the performance of sub-wavelength metallic thin-film bolometers

P. Renoux
S. Ingvarsson

Journal of optics **15**, 114011 (2013).

IOP Publishing Journal of Optics
J. Opt. **15** (2013) 114011 (7pp) doi:10.1088/2040-8978/15/11/114011

Sample size effects on the performance of sub-wavelength metallic thin-film bolometers

Pauline Renoux and Snorri Ingvarsson

Science Institute, University of Iceland, Dunhaga 3, Reykjavík IS-107, Iceland

E-mail: pauline@hi.is and sthi@hi.is

Received 31 May 2013, accepted for publication 19 July 2013
Published 28 October 2013
Online at stacks.iop.org/JOpt/15/114011

Abstract
This paper presents how reducing the width and length of a bolometer's sensing core affects its performance. Bolometer devices made of thin films of platinum with various lateral dimensions—widths ranging from 300 nm to 4 μm and lengths ranging from 300 nm to 19 μm were tested. Some are significantly smaller in size than the wavelengths they are exposed to, coming from a blackbody source with a λ_{peak} of 2.74 μm. A resonance effect is revealed for samples of specific dimensions, where the performance is enhanced. Further, a strong increase in responsivity appears when the sample's width is narrowed, whereas specific detectivity remains independent of any change in dimensions. We believe that some of these features are due to plasmonic effects, which may explain the high performance reached by smaller samples. It seems that graphene could be subject to similar geometrical effects to our thin-film bolometers.

Keywords: infrared sensors, bolometers, optoelectronic technology, thin-film devices and applications

(Some figures may appear in colour only in the online journal)

1. Introduction

Nowadays, uncooled infrared detectors are used in many different applications, from industrial to private use, and from civilian to military technologies. In this category fall bolometers, which have been extensively studied in the past. In these detectors, infrared radiation heats up a sensitive layer, causing a rise in temperature that changes its physical properties. As they are uncooled detectors, they present slower response times and a lower overall performance compared to photon detectors [1]. However, as their design can be quite simple, they are low cost and reliable. Two highly desirable technical attributes are good sensitivity and a fast response. For the user and for industry, ease of use and low cost are also essential. Different materials and techniques have been investigated to produce high-sensitivity IR sensing devices, from semi-conductors or vanadium oxides [2] to metal strips [3]. Some metallic bolometers have a sensitive core coupled to antennas, to optimize the IR collection [4]. Others use suspended metallic membranes to increase thermal isolation [5]. Recently even metamaterials [6] or carbon nanotubes [7] have been characterized as bolometers. Graphene has also sparked a strong interest, as it displays a good performance as a photodetector [8, 9] despite the fact that it absorbs only 2.3% of the incident light. We have developed metallic bolometers that have a simple design but reach high sensitivity, at a submicron size scale. We present here the effects of geometry on their performance. We believe that graphene sheets should also be subject to similar effects, i.e. the IR absorption properties should be dependent on the in-plane geometry of the graphene sheet.

In previous work [10], we presented results of our study on bolometers from lithographically patterned platinum nanowires of different lengths. The smallest elements have dimensions significantly smaller than the wavelength of IR radiation being detected. They proved to exhibit detectivities

2040-8978/13/114011+07$33.00

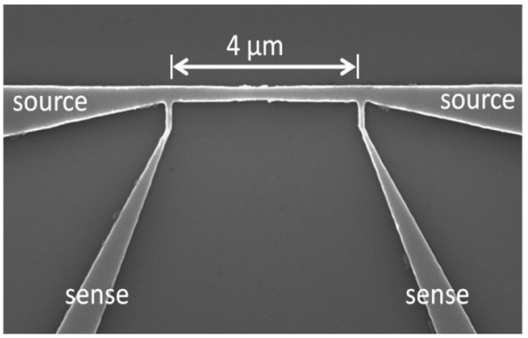

Figure 1. SEM image of the general sample design (without pads). Presented here is a 4000 × 300 nm bolometer.

comparable to or higher than other bolometers. The parameter chosen to be the reference, and hence kept constant, was either the Joule power dissipation or the bias current. In this paper, samples of different dimensions were measured. Our new and previous results are compared to study the influence of the dimensions of the sensing part on the bolometers' performance.

2. Sample fabrication and device physics

The sample design is presented in figure 1. We patterned a rectangular 'wire-like' structure, the sensing core of the bolometer, framed by four broadening leads with pads at their ends. The two outer leads are used for current bias while the two inner leads sense the voltage drop along the wire. We often refer to these samples as 'microheaters', as some of our previous work has focused on thermal emission from voltage biased, and thus hot, wires. Under modest bias (and thus low self-heating) the same samples work quite well as bolometers [10]. We therefore refer to our samples alternatively as heaters or bolometers, depending on the context.

Structures were patterned on photoresist-coated Si/SiO_2 (usually 105 nm) wafers in a single writing, using a state-of-the-art e-beam lithography system. Following development, 5 nm of adhesion layer and then 50 nm of platinum were deposited by sputtering. After lift-off, samples such as the one in figure 1 were obtained. We measured several sets of samples that were fabricated in different vacuum chambers and thus under slightly different conditions, both of them with platinum as the sensing layer. In our earlier work we used samples made at the Yorktown Heights laboratory of IBM. These samples have titanium as the adhesion material, and the wires have a fixed width of 300 nm for different lengths ranging from 300 nm to 19 μm. Another set of samples was fabricated at the Science Institute of the University of Iceland. These have chromium as the adhesion material, and the wires have widths ranging from 300 nm to 4 μm, and lengths from 300 nm to 15 μm. All samples from different sets have similar electrical properties. Their electrical resistance ranges from 6 to 300 Ω, depending on their lateral wire dimensions. The electrical resistivity has a value between 20 and 30 $\mu\Omega$ cm, a typical range for such metallic thin films. We chose to use platinum as the bolometric material as it has a rather low thermal conductance compared to other metals and a low $1/f$ noise. It has a temperature coefficient of resistance (TCR) of 0.002 K^{-1}. The average thermal conductance of our samples was calculated and we found an average value of 2×10^{-5} W K^{-1}. The details of our measurement setup are described in our previous paper [10].

2.1. Device physics

The performance of bolometers is expressed in terms of responsivity $\Re$ and specific detectivity D^*. Responsivity is defined as the ratio of the output signal generated to the incident power [1], hence it can be expressed in our case as:

$$\Re = (\Delta R \times I)/(\mathcal{A} \times \mathrm{Irr})\ [\mathrm{V\ W^{-1}}] \tag{1}$$

where I is the bias current, ΔR is the electrical resistance change, $\mathcal{A}$ is the area of the wire and Irr is the irradiance of the blackbody IR source.

Specific detectivity is the ultimate figure of merit to characterize the devices. It is expressed as [11]:

$$D^* = (\Re \times \sqrt{\mathcal{A}})/V_\mathrm{n}\ [\mathrm{cm\ Hz^{1/2}\ W^{-1}}] \tag{2}$$

where V_n is the root mean square (RMS) voltage fluctuation per unit bandwidth corresponding to the total voltage noise power spectral density S_n in the sample. It is evident from (2) that noise can severely limit the performance of the device. Concerning our devices, the noise estimation shows that $1/f$ noise is dominant. The calculation of the noise contribution was detailed previously [10].

2.2. Dependence of the responsivity and specific detectivity on sample dimensions

We can use (1) and (2) to study how the performance varies with the dimensions of the sensitive part of the sample. Our bolometers are essentially microscopic wires, as displayed in figure 1, with a well-defined length and width. If the samples are carefully designed then the change in temperature in the wire due to Joule heating by the electrical current is almost constant along the full length of the wire. In addition there is a temperature rise due to irradiation. The change in electrical resistance ΔR caused by these heating mechanisms may then be expressed as

$$\Delta R = R_0 \alpha \Delta T \tag{3}$$

where ΔT is the total temperature change with respect to a reference temperature with the corresponding electrical resistance value R_0. In this case the reference state is the biased wire and ΔT represents the temperature change due only to radiative heating. Here α is the temperature coefficient of resistance. We have found that α is independent of wire size within our size range, but can differ, for example, between different deposition techniques and thus film properties, or change upon annealing, presumably due to changes in grain size. However, for a given sample, after thermal cycling, α

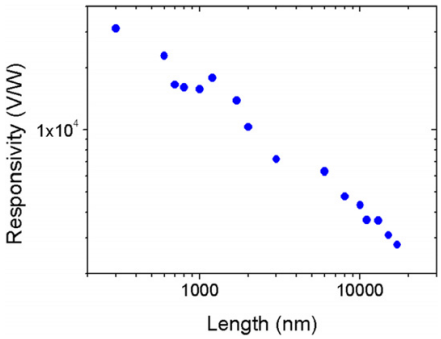

Figure 2. Responsivity of platinum bolometers, as a function of length. The Joule dissipation power is constant at 24 μW. The lengths of the samples range from 300 nm to 17 μm. The SiO_2 thickness is 105 nm.

remains constant. The wire electrical resistance can be written as

$$R = \frac{\rho \times L}{d \times W} \tag{4}$$

where ρ is the electrical resistivity, L and W are the length and width of the wire, respectively, and d is its thickness. Thus change in electrical resistance scales as

$$\Delta R \propto \frac{L}{W} \times \Delta T \tag{5}$$

assuming the sample thickness and electrical resistivity are constant. The former is fixed by sample design, the latter is expected to hold, as even in our smallest samples the sample width is at least two orders of magnitude larger than the electron mean free path. Thus we hardly expect to see a contribution from boundary scattering in the electrical resistance. Entering this into (2), and taking into account that the irradiance is constant and $\mathcal{A} = L \times W$, one obtains

$$\Re \propto (\Delta T \times I)/W^2 \tag{6}$$

for the responsivity. Noting that the energy absorbed from the incoming radiation is expected to be proportional to the sample area $L \times W$, and that the thermal conduction to the surroundings also scales the same way, it is reasonable to assume ΔT is constant for samples of unlike area. We are left with the simple relation

$$\Re \propto \frac{I}{W^2}. \tag{7}$$

Turning to the specific detectivity in (2), bearing in mind that metal film resistors such as our samples are limited by $1/f$ noise, we find:

$$D^* = \Re\sqrt{\mathcal{A}}/V_n \propto \Re \times \sqrt{LW} \times \sqrt{\frac{W^3}{LI^2}} \propto \Re \times \frac{W^2}{I} \tag{8}$$

with V_n the root mean square voltage fluctuation per unit bandwidth corresponding to the total voltage noise power spectral density in the sample. This results in

$$D^* \propto \text{constant}. \tag{9}$$

If the wire width is kept constant while its length is varied, the responsivity will be directly proportional to the bias current, as evident from (7). However, neither lateral dimensions of the sample nor bias current affect the specific detectivity. The evolution of performance with bias current has been extensively studied in a previous work [12].

Lately, we used a fixed bias current instead of a fixed power as reference values. Each of the samples was powered successively with 0.5, 1, 1.5 mA, etc. In this case, the self-heating contribution is not constant for all heaters and rapidly rises up to tens of kelvin. Despite this strong contribution of self-heating, a change in temperature is still sensed by the bolometers when they are exposed to the IR signal.

3. Influence of length on bolometer performance

It is interesting to compare the scaling relation (7) with results from a series of samples of constant width W. Figure 2 displays our previous results [10] from one set of samples, reproduced on a logarithmic scale. Note that the data look almost the same, apart from a multiplicative constant. This is in agreement with (7), which is directly proportional to I when W is constant, with no explicit dependence as discussed above. The length dependence appears through the current dependence at fixed power, as discussed below.

As illustrated in this figure, it is clear that shorter samples reach a better performance than the longer ones. The shorter sample of 300 × 300 nm^2 reaches a maximum responsivity of 3.1 × 10^4 V W^{-1}, an order of magnitude greater than for the longer samples of the same width. Interestingly one can see a local maximum of responsivity for the $L = 1200$ nm sample.

These samples were biased at a constant Joule dissipation power of $P_{\text{Joule}} = 24$ μW. This value limits the self-heating $\Delta T_{\text{self-heating}}$ to between 0.3 and 8.6 K, depending on the sample length. In comparison, the IR source causes a rise in temperature of around 1 K, so in this case bolometers detect a temperature change of less than one tenth of their own self-heating temperature rise. The bias current was calculated as follows:

$$I = \sqrt{\frac{P_{\text{Joule}}}{R_0}} \tag{10}$$

and the corresponding DC bias current was applied by a current source. Since P_{Joule} is kept constant, the bias current can be expressed as $I \propto \sqrt{1/L}$. Hence for responsivity one can find $\Re \propto 1/L$. Shorter samples were then biased by a larger current compared to the longer samples. The DC current values ranged from 1.9 to 0.3 mA, respectively, for the smaller sample, 300 × 300 nm^2, and the longer sample, 17 000 × 300 nm^2. Figure 3(a) presents the data of figure 2 as a function of $L^{-1/2}$, in an attempt to account for bias current changes.

In figure 3, the orange line represents the linear increase of the responsivity as a function of $L^{-1/2}$, as one would expect from theory. The responsivity of longer samples, with lengths

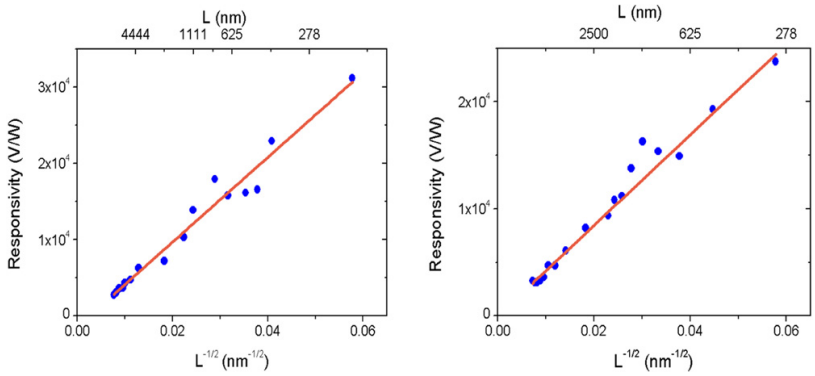

Figure 3. (a) and (b) Responsivity of platinum bolometers as a function of the square root of the inverse of their length [8]. Bias power kept constant at 24 μW. The orange line is a linear fit based on the longest samples' data. (a) Length ranging from 300 nm to 17 μm (data from figure 2), with a width of 300 nm and a SiO_2 thickness of 100 nm. (b) Length ranging from 300 nm to 19 μm, with a width of 300 nm and a SiO_2 thickness of 70 nm.

from 19 to 8 μm, does indeed increase linearly. Due to their macroscopic size, they are more likely to adhere to the simple scaling arguments made above. We used these data points to build the linear fit, and then extended it to the smaller lengths. This fit then represents the responsivity values expected for shorter samples according to theory. It appears that our measured data agrees with the suggested scaling. This means that shorter samples display a larger responsivity, mainly because of their larger bias current. Albeit this general fit to the scaling, there is a visible digression of measured responsivity for samples whose lengths range between 800 nm and 2 μm. In figure 3(a), a local maximum in responsivity is reached by the 1200 nm long bolometer.

We have repeated these measurements on another set of samples, made at the University of Iceland. There are some structural differences: the adhesion layer is Cr rather than Ti, and the SiO_2 thickness is 70 nm as opposed to 150 nm in figure 3(a). The responsivity for this set of samples is presented in figure 3(b).

Data from figure 3(b) exhibit a similar linear trend as before, confirming the scaling arguments, also with a similar digression having a local maximum of responsivity centered on $L = 1100$ nm. The responsivity at the local maxima is improved by 29% and 36% compared to the linear fit in figures 3(a) and (b) respectively.

The deviation from linearity in figures 3(a) and (b) represents an impact of the length of the wires on the bolometer performance in the wavelength range roughly from 600 to 2000 nm. We believe these local enhancements to be an antenna resonance. With our blackbody IR lamp having a λ_{peak} of 2.74 μm, we are at the threshold between optical and near-infrared frequencies. Classical antenna theory predicts a half-wavelength resonance at $L = \lambda/2 = 1370$ nm. Our experimental resonant lengths, 1100 nm and 1200 nm, are respectively 19.7% and 12.4% shorter. Recently, several experimental studies [13, 14] on metallic antennas showed that antenna resonances occur at lengths up to 20% shorter than predicted by classical antenna theory. A new model for a revised effective wavelength scaling for metallic rod antennas in the optical frequency regime was introduced by Novotny [15]. Our results seem to be in agreement with other experimental findings and with this revised optical antenna model. One should be careful in this comparison, however, as our samples are 'open-ended' antennas. This may result in a slightly longer effective 'optical length' than the physical length we name them by. Both experimental work [16] and the refined model [17] have demonstrated the importance of taking into account the optical properties of the surroundings. In particular we have a thin SiO_2 layer (105 nm), which will affect the antenna resonance condition in our samples. This suggests that the incoming infrared radiation gives rise to plasma oscillations in our samples, contributing within a specific bandwidth to the absorption.

4. Influence of width on bolometer performance

We have also studied the influence of width on bolometer performance. Following the same procedure as stated above, samples with different lengths (between 300 nm and 15 μm) and widths (between 300 nm and 4 μm) were fabricated on a commercial Si/SiO_2 (105 nm) substrate and measured. The lengths were specifically chosen to avoid the resonance range presented above. After fabrication, their real dimensions were measured by SEM. On average, the measured dimensions deviated slightly from nominal values, for example, due to proximity effects in e-beam lithography. In all our calculations we use the measured dimensions; however, we will refer to the samples by using their designed size. Also, to simplify the reading, a sample designed to have, for example, a width of 300 nm and a length of 1500 nm will be referred to as W300–L1500.

Each sample was measured several times with increasing DC bias currents: 0.5, 1, 1.5 mA, etc. After measuring the change in a sample's electrical resistance change (ΔR) upon exposure to IR illumination and using (1) and (2), one is

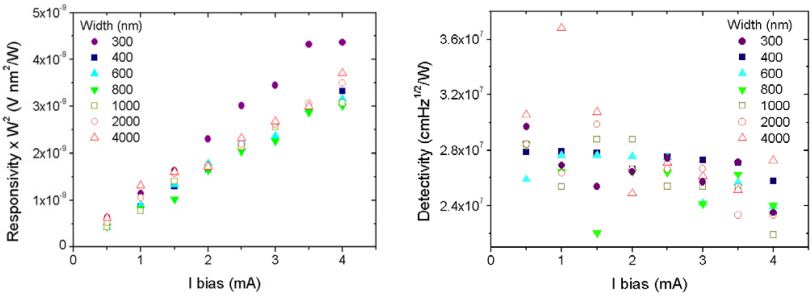

Figure 4. (a) and (b) Responsivity and specific detectivity of L9000 bolometers as a function of width and bias current. The data are plotted taking into account the width scaling expected according to (7) and (9) on the y-axes. The width ranges from 300 nm to 4 μm and the SiO_2 thickness is 105 nm.

able to calculate its responsivity and specific detectivity. Narrower samples with a width of 300 nm and a length of 9 μm reach a responsivity of 4.8×10^4 V W^{-1} when biased with a 4 mA current, and a specific detectivity of 2.7×10^7 cm Hz$^{1/2}$ W^{-1}. The results presented in figures 4(a) and (b) for a representative series of samples of fixed length of 9000 nm (L9000) appear to adhere to the scaling in (7) and (9), with a linear dependence on bias current for the responsivity. As the sample's width increases, its responsivity decreases, whereas the detectivity stays constant. This is a fundamental result of this study. Responsivity drops by more than two orders of magnitude, as the width of the samples vary from W300 to W4000.

As seen in figure 4(a), the larger samples tend to display a similar responsivity for each bias current value (accounting for the width dependence), but W300 samples appear stand out by displaying a higher responsivity. In figure 4(b), the specific detectivity is clearly not affected by either the bias current or the sample's width. This denotes two things: an overall higher performance for samples with a width of 300 nm, and also a departure from the simple scaling theory for such narrow samples. This suggests that for such reduced dimensions, the area may not be the main factor influencing the performance of the bolometers.

The same analysis was carried out for a large range of samples, with varying lengths and widths. The width effect observed for 9 μm-long samples is confirmed for samples of different lengths as well. Therefore, for a specific width and current, the experimental results of all lengths were averaged, to reduce fluctuations. (Samples with out-of-range values were excluded from the calculations, such as the W300–L300 and W2000–L3000 samples, which presented an unexplained higher performance.) Figure 5 displays the averaged responsivity, encompassing data for all our samples. Narrower samples with a width of 300 nm reach an averaged responsivity of 5.1×10^4 V W^{-1} when biased with 4 mA. Specific detectivity has an averaged value of 2.7×10^7 cm Hz$^{1/2}$ W^{-1}, with some samples reaching a value of 3×10^7 cm Hz$^{1/2}$ W^{-1}.

According to (7), figure 5 should display the same linear increase for all widths. This is evidently not the case. All the widths tend to fall together with the same linear increase

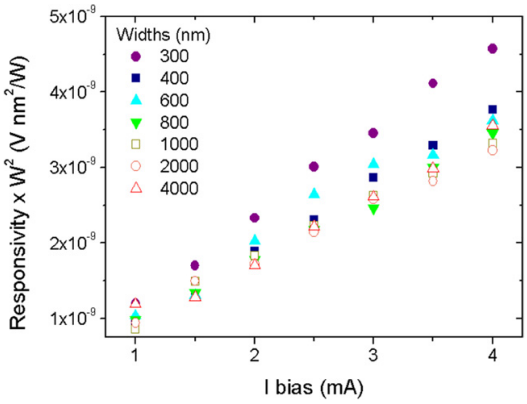

Figure 5. Responsivity. W^2 of bolometers as a function of bias current. Lengths range from 900 nm to 15 μm, and widths from 300 nm to 4 μm. Data from several length samples with the same width was averaged.

with the bias current, but some narrow widths tend to increase faster than the main trend. In figure 5, W300 obviously stands apart from the main trend, while W400 and W600 break slightly away from the main cluster. The rest of the samples whose width is 800 nm or larger are close together, with the same trend. This suggests that samples with a width lower than 800 nm do not have the same behavior as wider bolometers, and that their responsivity is enhanced beyond the scaling predictions.

The question arises as to why the responsivity is better for samples with widths below 800 nm. When looking at the data, one can see that the elevation in the electrical resistance of W300 samples due to IR illumination (ΔR) is more than for wider samples. As (2) states that responsivity is the ratio of the generated output signal ($\Delta V = \Delta R \times I$) to the incoming power ($\mathcal{A} \times$ Irr), this leads to a high responsivity value for W300 samples.

The electrical resistance of samples is proportional to $1/W$, as presented in (4). Hence narrow samples present a higher electrical resistance compared to their wider counterparts. Our samples have an electrical resistance

varying between hundreds of ohms for W300 samples to tens of ohms for W4000. Plotting the wire electrical resistance of same length samples as a function of $1/W$ reveals that the electrical resistance is higher than expected when the sample's width is lower than 800 nm. This may come from boundary scattering, which causes an increase in the wire electrical resistance. As the width is reduced, carriers are more and more scattered by the edges of the film, causing an increase of the electrical resistance. In our case, we measured an electrical resistance 30% higher than expected. This could also contribute to the high ΔR of narrow samples. Further, ΔR depends on the absorption properties of the sample. This means that samples with a width lower than 800 nm may absorb more IR than their wider counterparts. If edge scattering and enhanced absorption both contribute to a higher ΔR in narrow samples, the influence of each is not yet clearly defined.

By Kirchoff's law of thermal radiation, a parallel can be made between absorption and emission properties. In a previous paper [17] the thermal emission properties of similar samples (called 'heaters') were thoroughly studied, and one can compare those results with our findings on absorption. In this paper, the heater emission was studied along two polarization axes, either perpendicular or parallel to the long axis of the wire. The samples had a fixed length of 8 μm and a width varying between 200 nm and 8 μm. The experiments show that when the width is below 2 μm there is a blue-shift in the perpendicular polarized part of the emitted IR spectrum. Also, there is an extinction of emission along this polarization as the samples are made narrower. This continues to the point where, for samples narrower than 600 nm, there is almost no detectable IR emission perpendicularly polarized. This means that such samples mostly emit IR with a polarization parallel to their long axis.

Also, one would think that in this case the general intensity of emitted IR should decrease with the width, as according to the Stefan–Boltzmann law the total radiation should scale with the sample's surface area. The previous study [17] reveals that this is not the case. For larger samples, the emitted intensity for both polarizations decreases with the width, from 8 to 1 μm. For narrower samples, as the intensity along the perpendicular axis decreases drastically, the intensity along the parallel axis stabilizes at a constant value. This clearly means that at this dimension range, the sample size is no longer the dominant factor in the radiation intensity. That work showed that, at sub-wavelength widths, the emission properties of such heaters are modified, as we present in this paper for the absorption properties of similar samples.

Our present study does not take into account the polarization of the incoming infrared light, but the work mentioned above introduces the fact that the thermal emission spectra are strongly polarized when the width is narrowed. Hence we believe that the bolometers presented here become increasingly selective in the polarization of light they absorb as their width is reduced. This suggests that for samples with widths larger than 800 nm, the same amount of light with a polarization parallel and perpendicular to their long axis is absorbed. As the width narrows, the amount of parallel polarized light absorbed stays constant, despite the fact that the sensing area is smaller. Finally, W300 samples probably absorb very little or no perpendicularly polarized light. If this is verified, it is quite remarkable that W300 samples display an enhanced absorption, despite the fact that they only partially absorb the incoming infrared radiation.

5. Conclusion

As a conclusion, we have studied the performance of thin-film bolometers of sub-wavelength lateral dimensions and compared them using simple scaling arguments. Our results show that both the length and width of the bolometer sensing area influence their performance. From macroscopic models, responsivity should be linear with the bias current, whereas specific detectivity should stay constant. However, there is an indication that a certain range of lengths is more sensitive to IR illumination, when antenna-like resonances enhance the infrared absorption. Furthermore, this study demonstrates the critical role played by the width of the samples. The performance is drastically increased when the wire is narrowed, departing from the macroscopic scaling relations. For bolometers with a width under 800 nm, the sensing area is no longer the dominant factor on sensitivity. Edge scattering and enhanced absorption amplify the performance of narrow samples. Also, it is believed that for this dimension range, only a part of the IR irradiation is actually picked up by the bolometer. However, such small samples display a typical responsivity of 10^4 V W^{-1} and a specific detectivity of 10^7 cm Hz$^{1/2}$ W^{-1}. This performance is comparable to the latest achievements reported in the literature. We believe these findings could lead the path towards the improved engineering of graphene sheets for a maximized infrared sensing performance.

Acknowledgments

This research was funded in part by the Icelandic Research Fund and the University of Iceland Research Fund.

References

[1] Rogalski A 2003 *Infrared Detectors* 2nd edn (Boca Raton, FL: CRC Press)
[2] Fieldhouse N, Pursel S M, Horn M W and Bharadwaja S S N 2009 Electrical properties of vanadium oxide thin films for bolometer applications: processed by pulse DC sputtering *J. Phys. D: Appl. Phys.* **42** 055408
[3] Saxena R S, Bhan R K, Jalwania C R and Khurana K 2008 Effect of excessive bias heating on a titanium microbolometer infrared detector *IEEE Sens. J.* **8** 1801–4
[4] González F J and Boreman G D 2005 Comparison of dipole, bowtie, spiral and log-periodic IR antennas *Infrared Phys. Technol.* **46** 418–28
[5] Yoneoka S, Liger M, Yama G, Schuster R, Purkl F, Provine J, Prinz F B, Hove R T and Kenny T W 2011 ALD-metal uncooled bolometer *MEMS 2011 (Cancun)*
[6] Niesler F B P, Gansel J K, Fishbach S and Wegener M 2012 Metamaterial metal-based bolometers *Appl. Phys. Lett.* **100** 203508

[7] Aliev A E 2008 Bolometric detector on the basis of single-wall carbon nanotubes/polymer composite *Infrared Phys. Technol.* **51** 541–5
[8] Xia F, Mueller T, Lin Y M, Valdes-Garcia A and Avouris P 2009 Ultrafast graphene photodetector *Nature Nanotechnol.* **4** 839–43
[9] Bonaccorso F, Sun Z, Hasan T and Ferrari A C 2010 Graphene photonics and optoelectronics *Nature Photon.* **4** 611–22
[10] Renoux P, Jónsson S Æ, Klein L J, Hamann H F and Ingvarsson S 2011 Sub-wavelength bolometers: uncooled platinum wires as infrared sensors *Opt. Express* **19** 8721–7
[11] Chen C, Yi X, Zhao X and Xiong B 2001 Characterizations of VO_2-based uncooled microbolometer linear array *Sensors Actuators* A **90** 212–4
[12] Renoux P, Beauny A, Klein L J, Hamann H F and Ingvarsson S 2012 Thin-film platinum nanowires as sub-wavelength bolometers *Proc. SPIE* **8261** 82610I
[13] Bryant G W, García de Abajo F J and Aizpurua J 2008 Mapping the plasmon resonances of metallic nanoantennas *Nano Lett.* **8** 631–6
[14] Neubrech F, Kolb T, Lovrincic R, Fahsold G, Pucci A, Aizpurua J, Cornelius T W, Toimil-Molares M E, Neumann R and Karim S 2006 Resonances of individual metal nanowires in the infrared *Appl. Phys. Lett.* **89** 253104
[15] Novotny L 2007 Effective wavelength scalind for optical antennas *Phys. Rev. Lett.* **98** 266802
[16] Fumeaux C, Gritz M A, Codreanu I, Schaich W L, González F J and Boreman G D 2000 Measurement of the resonant lengths of infrared dipole antennas *Infrared Phys. Technol.* **41** 271–81
[17] Au Y Y, Skulason H S, Ingvarsson S, Klein L J and Hamann H F 2008 Thermal radiation spectra of individual subwavelength microheaters *Phys. Rev.* B **78** 085402

Paper IV

Optimisation of performance for platinum nanowires as sub-wavelength bolometers

P. Renoux
D. Charpentier
S. Augé
S. Ingvarsson

Proceedings of SPIE, **8868**, 88680C (2013).

Optimisation of performance for platinum nanowires as sub-wavelength bolometers

Pauline Renoux [a†], Dorine Charpentier[b], Sylvain Augé[b] and Snorri Ingvarsson [a‡]
[a]Science Institute, University of Iceland, Dunhaga 3, Reykjavík IS-107, Iceland
[b]INSA Toulouse, Department of Physics, 135 avenue de Rangueil, 31077 Toulouse, France

ABSTRACT

Electronic properties and sensitivity of metallic bolometers were studied as a function of thin-film thickness in the active area. Our devices are made of platinum and chromium, with an active area of lateral dimensions 1 μm by 300 nm. The thickness of the metallic film was varied between 3.3 nm and 82.3 nm. Temperature coefficient of resistance and resisitvity were characterized, and are respectively increasing and decreasing with the thickness increasing. A threshold thickness of 40 nm is revealed where both parameters reach a constant value. Responsivity and detectivity were evaluated, unveiling the importance of 1/f noise. Responsivity reaches a maximum value of $2x10^5$ $V.W^{-1}$ for bolometers with a 7.5 nm thickness. Detectivity keeps a constant value of $1x10^8$ $cmHz^{1/2}/W$ for samples thicker than 40 nm, before dropping considerably as the thickness is decreased. This loss in detectivity is believed to be due to the prominence of 1/f noise in such thin samples.

Keywords: Thin-film devices and applications, Thermal (uncooled) IR detectors, Micro/nano bolometers, Platinum

1. INTRODUCTION

Infrared detectors have been studied thouroughly during the last decades. Development of microfabrication and lithography techniques has given new ways to improve their performance and selectivity. They can generally sense wavelengths from near-infrared region (several μm) to far-infrared one (up to 1 mm)[1]. Such versatile sensors are now used in various areas, from military applications to everyday use. Although two very desirable qualities are a good sensitivity and a fast response, the cost and ease of use play a role increasingly important.

The basic operating principle relies on the change of electrical properties of the sensor upon absorption of the infrared (IR) radiation. There is two categories of devices, each one having advantages and drawbacks. Photon detectors, composed of semiconductor active layers, rely on the excitation of electrons across a small band gap by IR photons. They present a high signal-to-noise ratio and a fast time response, but are selective in wavelength. Typically they involve a complex fabrication and packaging process that can lead to high prices and require careful use. Also, they are operated in vacuum due to the small band gap, hence adding some inconvenience. Thermal detectors are based on a change of electrical property (e.g. electrical polarisation or resistance) due to heating by the incident IR radiation. They have a simpler design and can be operated at room temperature without any need of encapsulation or specific apparatus. However, they often display a lower performance and slower time response. Bolometers are thermal sensors whose electrical resistance changes upon IR radiation. They have been intensively studied and various materials and designs have been tested, such as vanadium oxide[2], semiconductors[3], metals[4] or even graphene[5] or carbon nanotubes[6]. Also they can be coupled to antennas to improve selectivity [7,8].

† pauline@hi.is
‡ sthi@hi.is

Infrared Sensors, Devices, and Applications III, edited by Paul D. LeVan, Ashok K. Sood, Priyalal S. Wijewarnasuriya, Arvind I. D'Souza, Proc. of SPIE Vol. 8868, 88680C
 · doi: 10.1117/12.2022287

In this paper, we present thermal bolometers made of platinum litographically patterned as micro-stripes. They have a very simple design and fabrication process. Previously, we studied the effect of several physical parameters on the sensing performance: changing the active area's in-plane geometry[9,10], the thickness of the silicon dioxide underlayer or the bias current[11]. In this paper we studied the influence of the platinum's thickness on several electrical parameters and sensing performance. Thin-films down to only several monolayers of platinum were fabricated, leading to devices with dimensions as Atomic Layer Deposited-based bolometers[12].

2. FABRICATION AND DEVICE PHYSICS

The active part of our metallic microbolometers are simple rectangular-shaped thin-films of platinum, framed by four broadening leads with contact pads at their ends. Thanks to this design it is possible to bias the sample with a DC current while measuring accurately its voltage.

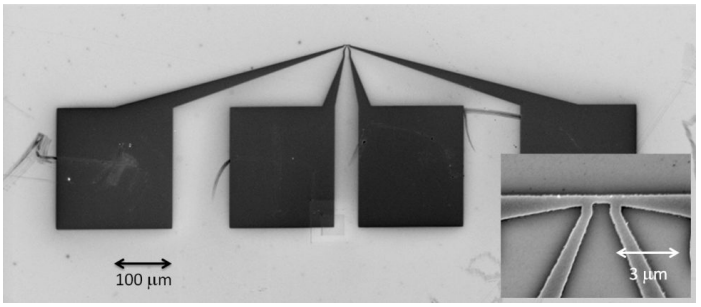

Fig. 1. SEM picture of a metallic bolometer patterned via e-beam lithography. Four microsized contact pads connected to biasing and sensing leads are framing a central metallic constriction that is the active area of the device. Inset is a close-up of the metal constriction.

Fabrication of such samples is quick and straightforward. Commercial Si/SiO_2(100 nm) wafers were used as a substrate. After a thourough cleaning procedure followed by a PMMA resist spin deposition, samples' design was patterned using state-of-the-art e-beam lithography. Developed chips were cleaned and inserted in a DC sputtering machine where they undergo a deposition of chromium and platinum. After lift-off, we obtained several chips of samples with a uniform metallic film on all the structure. The thickness of chromium and platinum layers for each deposition round was measured via grazing incidence X-ray diffraction (GIXRD) measurements. Chromium is used here as an adhesion layer; we used either 1 nm or 5 nm to secure the adherence of platinum on the substrate.

We deposited 14 chips with various thicknesses of platinum, ranging from 2 nm to 80 nm. On each chip, four identical samples were patterned, hence 56 samples were measured in total. We designed the active part with lateral dimensions of 1 µm long by 300 nm wide. The samples were exposed to a ceramic blackbody source at a temperature of 1060 K. This corresponds to a broad near- to mid-IR spectrum spanning from 2 µm to 8 µm, with a peak wavelength of λ_{peak} = 2.74 µm. Thus the dimensions of the bolometer´s sensing area are significantly smaller than the wavelength of the detected IR radiation.

With a 4-probe setup, samples were biased with a DC current through the outer leads, while their voltage was measured by a Keithley 2400 source-meter controlled by Labview. Upon IR illumination, a voltage increase is measured that corresponds to the heating effect in the active area. Samples have a base resistance between 10 Ω and 1 kΩ, dependent on their thickness. Measured thin film thicknesses and respective electrical properties are summarized in Table 1.

Two main figures of merit are used to characterize and assess the performance of IR sensors, namely the responsivity and the detectivity. Responsivity is simply the ratio between the output voltage of the device and the power received from the IR source. Adapted to our experiment, it is expressed as[9]:

$$\Re = {\Delta R \times I}/{\mathcal{A} \times Irr} \qquad [VW^{-1}] \tag{1}$$

where I is the bias current, ΔR is the resistance change, $\mathcal{A}$ is the area of the wire and Irr is the irradiance of the blackbody IR source.

Detectivity is the ultimate figure of merit to characterize the devices. It is expressed as[13]:

$$D^* = {\Re \times \sqrt{\mathcal{A}}}/{V_n} \qquad [cmHz^{1/2}W^{-1}] \tag{2}$$

where V_n is the root mean square (RMS) voltage fluctuation per unit bandwidth corresponding to the total voltage noise power spectral density S_n in the sample. It takes into account the intrinsic and extrinsic noise sources in the samples. It is generally assumed that such devices are Johnson-noise limited. Measuring the noise level in low-resistance samples such as ours can prove quite challenging. Hence we estimated the noise contribution by taking into account three main sources: Johnson-Nyquist noise, thermal conductance noise and 1/f noise. Details on the two aforementioned noise contributions calculation methods can be found in our previous work[9]. The calculation of the 1/f noise contribution is further explained in the last part of this paper.

3. INFLUENCE OF FILM THICKNESS OF ELECTRICAL PARAMETERS AND BOLOMETRIC PERFORMANCE

3.1 Temperature coefficient of resistance (TCR) and electrical resistivity

The temperature coefficient of resistance (TCR) directly affects the sensitivity of bolometers. It is expressed in K^{-1} and conveys the amplitude of resistance change upon IR illumination. It is evident from (1) that it is desirable to maximise ΔR in order to reach a higher responsivity. Metallic bolometers typically have a TCR value in the $10^{-3}\,K^{-1}$ range, a rather low value compared to other types of bolometric materials. The TCR value is a characteristic of the film and is greatly influenced by its thickness, thus one could find interesting to study the evolution of our samples' TCR values. We measured the resistance of each sample while heating it on a hot plate, from room temperature to 80°C. In this range of temperature, the resistance can safely be approximated by the linear equation:

$$R = R_0\,(1 + \alpha \Delta T) \tag{3}$$

with R_0 the room-temperature resistance of the sample, ΔT the rise in temperature above room temperature, and α the TCR. The TCR value of each sample with a specific thickness was extracted from the measurements, and Fig. 2 displays the results:

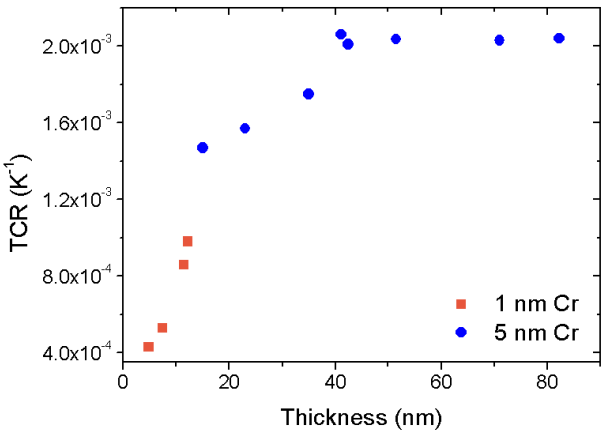

Fig. 2. Evolution of the temperature coefficient of resistance of bolometers with thickness of the metallic thin-film. Red squares and blue circles are for samples with a chromium adhesion layer of 1 nm and 5 nm respectively.

One can see that the TCR is constant for samples with a thickness equal to 40 nm or more, where it has a value of about $2x10^{-3}$ K^{-1}. This value is consistant with litterature for platinum thin-films[14]. This value for thin-films is around a half of the bulk platinum TCR value, reported[15] as $3.85x10^{-3}$ K^{-1}. However, as the thickness goes below 40 nm, the TCR value starts to decrease. A lowest value of $4x10^{-4}$ K^{-1} is reached by the thinnest measured sample, of a total thickness of 4.8 nm. It is lower by a factor of five compared to the thin-film "plateau" value of $2x10^{-3}$ K^{-1}, for a film of one tenth of the thickness. This pattern in TCR evolution with thickness was already reported by Zhang and al.[16], where the TCR of platinum thin-films is increasing from $4x10^{-4}$ K^{-1} (Pt thickness 15 nm) to a constant value of $1x10^{-3}$ K^{-1} (Pt thickness 30 nm and above).

As aforementioned, the TCR is strongly linked to the film thickness, i.e. to its grain size. In a previous work[17], the grain size of similar samples with a thickness of 55 nm was estimated to be 14 nm. Although this value depends on film thickness e.g., it gives an idea of the grain size obtained by our growth process. As the film thickness is reduced, the grain size decreases. This leads to an increase of conduction electron scattering, when they strike encounter grain boundaries. This phenomenon triggers a jump of the resistivity as well as a decrease of the TCR. In order to confirm this effect, the electrical resistivity of all samples was also measured.

After measuring the IV characteristics of our samples, their electrical resistivity was calculated according to:

$$\rho = \frac{hWR}{L} \tag{4}$$

with ρ the electrical resistivity, R the electrical resistance and L, W and h respectively the length, width and thickness of the active area of the bolometer. Fig. 3 below displays the evolution of resistivity with thickness:

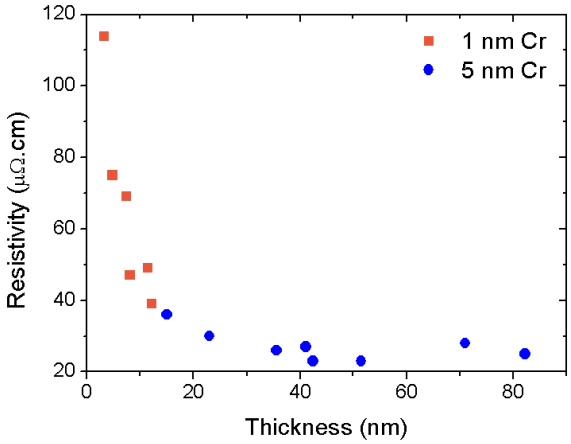

Fig. 3. Resistivity of bolometers' thin-films as a function of their thickness. Red squares and blue circles are for samples with a chromium adhesion layer of 1 nm and 5 nm respectively.

It is well known that the electrical resistance of thin-film increases greatly as their thickness decreases[18]. In this experiment, samples with a thickness of 3.3 nm have a resistance of 1 kΩ whereas thicker ones present a resistance down to 10 Ω (see Table 1). Hence there is a strong increase in our experimental electrical resistivity for thinner samples, due to increasing surface scattering. In Fig. 3, this is clearly seen. Resistivity is maximum for the 3.3 nm-thin sample, at 114 μΩ.cm, and then decreases with the thickness increasing. Resistivity for samples with a thickness of 40 nm or higher is constant around 23 μΩ.cm. This value is twice the bulk value of Pt, which is 10 μΩ.cm, and has been previously reported in previous experiments made by our group[17].

Table 1. Summary of thin-films dimensions (both nominal and measured) and corresponding electronic properties. Platinum thickness was measured via GIXRD, and added to nominal thickness of the chromium adhesion layer to obtain the total thickness h. TCR, resistivity and bias current are given for each chip.

Nominal h_{Pt} (nm)	Nominal h_{Cr} (nm)	Measured h_{Pt} (nm)	Total h (nm)	R_0 (Ω)	TCR (x10^{-3} K^{-1})	ρ (μΩ.cm)	I_b (mA)
2	1	2.3	**3.3**	1000	.	114	0.3
4	1	3.8	**4.8**	520	0.43	75	0.5
6	1	6.5	**7.5**	300	0.53	69	1
8	1	7.1	**8.1**	190	.	47	1
10	1	10.5	**11.5**	140	0.86	49	1
12	1	11.2	**12.2**	100	0.98	39	1
10	5	10	**15**	83	1.47	36	1
20	5	18	**23**	43	1.57	30	1
30	5	30.6	**35.6**	25	.	26	1
40	5	36.1	**41.1**	22	2.06	27	1
50	5	37.5	**42.5**	18	2.01	23	1
60	5	46.5	**51.5**	15	2.035	23	1
70	5	66	**71**	13	2.03	28	1
80	5	77.3	**82.3**	10	2.04	25	1

3.2 Responsivity

Responsivity is directly influenced by the DC bias current, as shown in (1). Hence it seems logical to keep the same bias current value for all the samples during the measurement of the bolometers' response to IR illumination. However, the current must also be limited in order to avoid excessive self-heating due to Joule dissipation. When samples are subjected to high current density, they undergo annealing that will change their electrical characteristics. Furthermore, they are damaged by electromigration, leading to their steady state destruction. Through previous experiments, it was found that a current density lower than 10^7 A.cm^{-2} is preventing any electromigration phenomena. With this in mind, we could set a suitable bias current value of 1 mA for most of the samples. However, the two thinnest samples having a resistance higher than 500 Ω, they had to be biased with a lower current. DC bias current values used for each samples are specified in Table 1.

Still from (1), we can define an expected evolution of responsivity as a function of the thin-film thickness. With both length L and width W being the same for all samples, only $\Delta V = \Delta R \times I_b$ is affected by the thickness h of the film. If I_b is constant for all samples, one finds that responsivity is proportionnal to the inverse of the film thickness (1/h). Responsivity of all samples is displayed below in Fig. 4, as a function of the inverse of thickness:

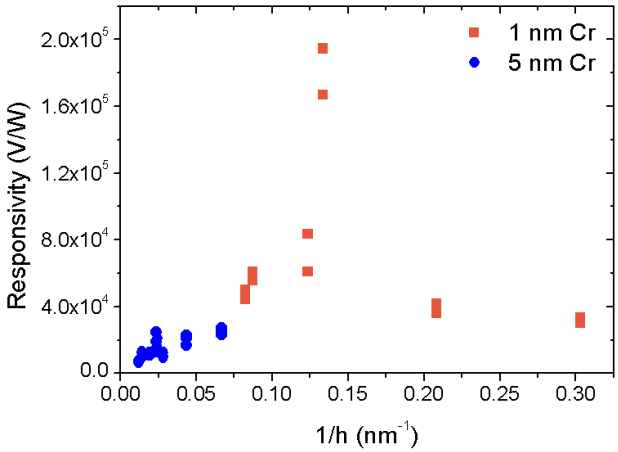

Fig. 4. Responsivity of bolometers as a function of the inverse of the thin-film thickness. Red squares and blue circles are for samples with a chromium adhesion layer of 1 nm and 5 nm respectively. Bias current is set at 1 mA for all samples except the two thinnest samples (4.8 and 3.3 nm) who were biased with 0.5 and 0.3 mA respectively.

For samples with a thickness from 77.3 nm to 12.2 nm, responsivity is increasing linearly with their thickness decreasing. However, there is an increase of responsivity when the thickness goes from 12.2 nm to 7.5 nm, with a peak responsivity of almost 2x10^5 V.W^{-1} reach by this last sample. The two finnest samples present a reduced responsivity compared to the 7.5 nm-thick sample, but one has to remember that they are biased by a lower bias current. It is likely that if powered with a current at 1 mA, they would display a slightly larger responsivity value (without exceeding 1.2x10^5 V.W^{-1} though). Through this experiment one can conclude that 7.5 nm is an optimum thickness for such bolometers, having a maximized responsivity.

3.3 Detectivity

From (2), one can see that the responsivity is taken into account, as well as the noise in the device. Therefore, detectivity is also influenced by the film thickness. In metallic samples, the Johnson-Nyquist noise is generally dominant, except when at very low frequency operation. However, when dealing with such thin samples, the contribution of the 1/f noise gets stronger. Calculation models for the 1/f noise in metal devices has been extensively studied in the past. While the empirical formula introduced by Hooge[19] is widely used, it doesn´t take into account the sample´s resistivity. Fleetwood et al.[20] introduced a revised Hooge formula defining a minimum 1/f noise level using the resistivity:

$$S_{\frac{1}{f},\min} = \frac{\rho_0}{\rho}\frac{V^2}{Nf^{\alpha}}$$

where ρ_0 is a constant value of $6\text{x}10^{-3}$ μΩ.cm, ρ the resistivity of the sample, N its number of free carriers in the active area and V its output voltage. In our case, we set f = 1 Hz as we work in the DC regime. This is a standard procedure and is commonly used when using frequency-dependant formulas while working with constant currents. Fig. 4 below displays the detectivity of our samples as a function of their film thickness:

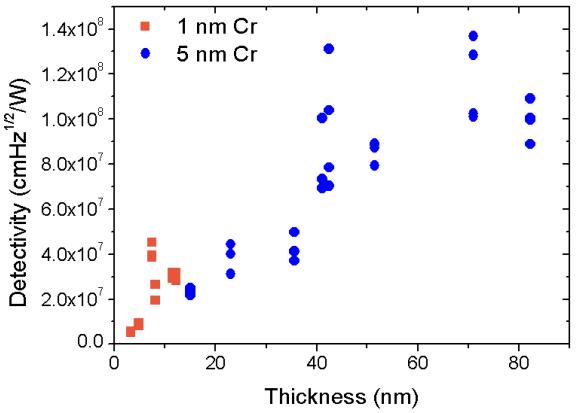

Fig. 4. Evolution of detectivity with the thin-film´s thickness. Red squares and blue circles are for samples with a chromium adhesion layer of 1 nm and 5 nm respectively. Bias current is set at 1 mA for all samples except the two thinnest samples (4.8 and 3.3 nm) who were biaised with 0.5 and 0.3 mA respectively.

Detectivity is increasing with the thickness of the thin-film, although for films of 40 nm thick and more, detectivity seems to stabilize towards a max value of $1\text{x}10^8$ $\text{cmHz}^{1/2}/\text{W}$. Thinnest samples display the lowest detectivity at $5\text{x}10^6$ $\text{cmHz}^{1/2}/\text{W}$, despite a large electrical resistance value. This corresponds to an increase of a factor 20 in detectivity when the thickness goes from 2.3 nm to 82.3 nm. The loss in detectivity with decreasing thickness is mainly due to the strong increase of 1/f noise in thin-films.

As an example, in the thickest sample the 1/f noise contribution is a 10^2 times higher than its Johnson-Nyquist counterpart. In the thinnest ones, this factor is up to a factor of 10^4. Thus the 1/f noise is the dominant noise factor in such samples, partly because of their increased resistivity. One way to reduce the 1/f noise contribution would be to use a lower bias current; however using 0.1 mA instead of 1 mA would only reduce the 1/f noise by a factor of 10^2. In this situation, Johnson-Nyquist noise and 1/f noise would be equivalent for thick samples, and 1/f noise still larger by a factor of 100 compared to the Johnson noise for the thin ones.

CONCLUSION

In conclusion, electronic properties and sensitivity of metallic bolometers were studied as a function of their film thickness. TCR and resisitivity respectively decreased and increased by a factor of 5 when the thickness was decreased from 82.3 nm to 3.3 nm. Bolometers as thick as 40 nm or thicker display a constant TCR and resistivity of respectively $2x10^{-3}$ K^{-1} and 23 μΩ.cm. A maximum responsivity was acheived for a thickness of 7.5 nm ($2x10^{5}$ $V.W^{-1}$), although detectivity only reach a constant maximum value ($1x10^{8}$ $cmHz^{1/2}/W$) for samples of thickness 40 nm or higher. Thus, a compromise has to be found between high responsivity and high detectivity. A major degradation of noise properties arises as the thickness is reduced, to the point that 1/f noise is the dominant the noise in the bolometers. Using AC or a reduced value of bias current should be considered in order to minimize this noise contribution.

ACKNOWLEDGMENTS

This research was funded in part by the Icelandic Research Fund and the University of Iceland Research Fund.

REFERENCES

[1] Rogalski, A., [Infrared detectors], CRC Press (2010)
[2] Ozcelik, A., Cabarcos, O., Allara, D. L., & Horn, M. W., "Vanadium Oxide Thin Films Alloyed with Ti, Zr, Nb, and Mo for Uncooled Infrared Imaging Applications," Journal of Electronic Materials, 1-5 (2013)
[3] Forsberg, F., Fischer, A. C., Roxhed, N., Samel, B., Ericsson, P., Stemme, G. and Niklaus, F., "Heterogeneous 3D integration of 17 μm pitch Si/SiGe quantum well bolometer arrays for infrared imaging systems," Journal of Micromechanics and Microengineering, 23(4), 045017 (2013)
[4] Liddiard, K. C., "Thin-film resistance bolometer IR detectors," Infrared physics, 24(1), 57-64 (1984)
[5] Xia, F., Mueller, T., Lin, Y. M., Valdes-Garcia, A., and Avouris, P., "Ultrafast graphene photodetector," Nature nanotechnology, 4(12), 839-843 (2009).
[6] Chen, H., Xi, N., Chen, L., and Lai, K. W. C., "Carbon nanotube based multi-spectrum infrared detector array," Proc. IEEE Solid-State Sensors, Actuators and Microsystems Conference (TRANSDUCERS), 16th International, 2566-2569 (2011)
[7] Mahjouri-Samani, M., Zhou, Y. S., He, X. N., Xiong, W., Hilger, P., and Lu, Y. F., "Plasmonic-enhanced carbon nanotube infrared bolometers," Nanotechnology, 24(3), 035502 (2013)
[8] Krenz, P. M., Tiwari, B., Szakmany, G. P., Orlov, A. O., González, F. J., Boreman, G. D., and Porod, W., "Response increase of IR antenna-coupled thermocouple using impedance matching," Quantum Electronics, IEEE Journal of, 48(5), 659-664 (2012)
[9] Renoux, P., Jónsson, S. Æ., Klein, L. J., Hamann, H. F. and Ingvarsson, S. "Sub-wavelength bolometers: uncooled platinum wires as infrared sensors," Opt. Express 19, 8721-8727 (2011)
[10] Renoux, P. and Ingvarsson, S. "Sample size effects on performance of sub-wavelength metallic thin-film bolometers," Journal of Optics, to be published (2013)
[11] Renoux, P., Beauny, A., Klein, L. J., Hamann, H. F. and Ingvarsson, S., "Thin-film platinum nanowires as sub-wavelength bolometers," Proc. SPIE 8261, 82610I (2012)
[12] Yoneoka, S., Lee, J., Liger, M., Yama, G., Kodama, T., Gunji, M., Provine, J., Howe, R. T., Goodson, K. E. and Kenny, T. W., "Electrical and thermal conduction in atomic layer deposition nanobridges down to 7 nm thickness," Nano Letters, 12(2), 683-686 (2012)
[13] Chen, C., Yi, X., Zhao, X. and Xiong, B., " Characterizations of VO2-based uncooled microbolometer linear array," Sensors ans Actuators A 90, 212-214 (2001).
[14] Tsutsumi, K., Yamashita, A., and Ohji, H., "The experimental study of high TCR Pt thin films for thermal sensors. In Sensors," Proceedings of IEEE (2), 1002-1005 (2002)
[15] Iniewski, K., [Smart Sensors for Industrial Applications], (Vol. 14) CRC Press (2013)

[16] Zhang, Q. G., Zhang, X., Cao, B. Y., Fujii, M., Takahashi, K., and Ikuta, T., "Influence of grain boundary scattering on the electrical properties of platinum nanofilms, " Applied physics letters, 89(11), 114102-114102 (2006)
[17] Elíasson, O. and Ingvarsson, S., "Grain growth in Pt microheaters subjected to high current density under constant power," to be submitted
[18] Yoneoka, S., Liger, M., Yama, G., Schuster, R., Purkl, F., Provine, J., Prinz, F. B., Howe, R. T. and Kenny, T. W., "ALD-metal uncooled bolometer," Proc. Micro Electro Mechanical Systems (MEMS), 2011 IEEE 24th International Conference on, 676-679 (2011)
[19] Kogan, S., [Electronic Noise and Fluctuations in Solids], Cambridge University Press, (1996)
[20] Fleetwood, D. M. and Giordano, N., "Resistivity dependence of 1/f noise in metal films," Physical Review B, 27(2), 667 (1983)

Bibliography

Aliev, A. E. (2008), 'Bolometric detector on the basis of single-wall carbon nanotube/polymer composite', *Infrared Physics & Technology* **51**(6), 541–545.

Aliev, V. S. & Bortnikov, S. G. (2011), Bolometer at semiconductor-metal phase transition in VO_2 thin films, *in* 'Micro/Nanotechnologies and Electron Devices (EDM), 2011 International Conference and Seminar of Young Specialists on', IEEE, pp. 129–131.

Andersen, O. K. (1970), 'Electronic structure of the fcc transition metals Ir, Rh, Pt, and Pd', *Physical Review B* **2**(4), 883.

Au, Y.-Y., Skulason, H. S., Ingvarsson, S., Klein, L. J. & Hamann, H. F. (2008), 'Thermal radiation spectra of individual subwavelength microheaters', *Phys. Rev. B* **78**, 085402.
URL: *http://link.aps.org/doi/10.1103/PhysRevB.78.085402*

Bean, J. A., Weeks, A. & Boreman, G. D. (2011), 'Performance optimization of antenna-coupled Al/AlOx/Pt tunnel diode infrared detectors', *IEEE J. Quantum Electron* **47**(1), 126–135.

Bhan, R., Saxena, R., Jalwania, C. & Lomash, S. (2009), 'Uncooled infrared microbolometer arrays and their characterisation techniques', *Defence Science Journal* **59**(6), 580–589.

Block, W. & Gaddy, O. (1973), 'Thin metal film room-temperature IR bolometers with nanosecond response time', *Quantum Electronics, IEEE Journal of* **9**(11), 1044–1053.

Boragno, C., Valbusa, U. & Pignatel, G. (1987), 'Fast P-doped silicon bolometer for detecting heat pulses', *Applied physics letters* **50**, 583.

Boreman, G. D. (2012), Infrared antennas and frequency-selective surfaces, *in* 'SPIE Optical Engineering + Applications', International Society for Optics and Photonics, pp. 84830D–84830D.

Bryant, G. W., García de Abajo, F. J. & Aizpurua, J. (2008), 'Mapping the plasmon resonances of metallic nanoantennas', *Nano letters* **8**(2), 631–636.

Bumble, B. & LeDuc, H. G. (1997), 'Fabrication of a diffusion cooled superconducting hot electron bolometer for THz mixing applications', *Applied Superconductivity, IEEE Transactions on* **7**(2), 3560–3563.

Chen, C., Yi, X., Zhao, X. & Xiong, B. (2001), 'Characterizations of VO_2-based uncooled microbolometer linear array', *Sensors and Actuators A: Physical* **90**(3), 212–214.

Chen, S., Ma, H., Xiang, S. & Yi, X. (2007), 'Fabrication and performance of microbolometer arrays based on nanostructured vanadium oxide thin films', *Smart materials and structures* **16**(3), 696.

Chi-Anh, N., Shin, H.-J., Kim, K., Han, Y.-H. & Moon, S. (2005), 'Characterization of uncooled bolometer with vanadium tungsten oxide infrared active layer', *Sensors and Actuators A: Physical* **123**, 87–91.

Codreanu, I. & Boreman, G. D. (2002), 'Influence of dielectric substrate on the responsivity of microstrip dipole-antenna-coupled infrared microbolometers', *Applied optics* **41**(10), 1835–1840.

Codreanu, I., Gonzalez, F. J. & Boreman, G. D. (2003), 'Detection mechanisms in microstrip dipole antenna-coupled infrared detectors', *Infrared physics & technology* **44**(3), 155–163.

Contreras, B. & Gaddy, O. (1970), 'Nanosecond response time room-temperature infrared detection with thin-film bolometers', *Applied Physics Letters* **17**(10), 450–453.

Cuadrado, A., Alda, J. & González, F. J. (2013), 'Multiphysics simulation for the optimization of optical nanoantennas working as distributed bolometers in the infrared', *Journal of Nanophotonics* **7**(1), 073093–073093.

Day, G., Gaddy, O. & Iversen, R. (1968), 'Detection of fast infrared laser pulses with thin film thermocouples', *Applied Physics Letters* **13**, 289.

Dillner, U., Kessler, E. & Meyer, H. (2013), 'Figures of merit of thermoelectric and bolometric thermal radiation sensors', *Journal of Sensors and Sensor Systems* **2**, 85–94.

Dobrovolsky, V. & Sizov, F. (2007), 'A room temperature, or moderately cooled, fast THz semiconductor hot electron bolometer', *Semiconductor science and technology* **22**(2), 103.

Dosdale, T. & Livesey, D. (1974), 'The electrical transport properties of platinum at room temperature', *Journal of Physics F: Metal Physics* **4**(1), 68.

Elíasson, O. & Ingvarsson, S. (, to be submitted), Grain growth in Pt microheaters subjected to high current density under constant power.

Eriksson, P., Andersson, J. & Stemme, G. (1997), 'Thermal characterization of surface-micromachined silicon nitride membranes for thermal infrared detectors', *Microelectromechanical Systems, Journal of* **6**(1), 55–61.

Fischer, G., Hoffmann, H. & Vancea, J. (1980), 'Mean free path and density of conductance electrons in platinum determined by the size effect in extremely thin films', *Physical Review B* **22**(12), 6065.

Fleetwood, D., Masden, J. & Giordano, N. (1983), '1/f noise in platinum films and ultrathin platinum wires: evidence for a common, bulk origin', *Physical Review Letters* **50**(6), 450–453.

Forsberg, F., Fischer, A. C., Roxhed, N., Samel, B., Ericsson, P., Stemme, G. & Niklaus, F. (2013), 'Heterogeneous 3D integration of 17 μm pitch Si/SiGe quantum well bolometer arrays for infrared imaging systems', *Journal of Micromechanics and Microengineering* **23**(4), 045017.

Fricke, J. & Tillotson, T. (1997), 'Aerogels: production, characterization, and applications', *Thin Solid Films* **297**(1-2), 212–223.

Fumeaux, C., Gritz, M. A., Codreanu, I., Schaich, W. L., González, F. J. & Boreman, G. D. (2000), 'Measurement of the resonant lengths of infrared dipole antennas', *Infrared physics & technology* **41**(5), 271–281.

Galkina, T., Klokov, A. Y., Sharkov, A., Khmelnitskiĭ, R., Gippius, A., Dravin, V., Ral'chenko, V. & Savel'ev, A. (2007), 'Bolometric detector embedded in a polycrystalline diamond grown by chemical vapor deposition', *Physics of the Solid State* **49**(4), 654–659.

Gawarikar, A. S., Shea, R. P. & Talghader, J. J. (2013), 'High detectivity uncooled thermal detectors with resonant cavity coupled absorption in the long-wave infrared', *Electron Devices, IEEE Transactions on* **60**(8), 2586–2591.

Gehrer, E. & Hayek, K. (1984), 'Ultrathin epitaxial deposits of platinum of NaCl to be used as model catalysts', *Thin solid films* **115**(4), 283–290.

González, F. (2006*a*), 'Noise measurements on optical detectors', *Revista mexicana de física* **52**(6), 550–554.

González, F., Ashley, C., Clem, P. & Boreman, G. (2004), 'Antenna-coupled microbolometer arrays with aerogel thermal isolation', *Infrared physics & technology* **45**(1), 47–51.

González, F. & Boreman, G. (2005), 'Comparison of dipole, bowtie, spiral and log-periodic IR antennas', *Infrared physics & technology* **46**(5), 418–428.

González, F., Fumeaux, C., Alda, J. & Boreman, G. (2000), 'Thermal impedance model of electrostatic discharge effects on microbolometers', *Microwave and Optical Technology Letters* **26**(5), 291–293.

González, F. J. (2006*b*), 'Thermal-impedance simulations of antenna-coupled microbolometers', *Infrared physics & technology* **48**(3), 223–226.

Grossman, E., Koch, J., Reintsema, C. & Green, A. (1998), 'Lithographic dipole antenna properties at 10 μm wavelength: Comparison of method-of-moments predictions with experiment', *International journal of infrared and millimeter waves* **19**(6), 817–825.

Han, Y.-H., Kim, K.-T., Shin, H.-J., Moon, S. & Choi, I.-H. (2005), 'Enhanced characteristics of an uncooled microbolometer using vanadium–tungsten oxide as a thermometric material', *Applied Physics Letters* **86**(25), 254101–254101.

Herschel, W. (1800), 'Experiments on the refrangibility of the invisible rays of the sun', *Philosophical Transactions of the Royal Society of London* **90**, 284–292.

Ingvarsson, S. (2001), *Magnetization dynamics in transition metal ferromagnets studied by magneto-tunneling and ferromagnetic resonance*, Ph.D. Thesis, Brown University.

Ingvarsson, S., Klein, L., Au, Y., Lacey, J., Hamann, H. et al. (2007), 'Enhanced thermal emission from individual antenna-like nanoheaters', *Opt. Express* **15**(18), 11249–11254.

Iniewski, K. (2013), *Smart Sensors for Industrial Applications*, Vol. 14, CRC PressI Llc.

Jónsson, S. (2009), *Nonlinear thermal electric analysis of platinum microheaters*, Master thesis, University of Iceland.

Karasik, B. S. & Cantor, R. (2011), 'Demonstration of high optical sensitivity in far-infrared hot-electron bolometer', *Applied Physics Letters* **98**(19), 193503–193503.

Ketterson, J. & Windmiller, L. (1970), 'de haas-van alphen effect in platinum', *Physical Review B* **2**(12), 4813.

Klein, L. J., Hamann, H. F., Au, Y.-Y. & Ingvarsson, S. (2008), 'Coherence properties of infrared thermal emission from heated metallic nanowires', *Applied Physics Letters* **92**(21), 213102–213102.

Klein, L. J., Ingvarsson, S. & Hamann, H. F. (2009), 'Changing the emission of polarized thermal radiation from metallic nanoheaters', *Optics express* **17**(20), 17963–17969.

Klokov, A. Y., Sharkov, A., Galkina, T., Khmelnitskii, R., Dravin, V. & Gippius, A. A. (2010), 'Fast bolometer built in an artificial HPHT diamond matrix', *Quantum Electronics* **40**(3), 269.

Kogan, S. (1996), *Electronic noise and fluctuations in solids*, Cambridge University Press (Cambridge England and New York, NY, USA).

Kosarev, A., Moreno, M., Torres, A. & Zuniga, C. (2008), 'IR sensors based on silicon–germanium–boron alloys deposited by plasma: Fabrication and characterization', *Journal of Non-Crystalline Solids* **354**(19), 2561–2564.

Krenz, P. M., Tiwari, B., Szakmany, G. P., Orlov, A. O., González, F. J., Boreman, G. D. & Porod, W. (2012), 'Response increase of IR antenna-coupled thermocouple using impedance matching', *Quantum Electronics, IEEE Journal of* **48**(5), 659–664.

Kuzmichev, V., Pogorelov, S. & Kohns, P. (2004), Transformation of the continuous laser power on wavelength 10.6 microns with thin-wire bolometer, *in* 'Laser and Fiber-Optical Networks Modeling, 2004. Proceedings of LFNM 2004. 6th International Conference on', IEEE, pp. 238–241.

Langley, S. (1881), 'The bolometer', *Nature* **25**(14-16).

Langley, S. P. (1880), The bolometer and radiant energy, *in* 'Proceedings of the American Academy of Arts and Sciences', Vol. 16, JSTOR, pp. 342–358.

Liddiard, K. (1984), 'Thin-film resistance bolometer IR detectors', *Infrared physics* **24**(1), 57–64.

Lu, R., Li, Z., Xu, G. & Wu, J. Z. (2009), 'Suspending single-wall carbon nanotube thin film infrared bolometers on microchannels', *Applied Physics Letters* **94**(16), 163110–163110.

Mahjouri-Samani, M., Zhou, Y., He, X., Xiong, W., Hilger, P. & Lu, Y. (2013), 'Plasmonic-enhanced carbon nanotube infrared bolometers', *Nanotechnology* **24**(3), 035502.

Mei, T., Neuzil, P., Karunasiri, G. & Zeng, W. (2002), 'Approach to measure thermal efficiency of bolometer sensors', *Applied physics letters* **80**(12), 2183–2185.

Mühlschlegel, P., Eisler, H.-J., Martin, O., Hecht, B. & Pohl, D. (2005), 'Resonant optical antennas', *Science* **308**(5728), 1607–1609.

Neubrech, F., Kolb, T., Lovrincic, R., Fahsold, G., Pucci, A., Aizpurua, J., Cornelius, T., Toimil-Molares, M., Neumann, R. & Karim, S. (2006), 'Resonances of individual metal nanowires in the infrared', *Applied Physics Letters* **89**(25), 253104–253104.

Niesler, F. B., Gansel, J. K., Fischbach, S. & Wegener, M. (2012), 'Metamaterial metal-based bolometers', *Applied Physics Letters* **100**(20), 203508–203508.

Novotny, L. (2007), 'Effective wavelength scaling for optical antennas', *Physical Review Letters* **98**(26), 266802.

Novotny, L. & van Hulst, N. (2011), 'Antennas for light', *Nature Photonics* **5**(2), 83–90.

Omega Engineering, I. (2002), *Transactions in Measurement and Control*, Vol. 1 - Non-contact temperature measurement, Omega Press.
URL: *http://www.omega.com/literature/transactions/volume1/trantocvol1.html*

Ozcelik, A., Cabarcos, O., Allara, D. L. & Horn, M. W. (2013), 'Vanadium oxide thin films alloyed with Ti, Zr, Nb, and Mo for uncooled infrared imaging applications', *Journal of Electronic Materials* pp. 1–5.

Rahman, A., de Lange, G. & Hu, Q. (1996), 'Micromachined room-temperature microbolometers for millimeter-wave detection', *Applied physics letters* **68**(14), 2020–2022.

Renoux, P., Beauny, A., Klein, L. J., Hamann, H. F. & Ingvarsson, S. (2012), Thin-film platinum nanowires as sub-wavelength bolometers, *in* 'Proceedings of SPIE', Vol. 8261, International Society for Optics and Photonics, p. 82610I.

Renoux, P., Charpentier, D., Augé, S. & Ingvarsson, S. (2013), Optimization of performance for platinum nanowires as sub-wavelength bolometers, *in* 'Proceedings of SPIE', Vol. 8868, International Society for Optics and Photonics, p. 88680C.

Renoux, P. & Ingvarsson, S. (2013), 'Sample size effects on performance of sub-wavelength metallic thin-film bolometers', *Journal of optics* **15**, 114011.

Renoux, P., Jónsson, S. Æ., Klein, L. J., Hamann, H. F. & Ingvarsson, S. (2011), 'Sub-wavelength bolometers: Uncooled platinum wires as infrared sensors', *Optics express* **19**(9), 8721–8727.

Rogalski, A. (2003), 'Infrared detectors: status and trends', *Progress in quantum electronics* **27**(2), 59–210.

Rogalski, A. (2011), *Infrared Detectors*, Taylor & Francis.

Rogalski, A. (2012), 'Progress in focal plane array technologies', *Progress in Quantum Electronics* **36**(2-3), 342 – 473.

Ruffner, J., Clem, P., Tuttle, B., Brinker, C., Sriram, C. & Bullington, J. (1998), 'Uncooled thin film infrared imaging device with aerogel thermal isolation: deposition and planarization techniques', *Thin Solid Films* **332**(1), 356–361.

Saxena, R., Bhan, R., Jalwania, C. & Khurana, K. (2008), 'Effect of excessive bias heating on a titanium microbolometer infrared detector', *Sensors Journal, IEEE* **8**(11), 1801–1804.

Saxena, R., Bhan, R., Jalwania, C., Rana, P. & Lomash, S. (2008), 'Characterization of area arrays of microbolometer-based un-cooled ir detectors without using roic', *Sensors and Actuators A: Physical* **141**(2), 359–366.

Schöpp, H., Sperl, A., Kozakov, R., Gött, G., Uhrlandt, D. & Wilhelm, G. (2012), 'Temperature and emissivity determination of liquid steel S235', *Journal of Physics D: Applied Physics* **45**(23), 235203.

Scofield, J. (1987), 'Ac method for measuring low-frequency resistance fluctuation spectra', *Review of scientific instruments* **58**(6), 985–993.

Scofield, J. H., Mantese, J. V. & Webb, W. W. (1985), '1/f noise of metals: A case for extrinsic origin', *Physical Review B* **32**(2), 736.

Sedky, S., Fiorini, P., Baert, K., Hermans, L. & Mertens, R. (1999), 'Characterization and optimization of infrared poly SiGe bolometers', *Electron Devices, IEEE Transactions on* **46**(4), 675–682.

Sedky, S., Fiorini, P., Caymax, M., Baert, C., Hermans, L. & Mertens, R. (1998), 'Characterization of bolometers based on polycrystalline silicon germanium alloys', *Electron Device Letters, IEEE* **19**(10), 376–378.

Sekiyama, A., Yamaguchi, J., Higashiya, A., Obara, M., Sugiyama, H., Kimura, M., Suga, S., Imada, S., Nekrasov, I., Yabashi, M. et al. (2010), 'The prominent 5d-orbital contribution to the conduction electrons in gold', *New Journal of Physics* **12**(4), 043045.

Serway, R. (1998), *Principles of Physics*, Saunders College Publishing, London UK.

Shie, J., Chen, Y., Ou-Yang, M. & Chou, B. (1996), 'Characterization and modeling of metal-film microbolometer', *Microelectromechanical Systems, Journal of* **5**(4), 298–306.

Siebert, R. & Müller, J. (2005), 'Infrared integrated optical evanescent field sensor for gas analysis: Part I: System design', *Sensors and Actuators A: Physical* **119**(1), 138 – 149.

Smith, R., Jones, F. & Chasmar, R. (1957), *The detection and measurement of infrared radiation*, Clarendon Press.

Talghader, J. J., Gawarikar, A. S. & Shea, R. P. (2012), 'Spectral selectivity in infrared thermal detection', *Light: Science & Applications* **1**(8), e24.

Tanaka, A., Matsumoto, S., Tsukamoto, N., Itoh, S., Chiba, K., Endoh, T., Nakazato, A., Okuyama, K., Kumazawa, Y., Hijikawa, M., Gotoh, H., Tanaka, T. & Teranishi, N. (1996), 'Infrared focal plane array incorporating silicon IC process compatible bolometer', *Electron Devices, IEEE Transactions on* **43**(11), 1844 –1850.

Torres, A., Kosarev, A., García Cruz, M. & Ambrosio, R. (2003), 'Uncooled microbolometer based on amorphous germanium film', *Journal of non-crystalline solids* **329**(1), 179–183.

Tsutsumi, K., Yamashita, A. & Ohji, H. (2002), The experimental study of high TCR Pt thin films for thermal sensors, *in* 'Sensors, 2002. Proceedings of IEEE', Vol. 2, IEEE, pp. 1002–1005.

Vancea, J., Hoffmann, H. & Kastner, K. (1984), 'Mean free path and effective density of conduction electrons in polycrystalline metal films', *Thin Solid Films* **121**(3), 201–216.

Verghese, S., Richards, P., Char, K. & Sachtjen, S. (1991), 'Fabrication of an infrared bolometer with a high T_c superconducting thermometer', *Magnetics, IEEE Transactions on* **27**(2), 3077–3080.

Windmiller, L., Ketterson, J. & Hornfeldt, S. (1969), 'Experimental determination of the fermi radius, velocity, and g factor in Pd and Pt', *Journal of Applied Physics* **40**(3), 1291–1293.

Wood, R., Han, C. & Kruse, P. (1992), Integrated uncooled infrared detector imaging arrays, *in* 'Solid-State Sensor and Actuator Workshop, 1992. 5th Technical Digest., IEEE', IEEE, pp. 132–135.

Xia, F., Mueller, T., Lin, Y.-m., Valdes-Garcia, A. & Avouris, P. (2009), 'Ultrafast graphene photodetector', *Nature nanotechnology* **4**(12), 839–843.

Xiao, L., Zhang, Y., Wang, Y., Liu, K., Wang, Z., Li, T., Jiang, Z., Shi, J., Liu, L., Li, Q. et al. (2011), 'A polarized infrared thermal detector made from super-aligned multiwalled carbon nanotube films', *Nanotechnology* **22**(2), 025502.

Xin, Z., Xiao-Hui, S. & Dian-Lin, Z. (2010), 'Thickness dependence of grain size and surface roughness for DC magnetron sputtered Au films', *Chinese Physics B* **19**(8), 086802.

Yoneoka, S., Liger, M., Yama, G., Schuster, R., Purkl, F., Provine, J., Prinz, F., Howe, R. & Kenny, T. (2011), ALD-metal uncooled bolometer, *in* 'Micro Electro Mechanical Systems (MEMS), 2011 IEEE 24th International Conference on', IEEE, pp. 676–679.

Zhang, Q., Zhang, X., Cao, B., Fujii, M., Takahashi, K. & Ikuta, T. (2006), 'Influence of grain boundary scattering on the electrical properties of platinum nanofilms', *Applied physics letters* **89**(11), 114102–114102.

Zhang, X., Xie, H., Fujii, M., Ago, H., Takahashi, K., Ikuta, T., Abe, H. & Shimizu, T. (2005), 'Thermal and electrical conductivity of a suspended platinum nanofilm', *Applied Physics Letters* **86**(17), 171912–171912.